Spring 5-2011

# The Vogar Fissure Swarm, Reykjanes Peninsula, Iceland: Aseismic Kinematics of an Oblique Rift Zone

Keegan Timothy Runnals
*Bates College*, krunnals@bates.edu

# The Vogar Fissure Swarm, Reykjanes Peninsula, Iceland: Aseismic Kinematics of an Oblique Rift Zone

An Honors Thesis

Presented to

The Faculty of the Department of Geology

Bates College

In partial fulfillment of the requirements for the

Degree of Bachelor of Science

By

Keegan Timothy Runnals

Lewiston, Maine

March, 2011

**Abstract**

Exposure of the Mid-Atlantic ridge in Iceland offers a unique place to study hotspot-ridge interactions along an oblique rift zone. The Reykjanes Peninsula is a left lateral shear zone characterized by a series of NE striking en echelon fissure swarms oblique to the rift axis, and N-S trending dextral strike slip faults. This study focuses on the Vogar fissure swarm in southwest Iceland, in order to better constrain the mode of deformation within it. Movement of the faults and fissures that make up the fissure swarm is thought to either be related to seismic events along the ridge, or occur aseismically due to dike injections during eruptive episodes. GPS measurements and field based mapping were employed to examine a 7x3 km cross section of the fissure swarm in order to constrain its kinematics. The faults tend to terminate at the contact of a historical fissure lava and an ~12,000 year old shield lava. Cooling properties of the historical lava flow and overflown pre-existing faults were concluded to contribute to its present day structure. The faults' termination at the historical lava supports the theory that movement along the faults occurs primarily aseismically during eruptive episodes. With this assumption a hypothetical cross section was created of the Vogar fissure swarm extending to the base of the crust, relating the normal faults at the surface to dikes at depth. The continued activity along the Reykjanes Peninsula suggests that it is still a very active spreading center, making it important to constrain the types of deformation that characterize it.

**Acknowledgements**

This project was funded by a Bates Summer Research Grant, a Barlow Thesis Research Grant, and a Bates Student Research Fund grant which made it possible to conduct fieldwork in Iceland during May and June, and make a follow up trip in October. Without this funding the project would not have been, and I am very grateful for the opportunities Bates affords for student conducted research.

I would first like to thank Páll Einarsson at the University of Iceland for setting up this project for me. You were very accommodating and helpful as I developed and carried out this research, and were a limitless book of knowledge when it came to Icelandic geology. I would also like to thank the University of Iceland itself for providing me with the field equipment and software needed to conduct the research, as well as the company Loftmyndir for use of their aerial photographs.

A huge thanks to my advisor Dyk, I couldn't have asked for more from a thesis advisor. From your initial visit in Iceland to the final revisions you provided, I was always learning something new. You were always available and pushing me to look at different aspects of the project which I otherwise would not have been keen on, and it truly was a pleasure to work under you. To the rest of the Bates Geo professors, you have provided an awesome four years, and I've had a great time working with everyone throughout. Bev, without Global Change I probably wouldn't be a geology major. John, you have been a great resource and teacher to me during all four years. Mike, many great memories from your classes, and I hope you remember that I was in the middle of the canoe and had no control when it capsized.

To the Geo Seniors, it's been a great ride. I have many awesome memories from the countless hours we spent together in the field and lab, and even those late nights in Coram and Carnegie. Lots of support throughout has really been great, and without it I definitely would not be where I am today.

A huge thanks to everyone else that has supported me with this project and others during my time at Bates. Matt and Will, I feel like I just lived in your house for four years. You both have been incredible technical resources, and have helped me vastly improve my design and software skills. I'd like to thank Ken Hardcastle for helping me with the GPS files that I desperately needed for my thesis. Kenjo, it was only one day but that data we got was a huge part of my work as well.

Finally I'd like to thank my family. You have been extremely supportive of all the adventures and projects I embark on, and it is a great feeling to have you behind me.

# Table of Contents

**Table of Figures**

# CHAPTER 1: INTRODUCTION

## 1.1 Purpose

Iceland is the only place in the world where the Mid-Atlantic ridge is exposed above sea level, and thus offers a unique place to study rifting and volcanic structures. Fissure swarms are structures usually associated with volcanism along the ridge, and the stresses controlling the fissure swarm are not well understood by geologists. This project focuses on the Vogar fissure swarm in order to gain a comprehensive understanding of the mechanics involved in the active deformation of this structure. The main question being investigated is whether the mode of deformation is seismic or aseismic in nature. A seismic mode would indicate deformation related to the rifting plates, while an aseismic mode would point to volcanism as the source of deformation. GPS measurements and field observations were employed to examine a cross sectional swath through the Vogar fissure swarm to determine the mode of past and present deformation in the area. Determining the nature of the faulting could have important implications for earthquake-hazard assessment on the peninsula, as well as providing a better understanding of stresses in an active oblique spreading zone.

## 1.2 Introduction to Regional Tectonics

### *1.2.1 Iceland*

Iceland is located between a latitude of 63° and 67° N and between a longitude of -14° and -24° W. It sits on a divergent plate boundary called the Mid-Atlantic Ridge (MAR), which separates the North American plate from the Eurasian plate (Fig. 1.1). In Iceland, these plates are moving apart at an average rate of 18.2mm/year in a direction of N105°E according to the Nuvel-1A model (Einarsson, 2008). The MAR is characterized by rifting and transform segments along its axis, which can be clearly identified by the epicenters of earthquakes (Fig. 1.1). Iceland is also situated over a hot spot, which

coupled with the MAR creates an environment of frequent tectonism and volcanism in the region.

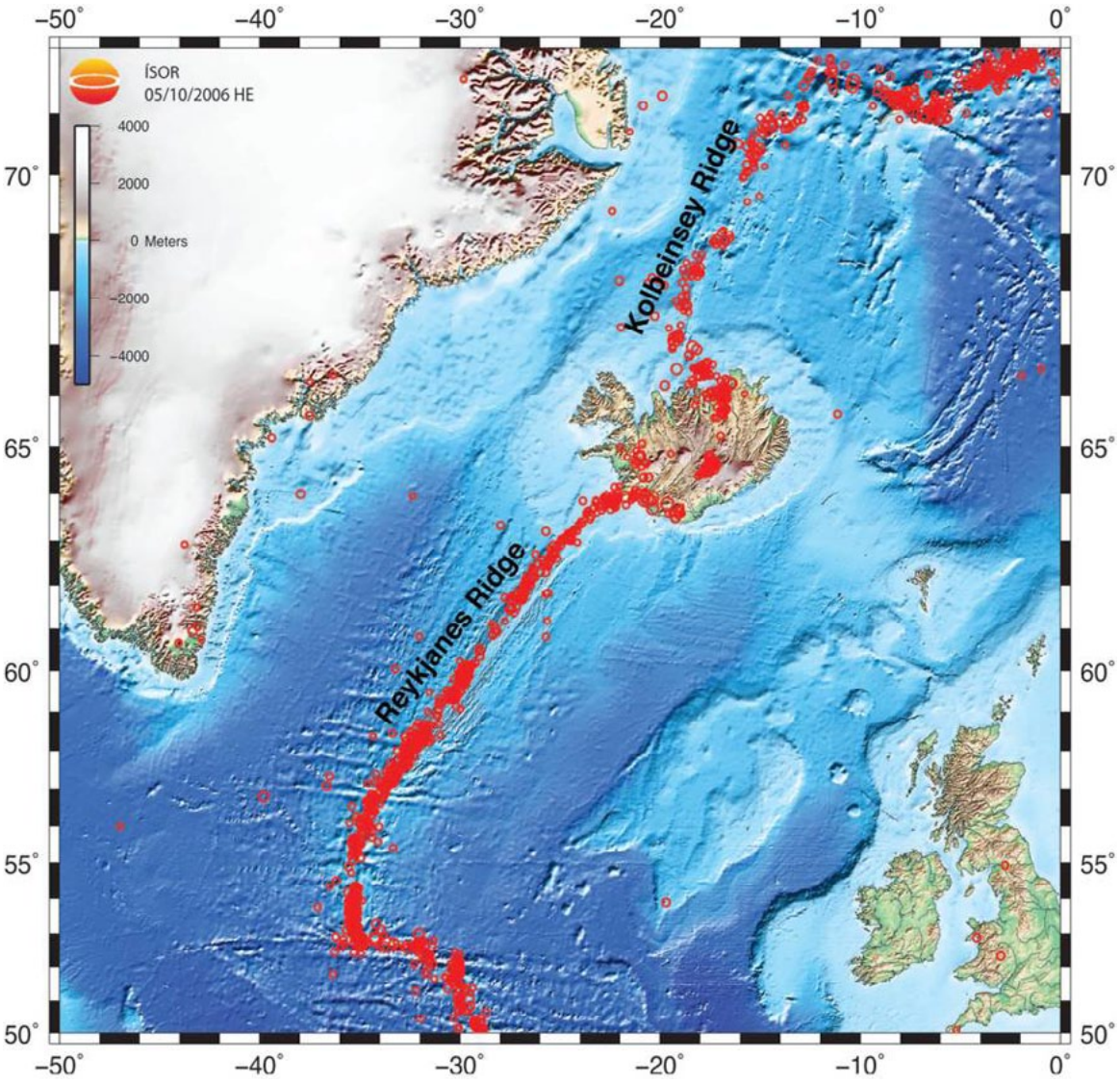


Figure 1.1 Map from Einarsson (2008) showing location and bathymetry around Iceland. The red circles indicate the epicenters of earthquakes between 1964 and 2006 and define the Mid Atlantic Ridge or plate boundary.

A hot spot is created by a mantle plume, which is a long subvertical column of hot buoyant material that flows upward from deep in the mantle to shallow levels in the crust (Gudmundsson, 2000). This shallow source of mantle material is the source of frequent volcanic events as it follows weaknesses in the crust to the surface of the earth. The center of the plume under Iceland is thought to lie below the western part of the Vatnajokull glacier (Fig. 1.2). The enhanced volcanic activity has thickened the crust, with a thickness of 20 km on the county's outer edge to 40 km at the source of the hotspot under Vatnajokull (Darbyshire et al. 2000). This varies significantly from the 8.3 ± 1.5 km thick oceanic crust normally found at a spreading center (White, 1992). The plume below Iceland is known to reach depths of 400 km with depths of 600-700 km possible (Gudmundsson, 2000; Dyment et al., 2007). The width of the plume is 200-300 km at its widest (Gudmundsson, 2000). The hotspot contributes to the volcanic systems that characterize Iceland, which are mostly large swarms of fissures and faults that arise from the stresses of the spreading plates (Gudmundsson, 2000).

According to Dyment et al. (2007), there are a series of interactions between a hotspot and spreading ridge as the ridge migrates over it. Currently the ridge is directly over the Iceland hotspot, and will linger here as it undergoes ridge jumps to the east due to the influence of the hot spot. A ridge jump is thought to be due to the interaction with the reheated and weakened lithosphere above the plume (Mittelstaedt, 2008). A ridge jump is currently in progress as the Western Volcanic Zone (WVZ) of Iceland is becoming less active and the activity in the Eastern Volcanic Zone (EVZ) is increasing (Fig. 1.3). A present day example of this activity can be seen in the recent eruption of Eyjafjallajokull, which is located in the EVZ. It must be pointed out that there are alternate theories to the Icelandic hot spot, such as that by Foulger and Anderson (2005) who attribute the melt underneath Iceland to recycled Caledonian crust. However, the mantle plume theory is the most widely accepted.

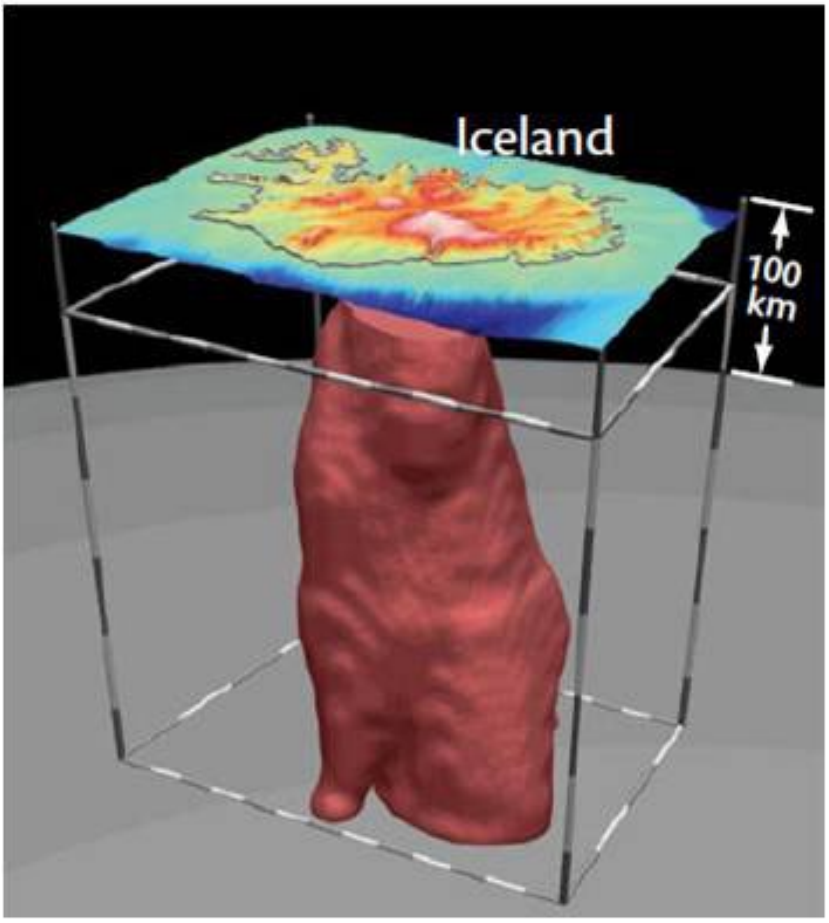


Figure 1.2 Model showing the hotspot or mantle root of magma below Iceland. This is thought to be centered under the largest glacier Vatnajokull (From Dyment et al., 2007).

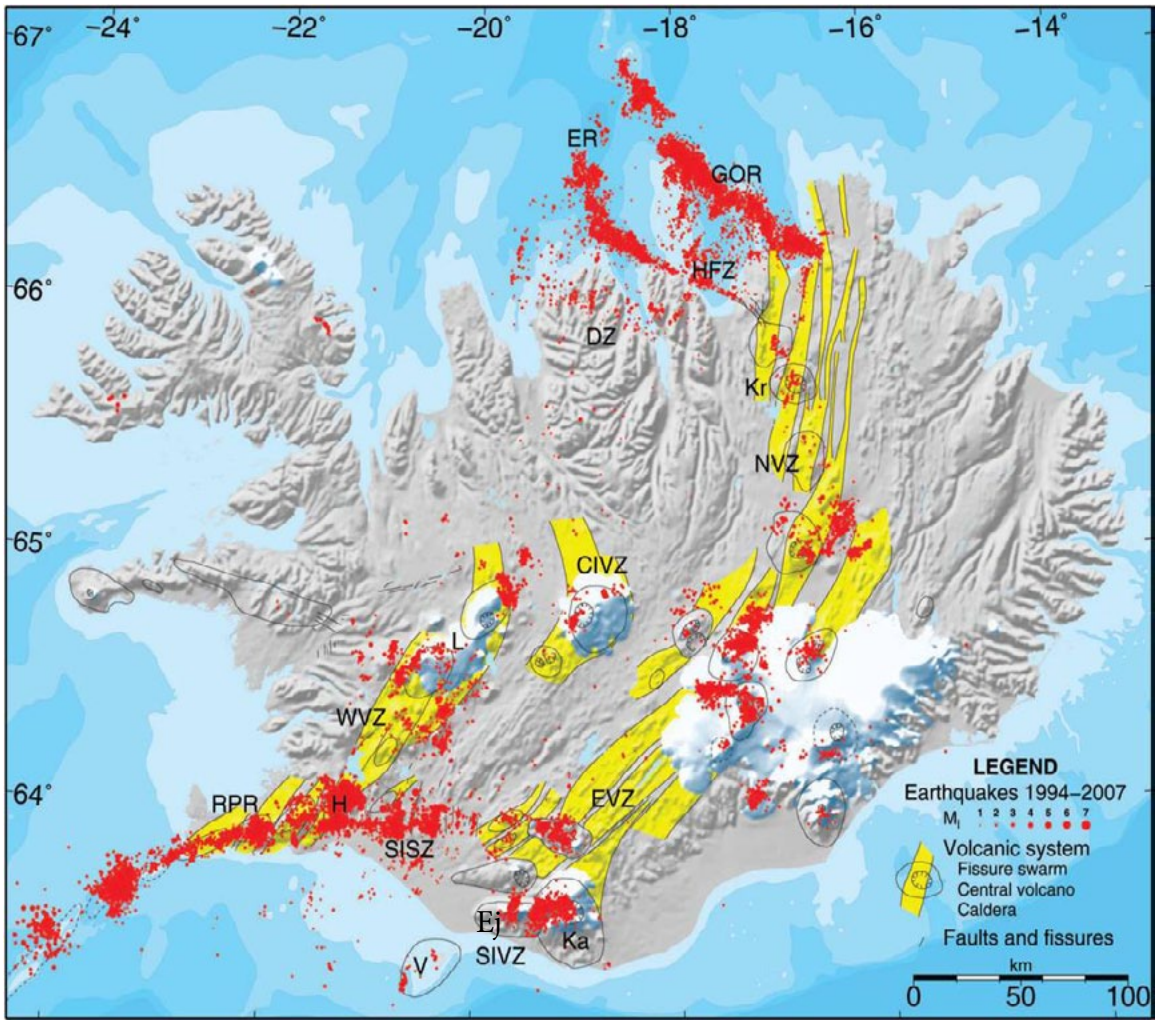


Figure 1.3 Tectonic map of Iceland indicating the epicenters of earthquakes from 1994-2007. The yellow areas are fissure swarms of the volcanic systems and the letters indicate the different active zones of Iceland. RPR=Reykjanes Peninsula Rift, WVZ = Western Volcanic Zone, SISZ=South Icelandic Seismic Zone, SIVZ=South Icelandic Volcanic Zone, EVZ=Eastern Volcanic Zone, CIVZ=Central Icelandic Volcanic Zone, NVZ=Northern Volcanic Zone, HVZ=Husavik-Flatey Zone, GOR=Grimsley Oblique Rift, ER=Eyjafjardarall Rift, DZ= Dalvik Zone. V, Ej, Ka, H, L, Kr= Central volcanoes of Vestmannaeyjar, Eyjafjallajokull, Katla, Hengill, Langjokull, and Krafla respectively (Modified from Einarsson, 2008).

The different ridge segments of the MAR are highly influenced by the rate of spreading and obliqueness to the plate velocity vector (Einarsson, 2008). Segments that are perpendicular to the velocity vector are purely divergent and are characterized by volcanism, normal faulting, and fissuring. In Iceland, examples of these zones are the Northern Volcanic Zone (NVZ), the WVZ, and EVZ (Fig. 1.3). Segments that are parallel or sub-parallel to the velocity vector are transform zones dominated by strike slip activity such as the South Icelandic Seismic Zone (SISZ) and the Husavik-Flatey Zone (HFZ). Segments that are neither parallel nor perpendicular but oblique to the velocity vector contain elements of both rift volcanism and strike slip activity, which may or may not influence each other. Examples of such oblique segments are the Grimsley Oblique Rift (GOR) and the Reykjanes Peninsula Rift (RPR) where the Vogar fissure swarm is located (Einarsson, 2008).

### *1.2.2 Reykjanes Peninsula*

The Reykjanes Peninsula is located in southwest Iceland, and represents a continuation of the Reykjanes Ridge onto the island (Fig. 1.4a). A ridge jump started the spreading on the Peninsula 6-7 million years ago. The ridge is obliquely oriented by about 30° counterclockwise to the NUVEL-1A direction of spreading of 103° (Demets et al., 1994). This creates for structures that accommodate both extensional strain and left lateral shear (Clifton and Kattenhorn, 2006). A major structural feature on the peninsula is the series of en echelon fissure swarms, each associated with a specific volcanic system. Other features include hyaloclastic ridges formed from subglacial eruptions, large lava shields, and eruptive and non-eruptive fissures, which dominate the landscape of the peninsula (Einarsson, 2008).

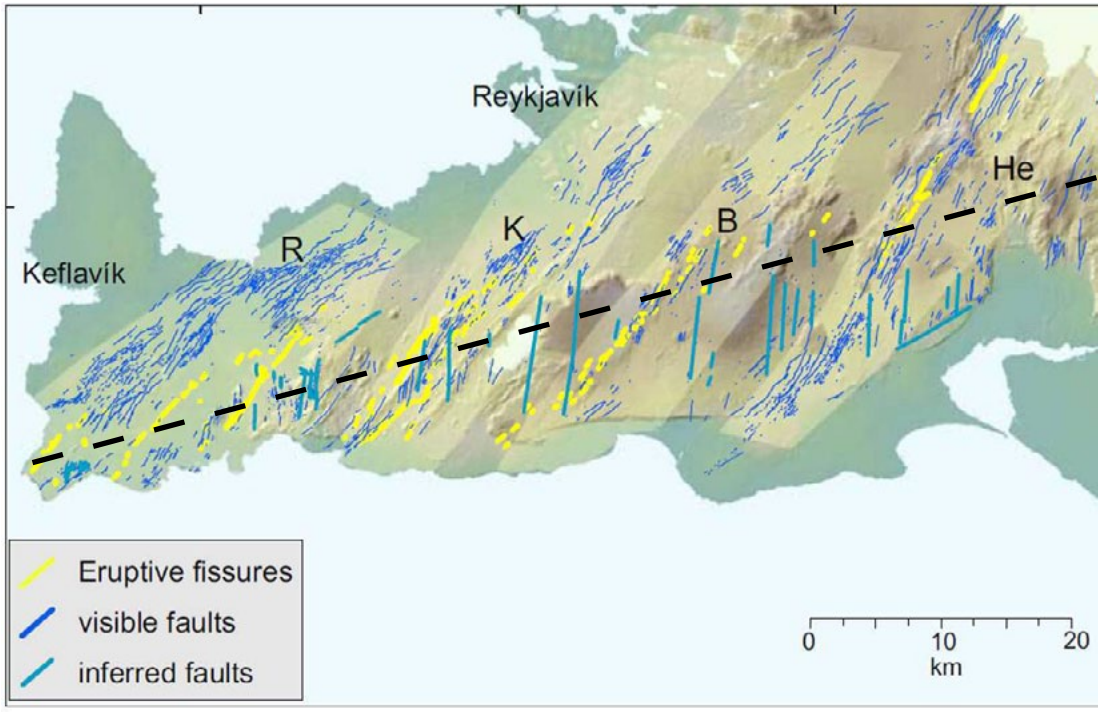


A

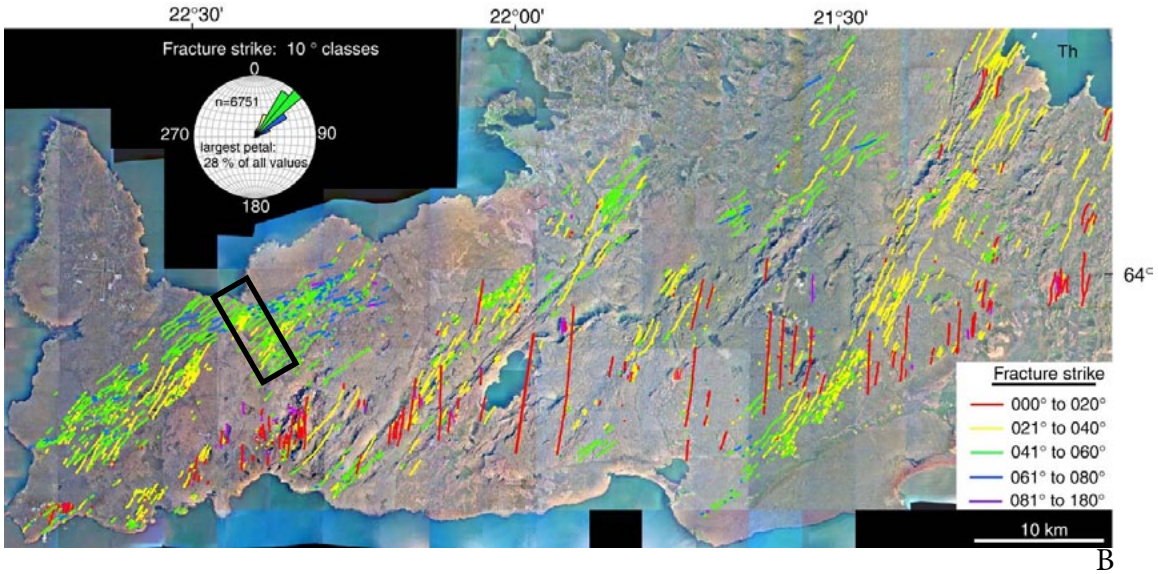


B

Figure 1.4 A) Map of Reykjanes Peninsula. Clusters of normal faults (dark blue) and eruptive fissures (yellow) signify fissure swarms. Each fissure swarm is associated with a volcanic complex. The north-south striking faults are strike slip faults. The combination of normal and strike slip movement is indicative of the obliquness of the ridge. Dashed line represents the approximate rift axis. Letters denote fissure swarms. R=Reykjanes, K=Krisuvik, B=Brennisteinsfjoll, He=Hengill (Modified from Jenness and Clifton, 2009). B) Map of faults in Reykjanes according to strike. Approximate study area is outlined by black box. (Modified from Clifton and Kattenhorn, 2006)

A zone of seismicity 2-5 km wide and trending at 75° runs through the peninsula and defines the active plate boundary (Einarsson, 2008). Where the fissure swarms intersect this boundary are zones of volcanism characterized by eruptive vents and craters from the Holocene (Clifton and Schlische, 2003). Seismicity in the zone is predominantly strike slip in nature, most likely a product of the left lateral transform zone. Earthquake swarms are quite frequent in the area and occur approximately every 30 years with the most recent in the year 2000 (Einarsson, 2008). Eruptive episodes are frequent on a geologic timescale and occur approximately every 1000 years. During these episodes eruptions can be highly episodic over hundreds of years. The most recent event occurred between the 10th and 13th centuries and erupted several different lavas onto the peninsula (Jenness and Clifton, 2009).

Clifton and Kattenhorn (2006) present a detailed interpretation of the structures located on the Reykjanes Peninsula. They determine that the pattern of faults and fissures are highly influenced by the obliquity angle, proximity to volcanic centers, and stage of the tectono-magmatic cycle. This creates for a localized mix of strain rates and strain fields across the peninsula. The fault and fracture sets studied by Clifton and Kattenhorn (2006) can be related to unique stress fields characterized by their differing orientations (Fig. 1.4b). They conclude these stress fields sometimes overlap which can lead to a sinuous fault strike appearance. This apparent sinuosity of the fractures is actually two different fracture sets that were formed at different periods in time. As will be discussed below, these types of fractures and faults are observed in the Vogar fissure swarm.

### 1.3 Volcanic Systems of the Peninsula and the Krafla Rifting Event

Volcanic systems in Iceland are numerous and feature most known volcano types and eruptive styles. The location of the Reykjanes Peninsula on the intersection of a spreading plate boundary and mantle plume leads to increased levels of volcanic activity. Volcanism on the Reykjanes Peninsula is dominantly effusive as opposed to explosive, and lavas are mostly basalts with a minor component of dacites and ryholites

(Thordarson, 2007). During the last ice age hyaloclastic table mountains, hyaloclastic ridges, and pillow mounds formed through subglacial eruptions. Postglacial lava shields of tholeiitic basalt constituted the dominant type of volcanism in the early Holocene creating vast (12 $km^2$) pahoehoe lava flows (Jenness and Clifton, 2009; Thordarson, 2007). More recently fissure eruptions have been dominant, initiating from the four to five fissure swarms located on the Reykjanes Peninsula and producing mostly A'a type lava flows.

Fissure swarms on the peninsula are made up of normal faults, extensional fractures, and fractures which exhibit both vertical shear and extension. Eruptive fissures and vents are also common where the fissure swarm intersects the 2-5 km wide zone considered the active plate boundary. These fissure swarms stike at about 60°-70° across the peninsula (Clifton and Kattenhorn, 2006; Clifton and Schlische, 2003), are arranged approximately 5 km apart from each other, and each exhibit an asymmetric or half graben regional structure. The swarms initiate at the end of the Reykjanes Peninsula where the Reykjanes Ridge comes onshore and are arranged in a gradually northeast stepping en-echelon style. Each fissure swarm has its own magma supply, geothermal system, and area of maximum volcanic production (Gudmundsson, 1987; Clifton and Kattenhorn, 2006). It has been suggested by multiple sources that the faults and fractures observed at the surface are the result of dike injections at depth during eruptive episodes (Paquet et al., 2007; Tentler, 2005; Sonnette, 2010 ).

The mode of fracture and fault formation within the fissure swarms is an important and well studied subject. A model for the development of normal faults in the Central Rift Zone of Iceland was presented by Tentler (2005), and points to the variable stresses exerted by changes in magma supply. When pressure in the magma reservoir is significant enough, vertical mode I fractures are initiated at the interface of the magma and the brittle crust. The fractures propagate upwards, with $\sigma 3$ being negative. As the dike moves higher in the crust away from the pressurized magma chamber, the

horizontal force of the bedrock overcomes the vertical force of the dike and the dike stops propagating. However, the stresses from the extensional setting allow the fracture to continue propagation as a mode II fracture inclined normal fault. As this plane of failure approaches the surface, mode I vertical fractures form at the surface in response to the concentrated stress at the tip of the upwardly propagating fracture. The geometry of these fractures at the surface is most likely influenced by cooling patterns and structures of old lava flows in the shallow crust. The fractures probably propagate downwards and intersect the upwardly propagating mode II fracture. The surface will display varied throw along the length of the fault depending on the dike kinematics and any pre-existing structures that could influence the path of the fracture to the surface (Tentler, 2005; Jenness and Clifton, 2009).

Activation of a fissure swarm was well studied in the Krafla eruptive episode between 1974 and 1989, which is located in the Northern Volcanic Zone (NVZ) (Fig. 1.3). During this episode, magma rose up into the 3 km deep magma chamber of the central volcano causing inflation (Einarsson, 2008). Though inflation dominated the episode, it was interspersed with rapid deflation events. Deflation occurred when the walls of the chamber ruptured and magma was injected laterally as dikes into the adjacent fissure swarm. Early deflation events were associated with shallow movement of magma in the crust, but later deflation events became increasingly tied with fissure eruptions lasting between 5 and 14 days. Significant subsidence and movement along normal faults in the fissure swarm was recorded, and a maximum cumulative extension of 8-9 m was measured. This event affected an area about 90 km long on the plate boundary (Einarsson, 2008). The hypocenters that were related to the propagation of the dikes were between 1 and 4 km deep, and showed northward propagation of 30 km from the central magma source. Paquet et al. (2007) suggest that shallow magma chambers and lateral flow of magmas that are controlled by regional stresses are common in the upper crust of Iceland. Their 3-D model of a dike swarm with a central volcano provides a

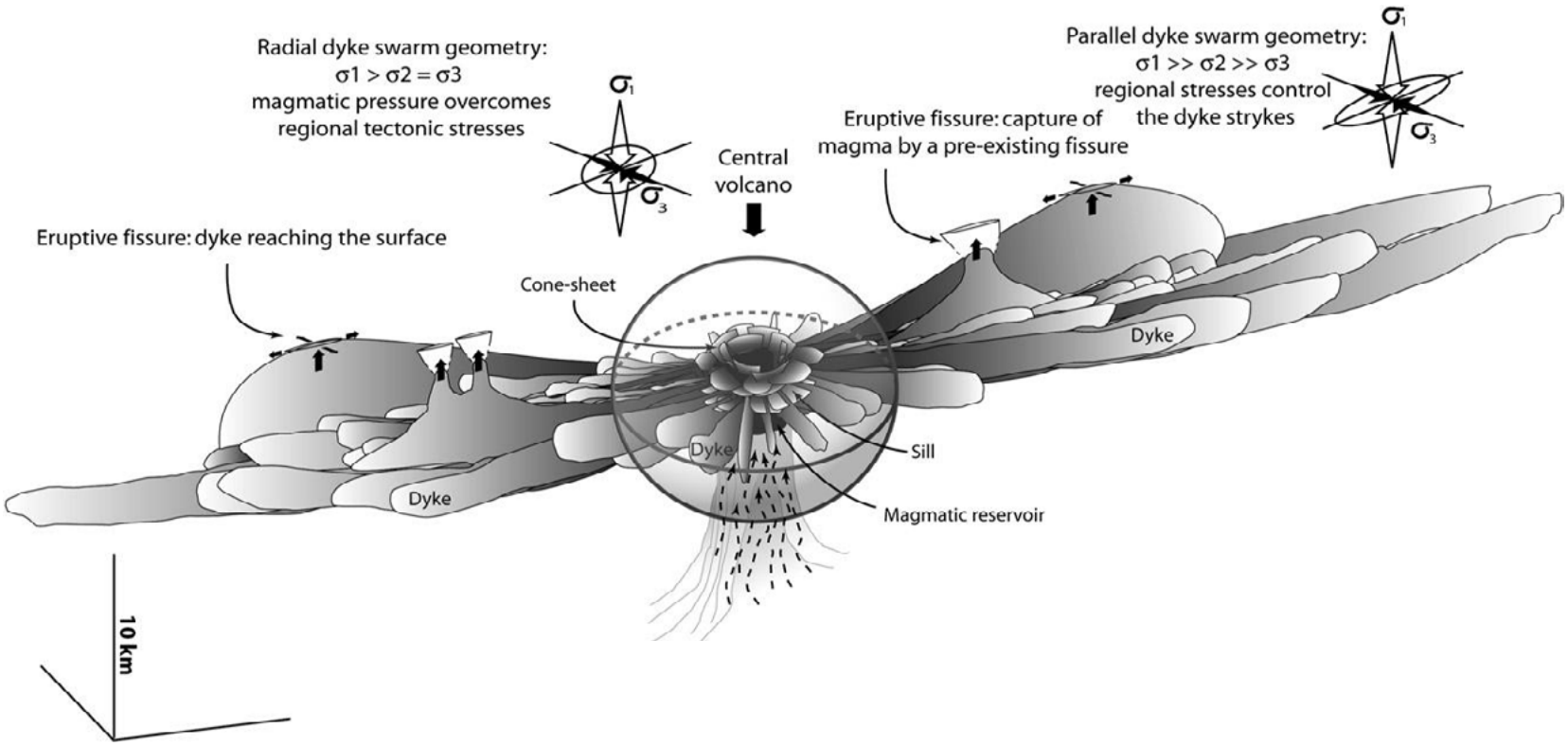


Figure 1.5 3D representation of a dike swarm in Iceland. Dikes are shown to radiate out laterally from a central reservoir or volcano. The strikes of the propagating dikes vary depending on the local stress conditions. Some dikes will propagate vertically to the surface, resulting in an eruptive fissure such as those seen during the Krafla rifting episode. $\sigma_3$ is the dominant stress of the region. (Modified from Paquet et al., 2007)

visual representation of this type of volcanic system. (Fig. 1.5).

It has been suggested by Hreinsdottir et al. (2001) and Einarsson (2008) that deformation on the peninsula occurs in two modes. The first is a dry mode when magma is not available and deformation occurs primarily along the north-south trending dextral strike slip faults. A wet mode is when magma is available and the peninsula is undergoing an eruptive episode. During these episodes the fissure swarms are activated, and deformation is primarily due to dikes propagating along the fissure swarms.

### 1.4 The Vogar Fissure Swarm

The Reykjanes fissure swarm is located on the southwestern end of the Reykjanes Peninsula (Fig. 1.4a). It is the first and the largest of a set of right stepping en echelon fissure swarms, with a length of 30 km and a maximum width of 7 km. These swarms are spaced about 5 km apart from each other across the peninsula (Clifton and Kattenhorn, 2006). This study focuses on an area in the northeastern section of the Reykjanes fissure swarm, just south of Vogar (Fig. 1.4b). The area is part of the Vogar fissure swarm (Grant and Kattenhorn, 2004), and consists of a highly asymmetric graben about 5 km wide made up of normal faults and fissures (Clifton and Schlische, 2003).

The Vogar fissure swarms lies predominately in basalt erupted from the Thrainsskjoldur shield volcano about 12,500 year ago (Fig. 1.6) (Saemundsson and Einarsson, 1980). The northernmost part of the graben reaches into supraglacial to interglacial lavas younger than .7 m.y. The southwest end of the graben has been covered by historical and Holocene fissure eruption lavas from the Eldvorp crater row. Jakobsson et al. (1977) group the extrusive rocks into picrite basalt shield lavas, olivine tholeiite shield lavas, and tholeiite fissure lavas. These are characterized by low concentrations of alkalies and high values of CaO. They also found there to be a chemical trend in the amount of $K_2O$ which increased from .02% to .24% over the last 12,000 years.

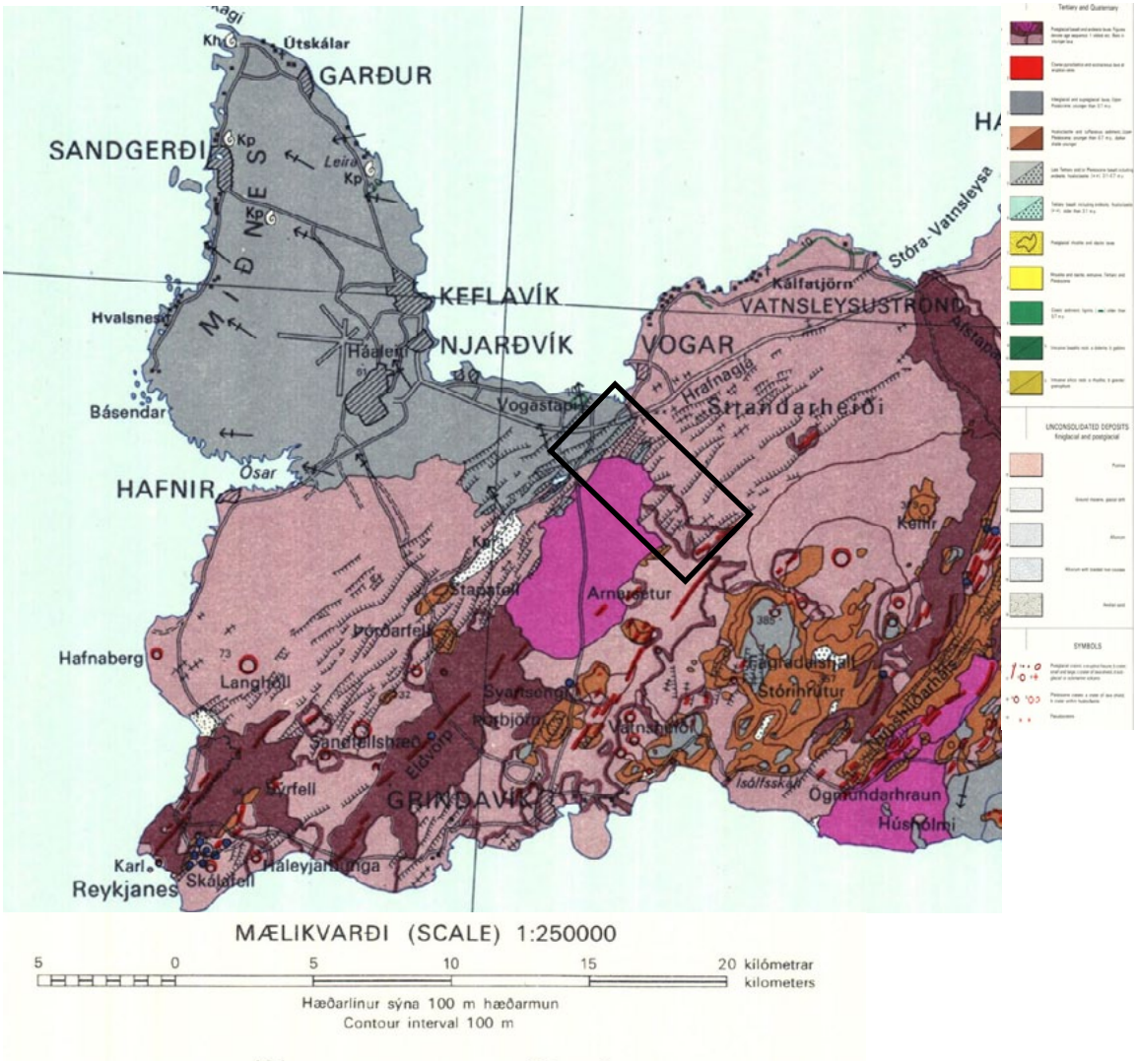


Figure 1.6 Map of the different bedrock units on the western half of the Reykjanes Peninsula. The black box outlines the study area. (Modified from Saemundsson and Einarsson, 1980)

The asymmetry of the graben can be seen in the vertical and horizontal sizes of each wall (Fig. 1.7). The northern graben wall is characterized by sub vertical normal faults, with the hanging walls on the south side of the fault. Most faults have throws greater than 10 m and are dipping to the southeast. On the southern graben wall, the normal faults are typically vertical with the hanging wall on the north side of the fault. These faults are characterized by less than 10 m of throw, and are more numerous than on the northern graben wall. The faults in this area are described as blocks that are tilted back towards the rift axis (Clifton and Schlishe, 2003). There are fault-bounded lakes in the lowest elevation region of the graben (Fig. 1.7).

The faults and fissures themselves are highly segmented, display curvilinear geometry and have a regular spacing between them (Grant and Kattenhorn, 2004). The fracture and fault segments are arranged in either a right stepping or left stepping en echelon pattern, and are rotated out of the general trend of the fault trace. Frequently the faults contain a fracture along some or all of their length. These vary in depth, but some can be as deep as 20 m or more. The fault surfaces exhibit no sign of slickenlines, and the exposed surface of the fault is easily weathered and eroded creating a rough uneven surface. The blocks that are eroded either build up at the base of the fault, or fall into the open fractures when they are present. Some faults exhibit a monocline at their base that follows the trace of the fault. The faults are mostly in the shield derived tholeiitic basalt, however a number of them are overflown by a historical A'a lava flow (Fig. 1.6).

There have been several recorded earthquake swarms along the plate boundary in the Reykjanes Peninsula, occurring on a cycle of about 30 years (Einarsson, 2008). Repeated precision leveling was done on an area of the Vogar graben in the Reykjanes Fissure swarm before and after an earthquake swarm that occurred in 1967 (Tryggvason, 1970). The data showed up to 8 mm of dip slip displacement on some of the faults that were measured. A fault further south in the Reykjanes fissure swarm also displayed dip

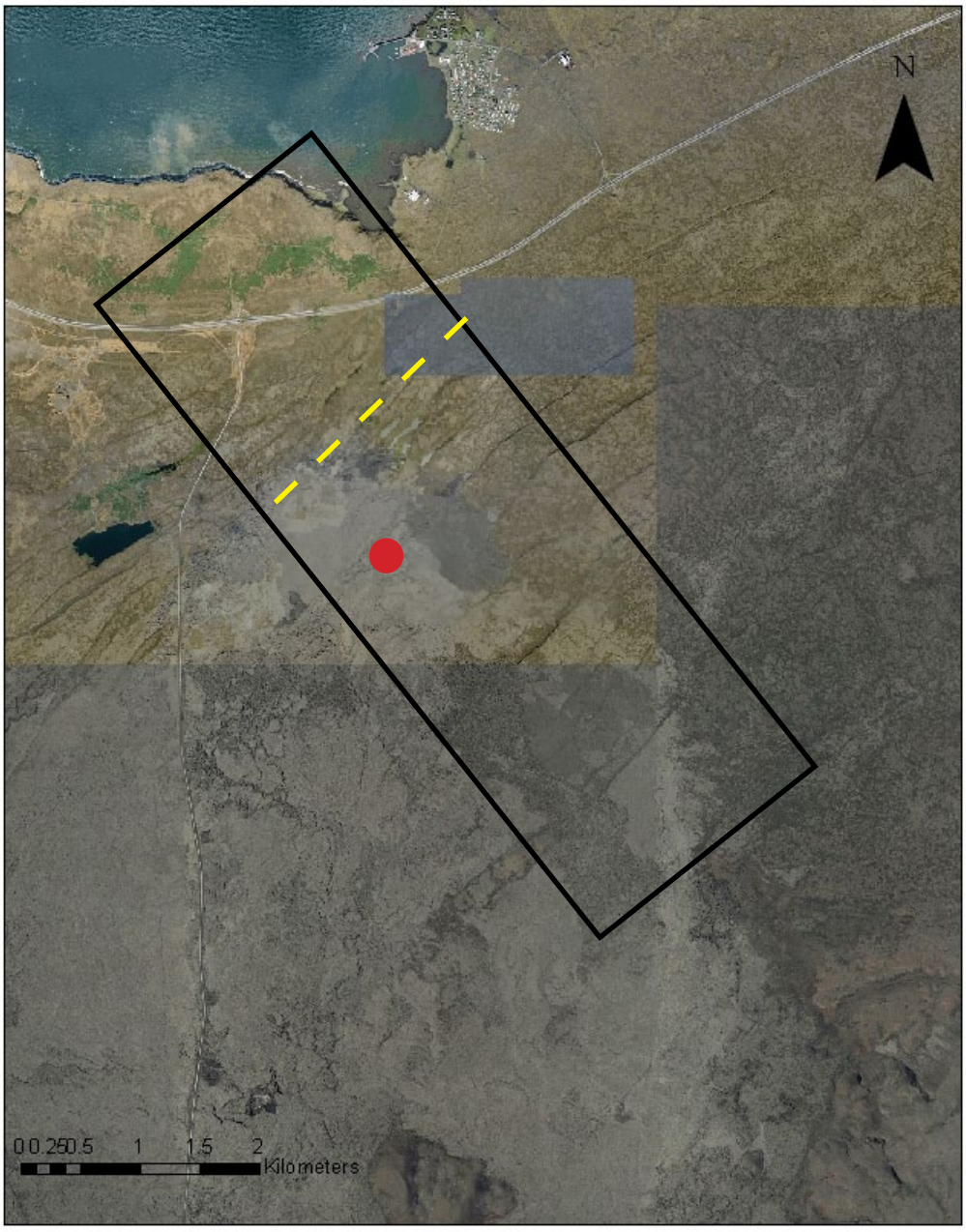


Figure 1.7 Aerial photograph of the Vogar fissure swarm with study area outlined by box. The dashed yellow line represents the bottom of the graben. Fault scarps are seen as the semi-linear lines striking approximately northeast. Historical lava flow is the darker gray unit identified by the red circle.

slip movement immediately after the same earthquake swarm. Clifton and Kattenhorn (2006) state that some faults in the Vogar graben displayed at least 3mm/yr of vertical displacement between 1966 and 2004.

### 1.5 Objectives of study

Iceland is located in an ideal location to study rift tectonics as influenced by a mantle plume. The associated structures that result from the different styles of rifting are varied and clearly exposed on the Reykjanes Peninsula. The peninsula is an oblique rift zone that is characterized by both volcanism and seismicity related to the active spreading. Fissure swarms made up of normal faults and fissures are prominent features on the peninsula, however their active deformation is not well understood. Previous work suggests that both seismic and aseismic stresses and events play roles in the deformation of the fissure swarms. This study constrains the timing of the movement and stresses acting on the Vogar fissure swarm, and provides a detailed descriptive and kinematic analysis of the graben. This was done by mapping fault scarp heights in lavas of different ages to evaluate their movement during the Holocene. These data constrain the overall structure and deformation of the graben. This information is helpful in preparing earthquake hazard assessments of the peninsula, as well as adding to the understanding of oblique rift tectonics.

# CHAPTER 2: METHODS

## 2.1 Field Methods

Field work for this study was carried out in May and June, 2010, with some follow up work done between the 14th and 24th of October. Two days of field work were performed at the start of the project under the supervision of professors Pall Einarsson and Dykstra Eusden. The majority of the remaining field work was carried out alone, but with constant communication with professor Einarsson. Aerial photographs with a resolution of approximately .5 m per pixel obtained from the Icelandic company Loftmyndir were used to make a field map of the lava flows, faults and fissures. A Trimble GPS unit was used to take two transects .5 km apart across the graben measuring lat, long and elevation coordinates. In addition to the transects eight fault scarps that cut the historical lava flow were mapped by walking along the hanging wall and foot wall in order to obtain the offset of the fault. The boundary of the historical lava flow was also traced using the Trimble. A Garmin eTrex Venture GPS was used to take waypoints at spots of interest, where fissures were measured, and to mark other lava flow contacts in the study area. This had a consistent uncertainty of ±3 m. Six hand samples were collected of different lava flow units in order to be cut into thin sections for microscope analysis. Using a Brunton, strike of the faults and fissures was recorded to the best field approximation, as the fault scarps were often made up of smaller segments that varied (± 10°) within the general strike of the whole fault. All faults were vertical, so dip was not recorded, but the up thrown and down thrown sides were observed and recorded.

## 2.2 Data Collection

The waypoints from the Garmin were downloaded using the DNR Garmin application available through the Minnesota Department of Natural Resources, and converted to a shapefile. The data from the Trimble was downloaded using GPS Pathfinder Office 3.1 software, differentially corrected to approximately one meter

accuracy, and then exported as shapefiles. Aerial photographs were obtained from the company Loftmyndir through the University of Iceland. ArcGIS v. 9.30 was used to generate maps of the faults, fissures, lava flows, and in conjunction with Microsoft Excel to build the along strike profiles of the scarps. Adobe Illustrator CS5 was used to construct the cross sections of the fissure swarm. Equal area plots using the strikes of the structures were made with Allmendinger's StereoWin v. 1.2.0 program. The rock samples collected were cut into blocks and sent to Spectrum Petrographics to be polished to 30 μm thick microprobe thin sections for transmitted light microscope and SEM-EDS anaylsis.

### 2.3 Thin Section Analysis

An Olympus microscope was used to examine the thin section under single and cross polarized light. An Olympus camera was used to take photomicrographs of the thin section at various levels of magnification. After preliminary mineral identification and textural analysis, certain mineral assemblages on the sections were examined with a JEOL JSM 6100 digital SEM using a Kevex EDS. Areas of interest were marked with aluminum tape on each slide, and photomicrographs were taken to use as a map to find minerals under the SEM. Samples were carbon coated using a Denton Vacuum DV-401 before each analysis was run. In each sample, two spectra were taken from three different grains of olivine and plagioclase, for a total of 12 spectra per slide. An analysis with SPI standards of olivine and plagioclase was done to get relative amounts of their chemical constituents. These were run using an accelerating voltage of 20 kev, a working distance of 39, a deadtime of around 25, and an acquisition time of 100 seconds. The oxide weight percentages and numbers of cations were then calculated using a ZAF analysis and compared against each other.

### 2.4 Map Generation

A map of the different lava flows was generated by using aerial photographs,

and these boundaries were then confirmed in the field. Faults and fissures were also traced using the aerial photographs, and field checked using GPS locations to confirm the existence of the different features. Strikes from measurements of the faults and fissures were put on the map using the advanced rotate tool in ArcMap symbology. Topographic profiles for the two cross sections across the Vogar fissure swarm were created by rendering the Trimble GPS point data from the transects into a line file, and then splitting the line at the vertices. Before this was done clumps of data points in one area, where the Trimble GPS had stopped moving but continued to take data, were removed to get continuous data across the swarm. Using the split line file, the distance between each point was calculated. A graph was created in Excel with the y-axis being the z coordinate or height of each point, and the x-axis defining the distance from the starting point. To illustrate both the shallow and deeper geologic subsurface, a verticall exaggerated 1:15 scale profile and a 1:1 scale profile, respectively, were made in Excel. The 1:1 profile was then imported into Adobe Illustrator and a cross section of the faults down to 5 km in the crust was created. A section showing details of the flows to a depth of 250 m and how they are cut by the faults was created using the 1:15 profile.

Six profiles of the fault scarps were created by using the continuous Trimble GPS point measurements taken while walking along the bottom and top of the scarp. Four profiles were taken of the faults that the historical lava had over flown, to see if they could continue to be traced into it, and two profiles of faults that had not been over flown were taken for comparison. This data was input into ArcMap as a set of points. Points that were clustered together, at the same latitude, or at a lower latitude than the previous point were deleted so that a continuous line of points was made along the top and bottom of the scarp. X Tools Pro was then used to convert the points into a polyline. The polyline was split at its vertices (the points) to form line segments, and the length of each segment was calculated. This was imported into Excel where all the line segment lengths were added to get the total length of the scarp. Each line segment correlated to two

points, one on the bottom of the scarp and one on the top (Fig. 2.1). The bottom Z value was subtracted from the top Z value to give the height of the scarp at that specific point. This was graphed, with the distance of the line segments on the x-axis and the height of the scarp on the y-axis, to give an along strike profile of the fault.

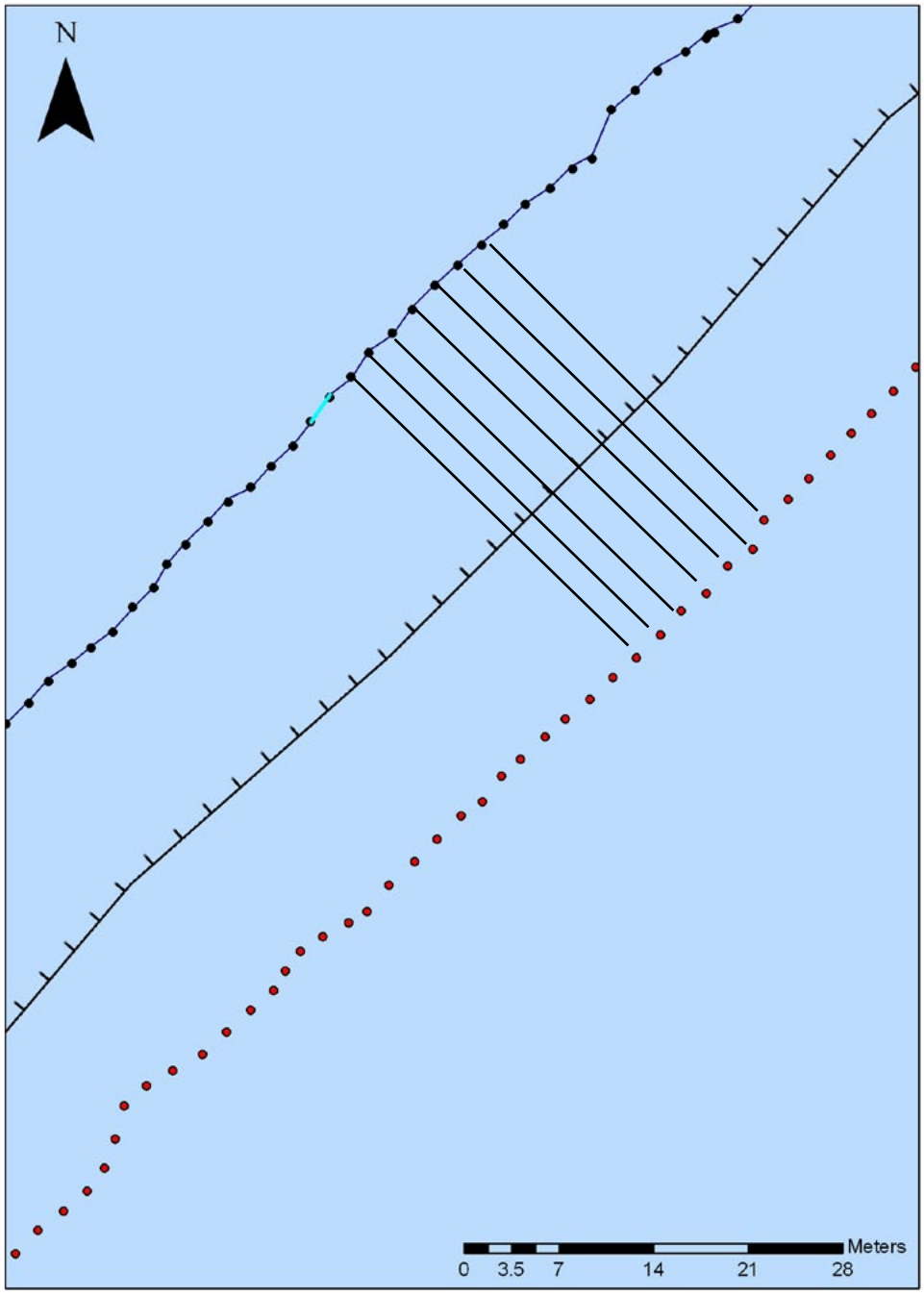


Figure 2.1 Method for creating the scarp profiles. Black dots are GPS points along the hanging wall, and red dots mark the footwall. Distances between the dots (light blue line) were added to get the total length of the scarp profile (dark blue line). This length was plotted against the difference in heights of corresponding points, marked by the black lines, to get the height profile of the scarp.

# CHAPTER 3: RESULTS

## 3.1 Overview and General Observations

### *3.1.1 Overview of Results*

Field results focused largely on observing the faults, fissures, and flows, and their relative attributes such as height, length, area, strike, dip, and relative relationships in the field. Larger scale characteristics of the overall graben were also observed and GPS data was used to create profiles of the scarps, as well as a cross section of the graben. Thin sections were created from samples collected from different lava flows in the field, and were analyzed to determine their optical properties and mineralogical constituents to compliment the other data.

### *3.1.2 Flows*

Fieldwork was carried out across a 7 km x 3 km swath of the Vogar graben, which included lava flows, faults, and fissures of varying sizes and geometries (Fig. 3.1a). Within the boundary of the study area, eight different lava flows were identified through field observation and aerial photographs, and are shown in Figure 3.1b. Each lava flow will be discussed from oldest to youngest below. Supraglacial lava covers 5.6 $km^2$ of the field area and is found mostly in the northwestern section, with some comprising the small mountain Litla Skógfell in the southern half of the area (Fig. 3.1b). It is bounded by a 20 m high, and a 3 km long scarp (E on Fig. 3.1a) which separates it from a pahoehoe lava flow (Fig. 3.2a). This ~12,000 year old pahoehoe lava covers the largest area of 11.2 $km^2$, was erupted from the lava shield Thráinsskjaldarhraun, and flowed from south to north in the field area (Fig. 3.1b) (Saemundsson and Einarsson, 1980). On top of the shield lava is an A'a fissure lava, referred to as the first fissure lava, which has an area of 2.7 $km^2$ and a flow direction of west to east (Fig. 3.1b). The first fissure lava has a small volume lava channel flow on top of it, which flowed northwest over fault P,

and had the smallest area of .2 $km^2$ (Fig. 3.1b). The first fissure lava is also covered by another A'a fissure flow, referred to as the second fissure lava. The second fissure lava has an area of 1.7 $km^2$ and flowed from west to east into the field area. This is covered by the northern edge of the ~2,000 year old Sundhnukur A'A lava flow, which is also on top of the first fissure flow (Fig. 3.1b). The Sundhnukur flow covers an area of .3 $km^2$ and flowed from southwest to northeast into the southern edge of the field area (Fig. 3.1b). An unknown A'a lava exists on either side of the mountain Litla Skógfell, is underneath the second fissure flow lava, and covers an area of .6 $km^2$ (Fig. 3.1b). The 800-1100 year old historical A'a lava flow, labeled New Lava in Figure 3.1b, is the youngest, and is on top of the shield, first fissure, second fissure, and unknown lava flows (Fig. 3.2b). It covers 3.8 $km^2$ and flowed from southwest to northeast into the field area. It is bounded to the north by fault scarp F (Fig. 3.1a) and to the south by Litla Skógfell (Fig. 3.1b).

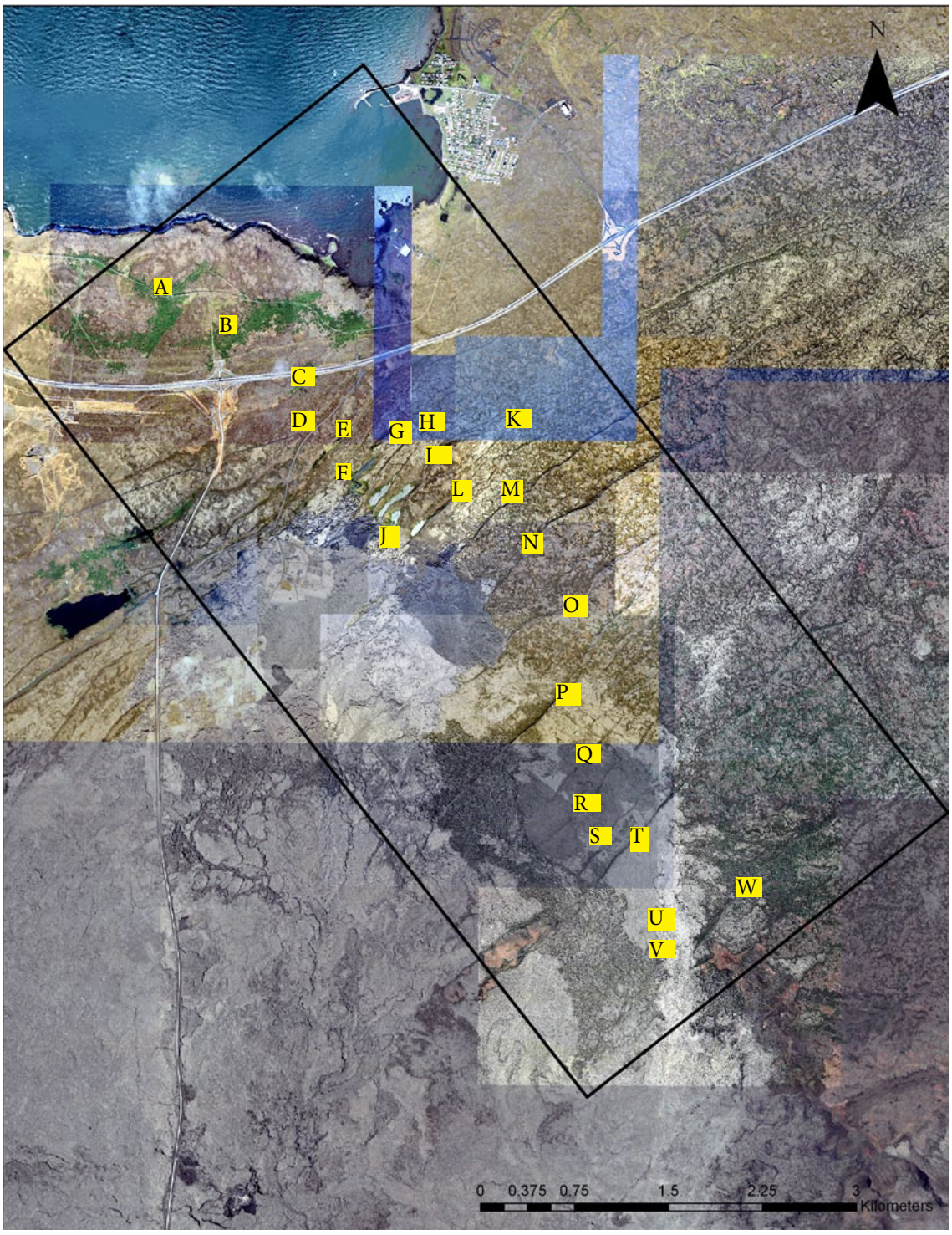


Figure 3.1 A) 1:35,000 scale aerial photograph of the Vogar graben with the study area outlined in black. The town of Vogar is seen at the top center of the image. The labels are faults corresponding with 1b.

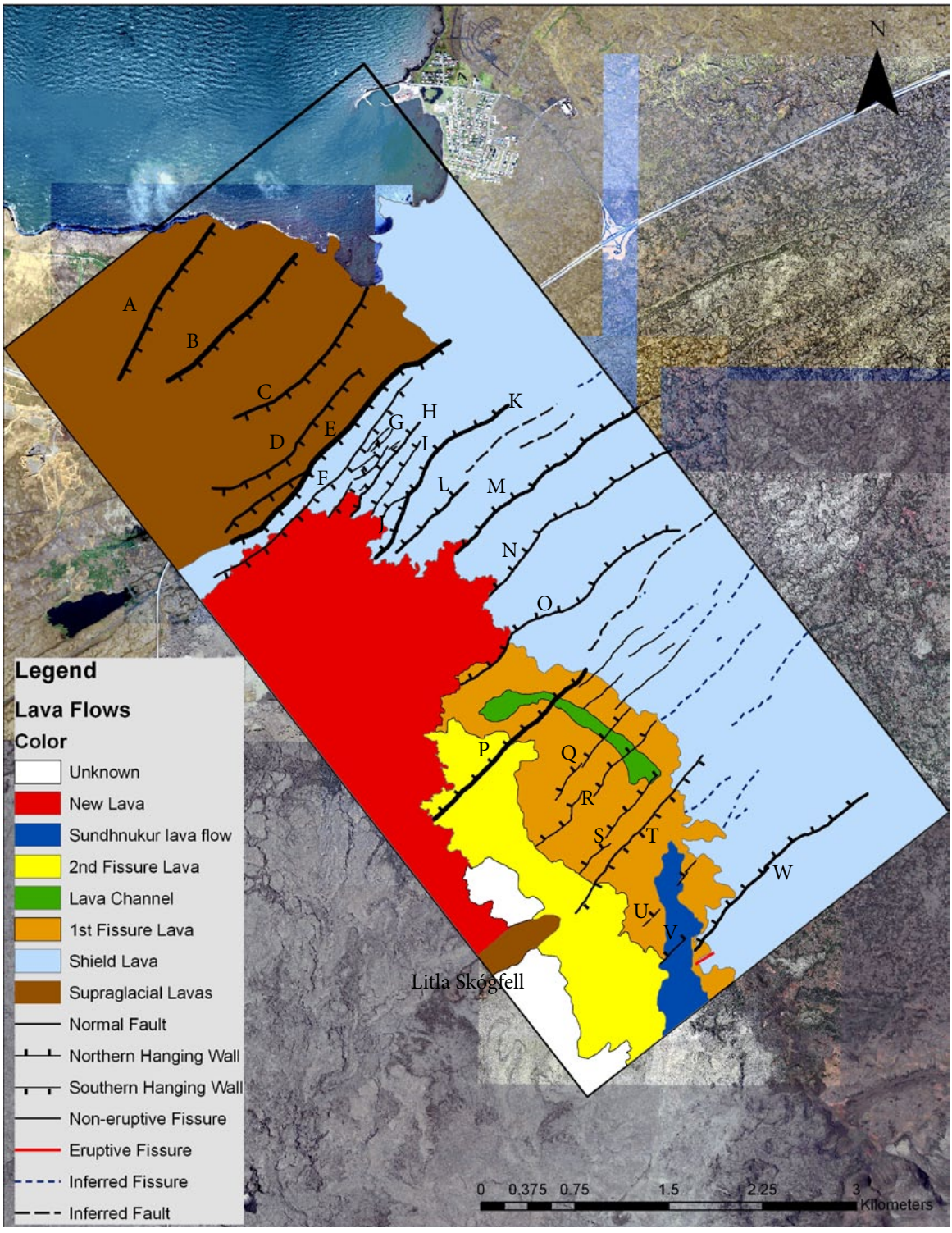


B) Map depicting all the lava flows, faults, and fissures observed in the field area, with the faults labeled. The thickness of the fault lines refelects their relative throw, with the thinnest corresponding to 2 m and the thickest 20 m. Scale is 1:35,000. The letters indicate specific faults.

A

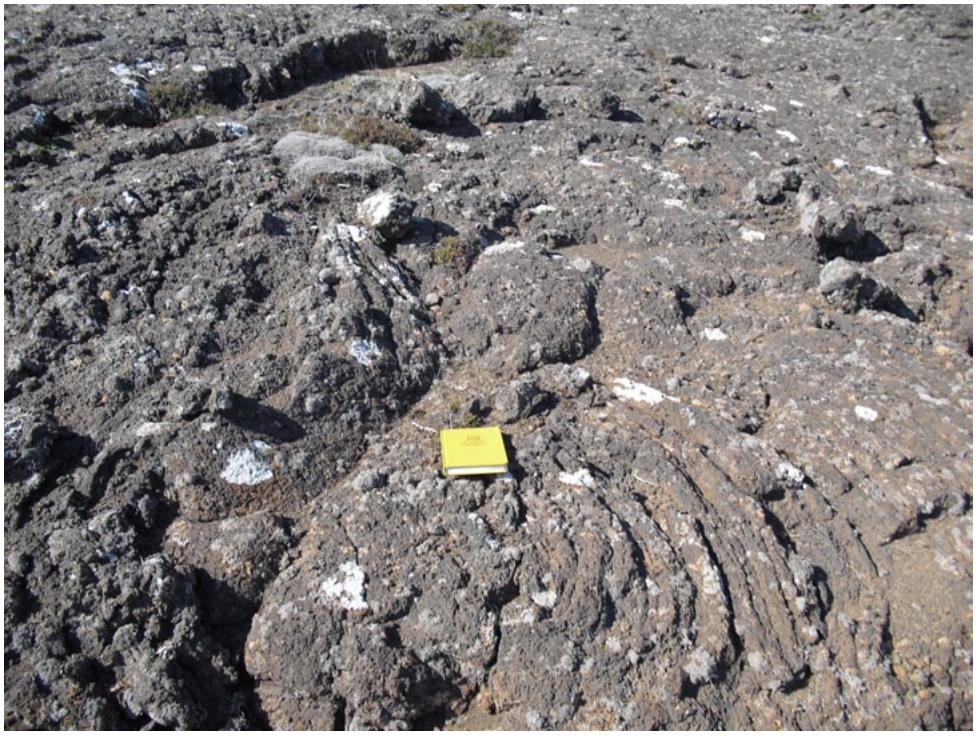

B

Figure 3.2 Examples of pahoehoe and A'a lava flows seen in field. A) 18,000 year old Thráinsskjaldarhraun pahoehoe shield basalt. B) Front of the 800-1100 year old historical lava flow on top of the Thráinsskjaldarhraun shield basalt. Scarp F bounds it on the right.

### *3.1.3 General Observations of the Graben*

The overall graben shape is highly asymmetric, with the northern half being 2 km wide as measured from the graben lowpoint (assumed to be the center), and the southern half being 5 km wide (Fig. 3.3) as measured similarly. The faults show the most offset in the shield and supraglacial lavas (Fig. 3.1b). The historical flow covers the fault scarps in the shield lava, and no offset is apparent along strike of the faults in the historical lava (Fig. 3.1b). The center of the graben contains a series of five lakes in successive order that are bounded by a fault scarp and an apparent dipping block (Fig. 3.4). These faults are labeled H, I, J, K, and L in Figure 3.1a. A fundamental change in fault hanging wall orientation also defines the structural center of the graben. The faults in the northern half of the graben have hanging walls on the southern side, while the faults in the southern half have all their hanging walls on the northern side, except for fault T which has its hanging wall on the southern side (Fig. 3.5). This scarp runs into the southern side of the 300 m high mountain Litla Skógfell (Fig. 3.1b). One kilometer south of fault T is the final fault scarp W that bounds the Vogar graben. The strikes of 66 faults and fissures were measured and fell mostly between 30° and 50° (Fig. 3.6).

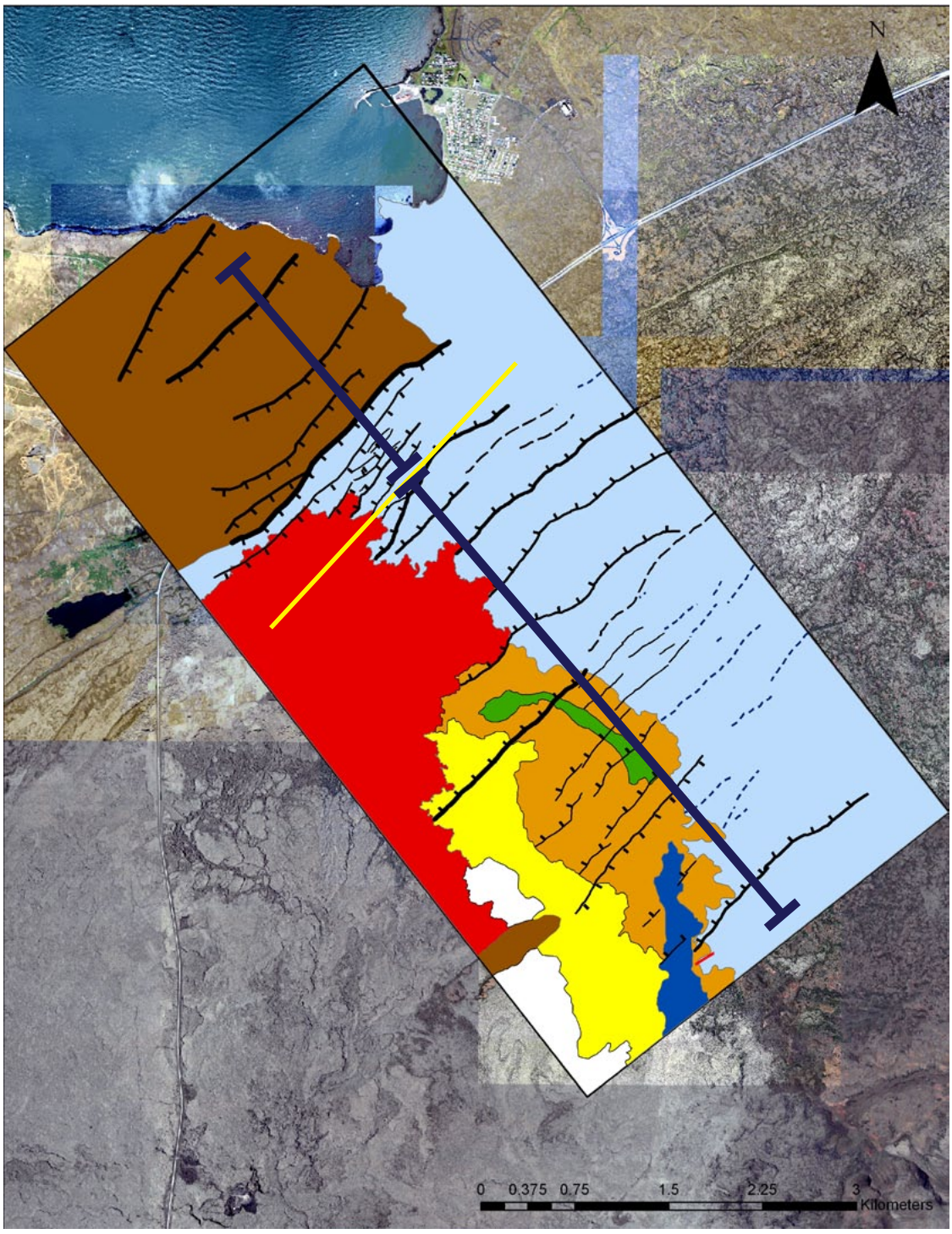


Figure 3.3 Map showing the faults and flows and size of the graben walls. The yellow line traces the lowest measured point of the graben. The two dark blue lines trace the distance from the bottom of the graben to its bounding faults. The northern half is 2 km and the southern half 5 km. Legend for the figure is the same as Figure 1b.

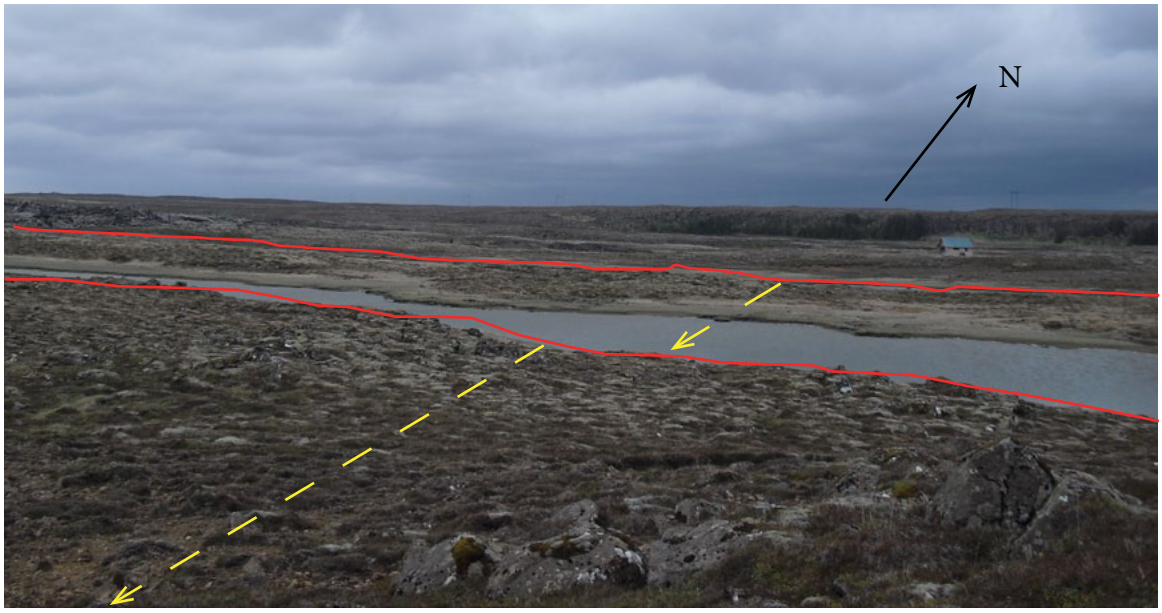


Figure 3.4 Photograph taken from the top of scarp K near the center of the graben. The yellow lines depict the observed dipping blocks bounded by the fault scarps and the red lines indicate the tops of the scarps. The house in the background is about 5 meters for scale.

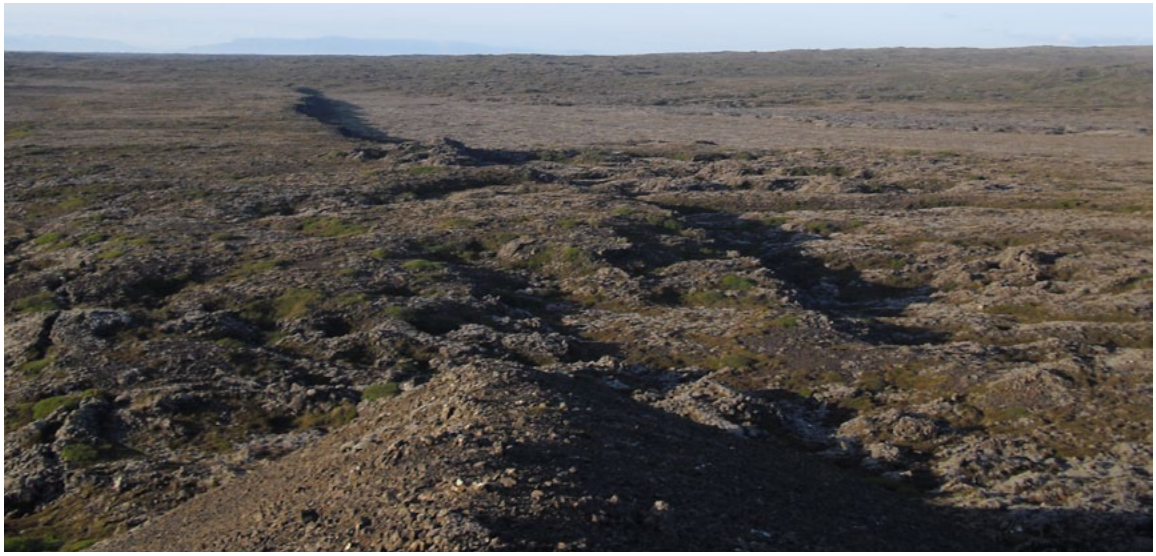

Figure 3.5 Photograph of the observed opposite dipping scarp (T) looking northeast from the mountain Litla Skógfell. The summit of Thráinsskjaldarhraun, the lava shield, is located just out of view at the top right of the photo.

A

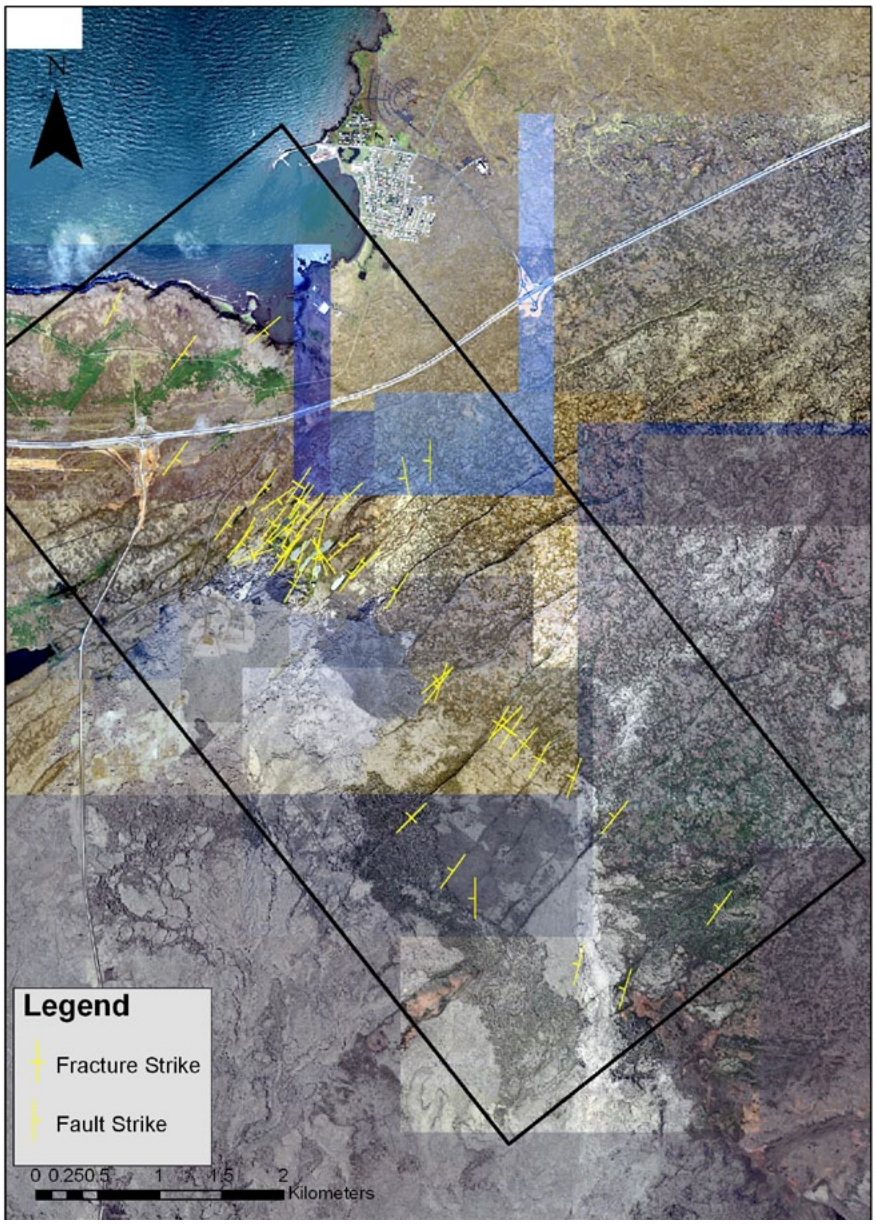


B

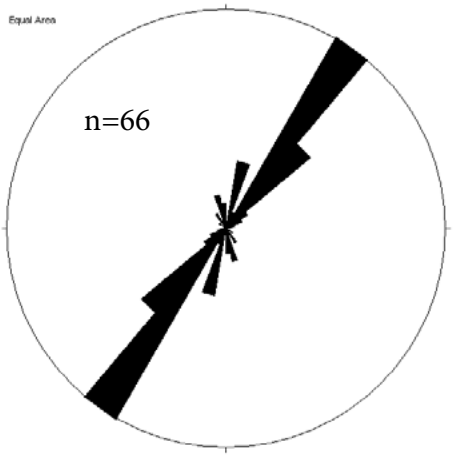


Figure 3.6 A) Strikes of fractures and faults taken in the field and put onto an aerial photograph of the area. B) Rose plot of the strikes of the faults and fissures put into 10 ° bins. Mean direction is N41 °E.

## 3.2 Structures

### *3.2.1 Faults*

Twenty five fault scarps were identified in the 7x3 km field area. The length of the faults varies from .5 km to 2 km, with most faults falling in the range between 1 and 2 km. The faults are not linear but often display a sinuous tendency, which is apparent in the aerial photographs (Fig. 3.1a). Vertical offset along the faults ranges from 2 m up to 20 m, with the northern part of the graben containing faults with the largest offsets (Fig. 3.1b). Of the seven faults that make up the northern wall, five have throws greater than 10 m along them. All the faults are assumed to be dipping at 90° (Fig. 3.7). The basalt that makes up the scarp surface is easily eroded which makes accurate field measurements of the dip hard to take. It has been well documented that these faults are almost always vertical at the surface, therefore this is the assumption that is made when analyzing the data for this study (Grant and Kattenhorn 2004, Tentler 2005). The faults are made up of both left stepping and right stepping en echelon segments that are rotated out of the general trend of the faults (Fig. 3.8). Strikes that were taken of these segments varied from 10° up to 90° from the general trend.

Some of the faults that are over flown by the historical lava appear to have a change in offset along the fault in the historical lava (Fig. 3.9a). There is typically a fissure or crack in the historical lava along strike of these faults, which range from .5 m to 1 m wide and 1-2 m deep. The historical lava also appears to pile up much higher along the hanging wall side than on the footwall side (Fig. 3.9b).

Figure 3.7 Picture of fault P, representing a typical vertical scarp seen in the field. Field notebook for scale.

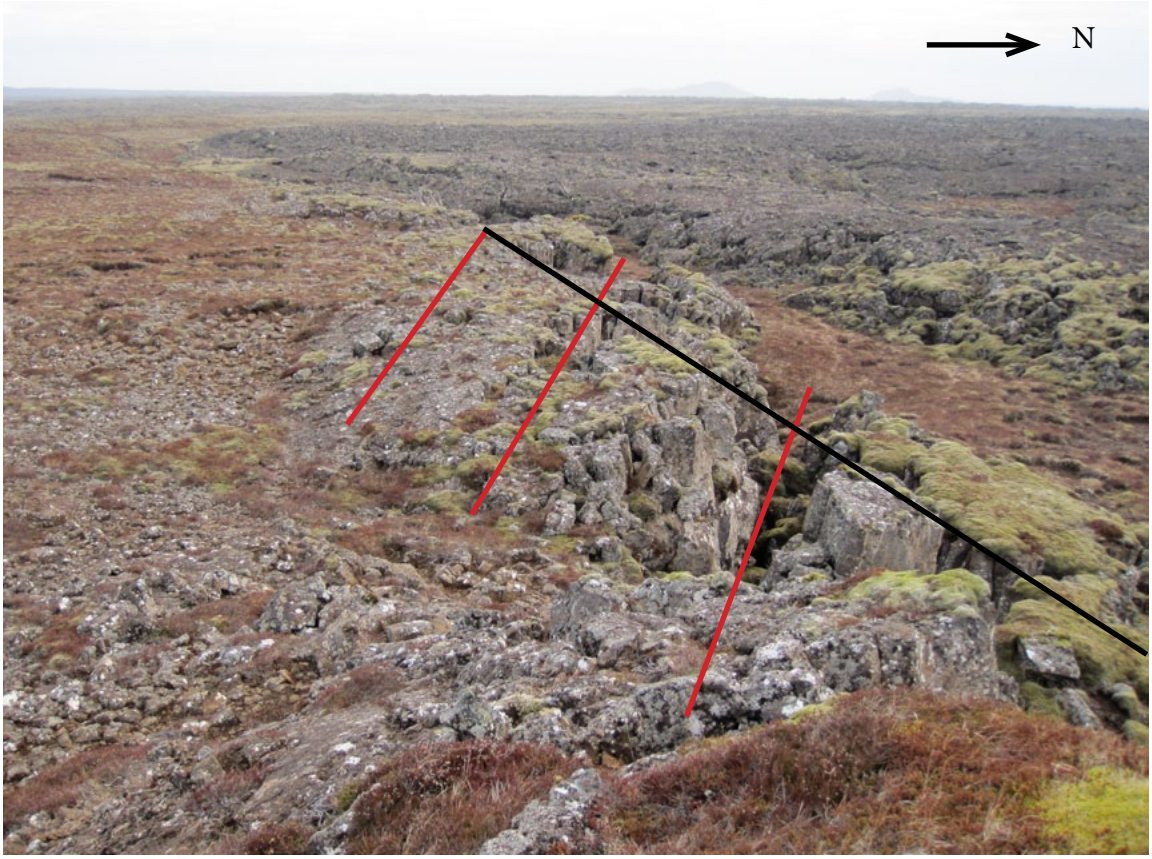


Figure 3.8 Figure showing an example of left stepping en echelon segments that are seen within fault scarp O. The black line indicates the general trend of the scarp and the red lines indicate the segments.

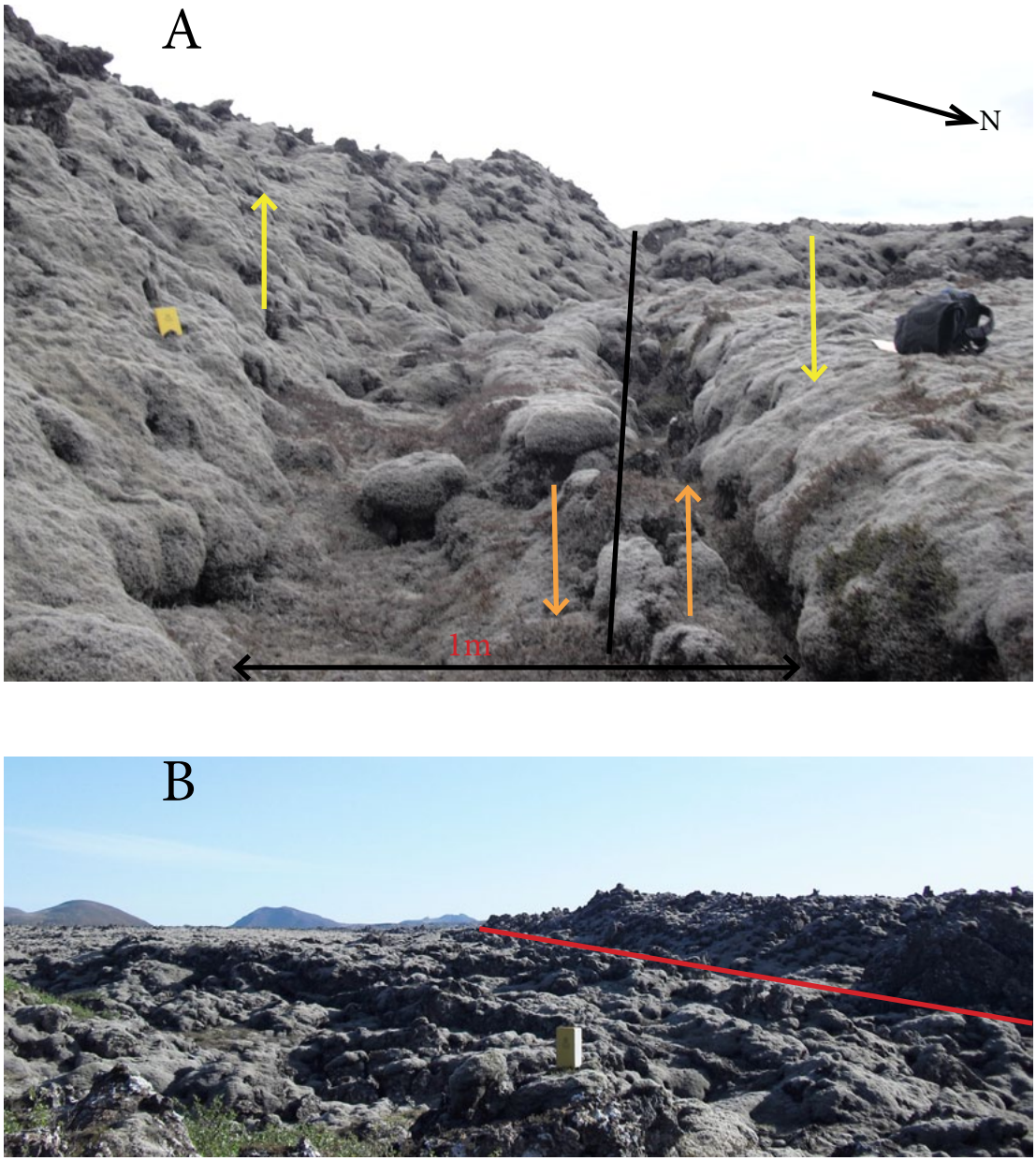


Figure 3.9 Structures seen along strike of faults in the historical lava. A) Apparent change in offset is observed along strike of fault F. The black line indicates the strike of the fault and the orange arrows indicate the upthrown and downthrown sides of the fault before it enters the historical lava. The yellow arrows indicate the observed upthrown and downthrown sides in the historical lava, which have apparently changed. B) Pile up of historical lava seen along strike (red line) of fault P. The elevated historical lava is on the hanging wall side of the fault, and the non elevated historical lava is on the footwall side of the fault.

The following paragraphs will give an individual description of each scarp. Fault scarp A is the northernmost scarp and extends for about 1.5 km with a throw around 18 m (Fig. 3.1b). The scarp displays significant erosion, that makes it appear to have a non vertical dip, and the hanging wall is on the southern side. Scarp B is about 500 m southeast of scarp A and is 2.5 km long (Fig. 3.1b). Throw along the fault reaches up to 15 m, the hanging wall is on the southern side, and has undergone significant erosion. The eroded scarp C is 700 m southeast of B, 1.5 km long, and has a throw of around 10 m with its hanging wall to the south (Fig. 3.1b). Scarp D is 350 m southeast of C and is 1.5 km long with a hanging wall on its southern side and up to 10 m of throw (Fig. 3.1b). It has also undergone significant erosion. Scarp E is 300 m southwest of D, and is one of the longest with a length of 2.3 km long (Fig. 3.1b). The throw along the scarp is 20 m which is the greatest throw seen in the field, and the hanging wall is on the southern side (Fig. 3.10). The scarp is vertical, and does not exhibit the tectonic weathering that is seen in the previous faults. Scarp F is 200 m south of E, and bounds the historical lava flow on the northern end (Fig. 3.1b). It has a maximum throw of 5 m, is 2.25 km long, and has its hanging wall on the southern side. The base of the fault also has a small pond along it adjacent to the front of the historical lava flow. There is what appears to be a change in offset in small lobes of historical lava that have overflowed the scarp (Fig. 3.9a). Several scarps labeled G are small and collectively define the bottom of the graben (Fig. 3.1b). The northern bounding scarps have their hanging walls on the southern side, and the southern bounding scarps have their hanging walls on the northern side. Maximum throw (that can be seen above water) is 3 m seen on the northern bounding scarp. This scarp also terminates in a fissure approximately 15 m long (Fig. 3.11).


Figure 3.10 Photograph of fault E, with backpack for scale, showing vertical 20m high scarp. Scarp is made up of supraglacial basalt while the hanging wall is comprised of shield lava.

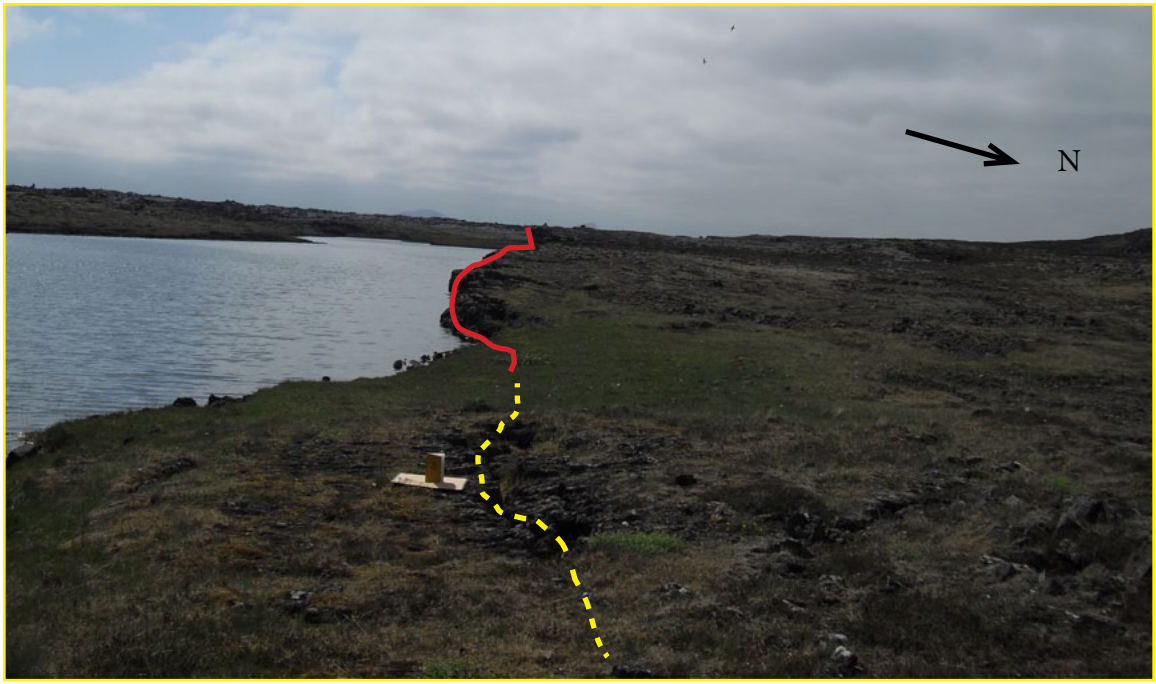


Figure 3.11 Photograph of the bottom of the graben showing lake bounded by two faults. The fault in the center of the picture (red) terminates in a fissure (yellow) which is seen next to the field notebook.

Scarp H is located 50 m from the southernmost scarp of G, and is 1 km long (Fig. 3.1b). It has a maximum throw of approximately 3 m and the hanging wall is on its northern side. It strikes into the historical lava, but no offset in the historical lava is seen. 70 m before the scarp reaches the historical lava the scarp turns into a fissure that is >5 m deep and filled with water. The historical lava runs along the scarp and into a small lake that it bounds. Scarp I is located about 140 m southeast of H, is 700 m long and has its hanging wall on the northern side (Fig. 3.1b). It has a maximum throw of approximately 3 m and terminates with a fissure ~25 m long at its northern end. Scarp J is 100 m southwest of scarp I and is partially covered by the historical lava to its south (Fig. 3.1b). It terminates at scarp K to its north, and there is a lake that runs along its base (Fig. 3.1a). It has a maximum throw of 5 m, is 150 m long, and has its hanging wall on the northern side. In the historical lava there is ~6 m of raised topography along strike of the fault in the shield lava on what would be the hanging wall of the fault (Fig. 3.12). Fault K is 1.6 km, has a maximum throw of 14 m, and has its hanging wall on its northern side (Fig. 3.1b). On the southwestern end there is a small lake that it bounds with scarp J. After the intersection between the two faults another pond is seen present along the hanging wall of the fault (Fig. 3.1a). Fault L is 250 m southeast of K and is the last fault to have a lake along its base. The fault is 800m long, has a maximum throw of 8m, and has its hanging wall on the northern side. Fault M is 400 m southeast of L and is partially covered by the historical lava flow (Fig. 3.1b). It is over 3 km long, extending out of the study area, and has a maximum measured throw of 9 m with the hanging wall on the northern side. The historical lava completely covers an unknown portion of the fault, and then after the footwall becomes exposed, extends for 200 m against the scarp along the hanging wall (Fig. 3.1b). No offset is observed where the historical lava completely covers the fault. Fault N is 400 m southeast of M and is covered by the historical lava flow (Fig. 3.1b). It is also over 3 km long, extending out of the study area, and has a maximum measured throw of 6 m with the hanging wall on the northern side. 50 m before the fault enters the

historical lava flow offset ceases and the fault turns into a fissure (Fig. 3.1b). There is also an apparent monocline that is seen at the base, and like in fault M, the historical lava follows the base of the fault for ~150 m (Fig. 3.13).

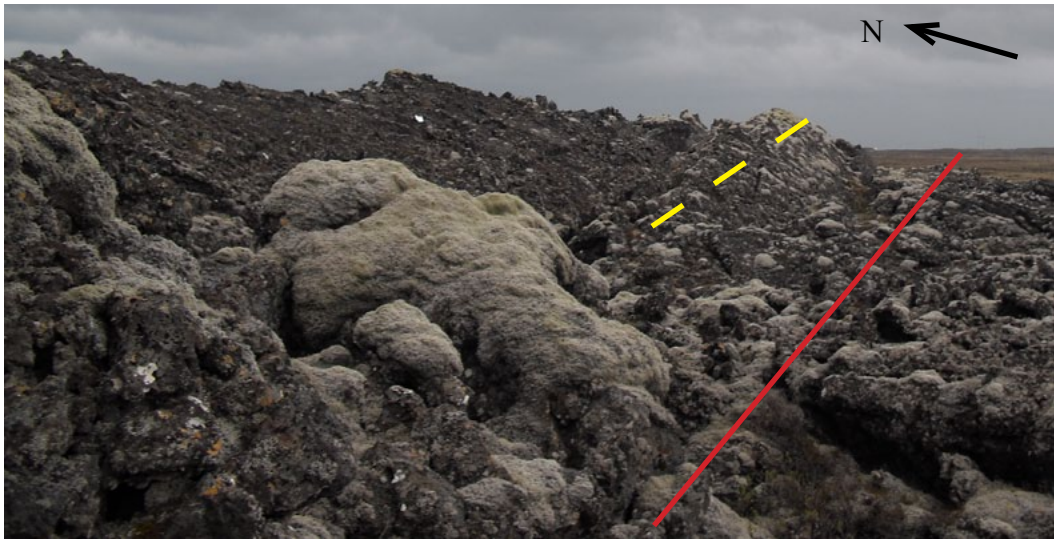


Figure 3.12 Photograph in historical lava of strucure that parallels the strike of fault J. The lava appears to pile up alongside strike identified by the red line. The yellow line indicates a fissure or crack in the lava.

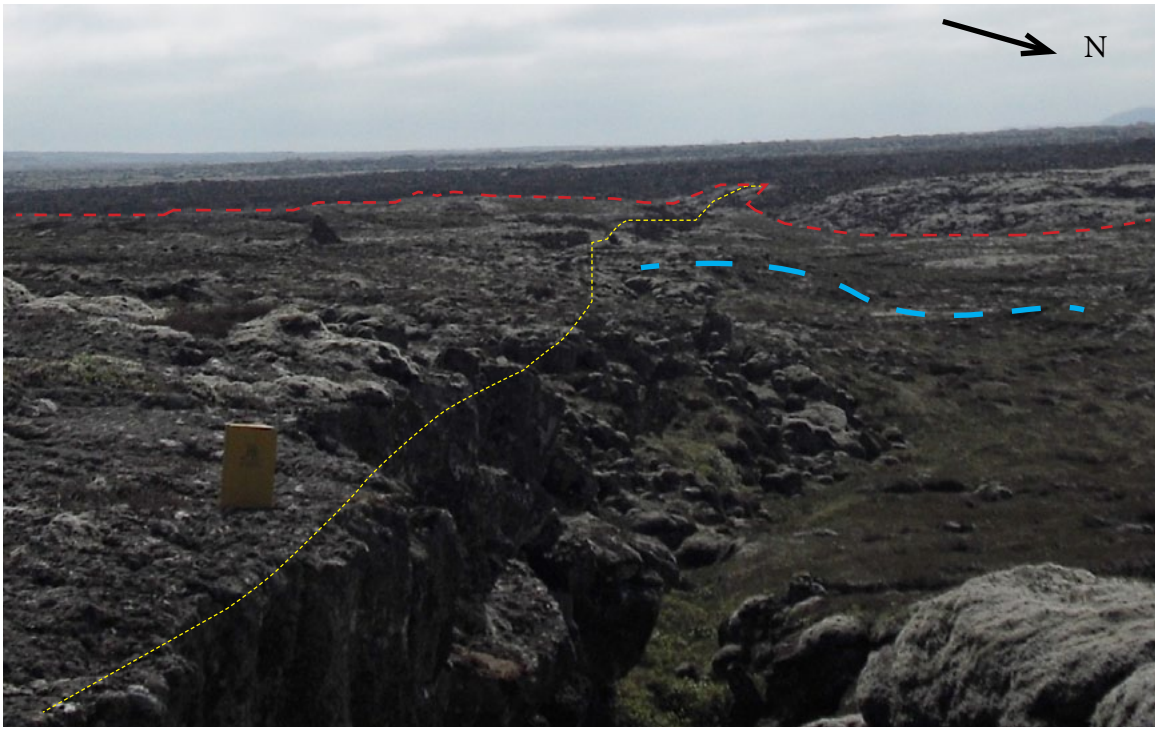


Figure 3.13 Photograph looking down fault N (yellow line) into the historic lava (red line). You can see the historic flow running along a segment of the hanging wall parallel to the scarp. The blue line shows the observed monocline at the base of the fault. In the foreground significant erosion is evidenced by the basalt blocks at the base of the scarp.

Faults O through W all cut more than one flow. In the field there was no significant variance in the throws between the different flows. Fault O is 500 m southeast of fault N, 2 km long, and has a maximum measured throw of 5 m (Fig. 3.1b). It is not covered by the historical lava flow, but does bound it at its southwestern end. There are multiple fissures or openings in the base of the scarp, with the deepest one >10 m. Fault P is 500 m southeast of O, is 2 km long, and displays a maximum throw of 15 m with its hanging wall on the northern side (Fig. 3.1b). It cuts through the shield, lava channel, first fissure, and second fissure flows. Throw is smallest in the shield lava and largest in the second fissure lava. In the historical lava there appears to be raised topography along strike of the fault (Fig. 3.9b). The fault frequently displays fracture openings along its crest, with one fracture extending from the northeastern termination 500 m down strike. The fractures are typically 1-2 m wide and are in some cases greater than 15 m deep. A monocline also exists at the northeastern end of the fault. Fault Q is 500 m southeast of P, 1 km long, and has a maximum throw of 2 m (Fig. 3.1b). It cuts the channel lava, and first fissure flow, and has its hanging wall on the northern side. Fault R is 225 m southeast of Q, is 1.3 km long, and has a maximum throw of 2 m with the hanging wall on the northern side (Fig. 3.1b). It cuts the channel lava and first fissure flow, and terminates at the contact with the second fissure lava. Fault S is 300 m southeast of R, 1 km long, and displays a maximum throw of 2 m with its hanging wall on its northern side. It cuts the lava channel and first fissure lavas and terminates at the contact of the second fissure lava. Fault T is 125 m southeast of S, is 1.3 km long extending out of the study area, and has a maximum throw of 4 m with the hanging wall on its southern side (Fig. 3.1b) (Fig. 3.5). Fault U is 500 m southeast of T, 500 m long, and has a maximum throw of 2 m with the hanging wall on the northern side (Fig. 3.1b). It is covered in its middle by the Sundhnukur lava, which does not appear to be cut by the fault. Fault V is 300 m south of U, 300 m long, and shows a maximum offset of 2 m with the hanging wall on the

northern side (Fig. 3.1b). The fault does appear to cut the Sundhnukur lava flow as well as the first fissure lava. Fault W is the final fault of the graben, and is 125 m southeast of V (Fig. 3.1b). The fault is 2 km long, has a maximum throw of 6 m, and cuts the shield lava and first fissure lava.

Profiles along two scarps (K and L) not in contact with the historical lava flow, and four fault scarps that are completely covered by the historical lava (J, M, N, P) were constructed using high resolution GPS data. Figure 3.14 shows the faults that are not over flown by the historical lava, with these profiles covering the length of the entire scarp. Scarp K has a maximum throw of 14 m, and a minimum of -2 m (Fig. 3.14a). Negative throws indicate that the footwall has dipped below the hanging wall, and this occurred on either end of the fault. This would seem to imply a reversal of slip. Scarp L also has an overall curved profile, with the highest points in the center and lowest points at its ends (Fig. 3.14b). L has a maximum throw of about 8 m and a minimum of -2 m. The minimum occurs at the end of the profile. For both scarps K and L, the overall throw pattern of the fault profile is systematically variable, with the maximum throw in the center of the scarp and the minimum throw at the scarp terminations.

A

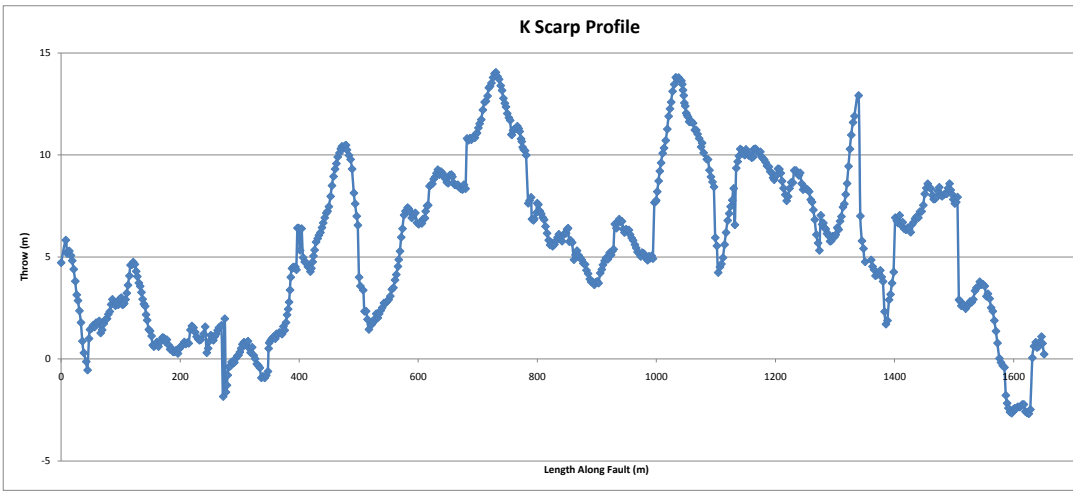


B

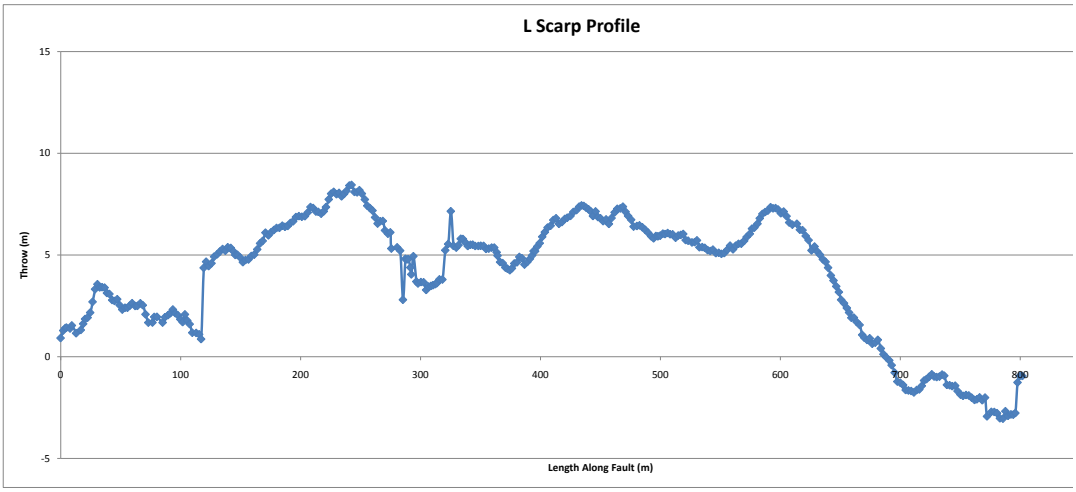


Figure 3.14 Profiles of scarps not covered by the historical lava flow. A) Fault scarp profile for K. B) Fault scarp profile for L.

Figure 3.15 shows the faults that are all partially covered by the historical lava. All of these profiles display a consistent trend of a negative throw in the historical lava, that switches to a positive throw at the contact margin. After the contact margin, the faults J, M, and N (Fig. 3.15 a-c) display a positive throw along the rest of their profile. These profiles do not extend the complete length of the fault and terminate somewhere in the middle of the scarp. The maximum throw of the faults that are covered by the historical lava is approximately 15m, found along the P profile (Fig. 3.15d). Systematic variation in throw is seen along these partial profiles, but cannot be confirmed without the rest of the fault.

A

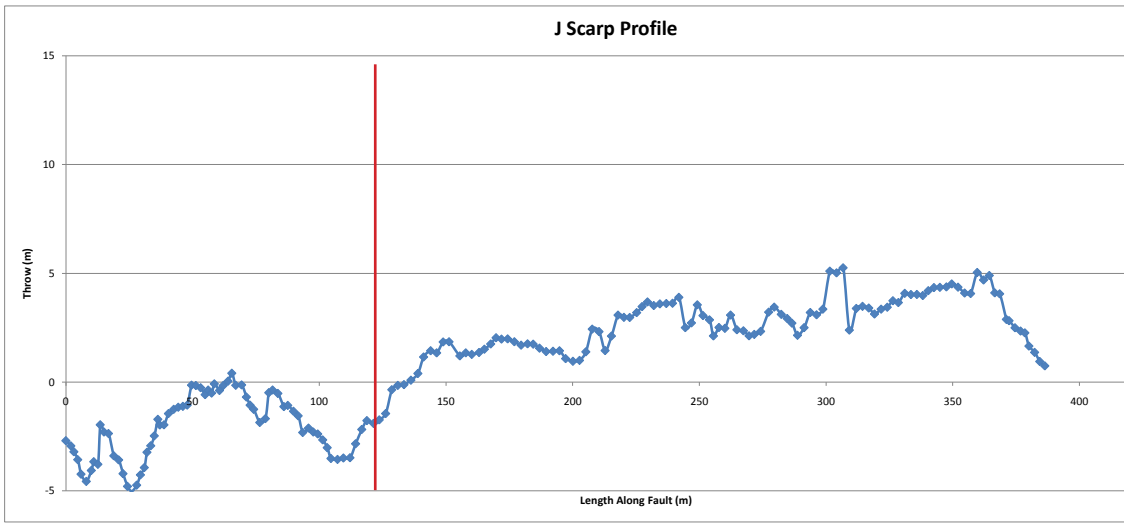


B

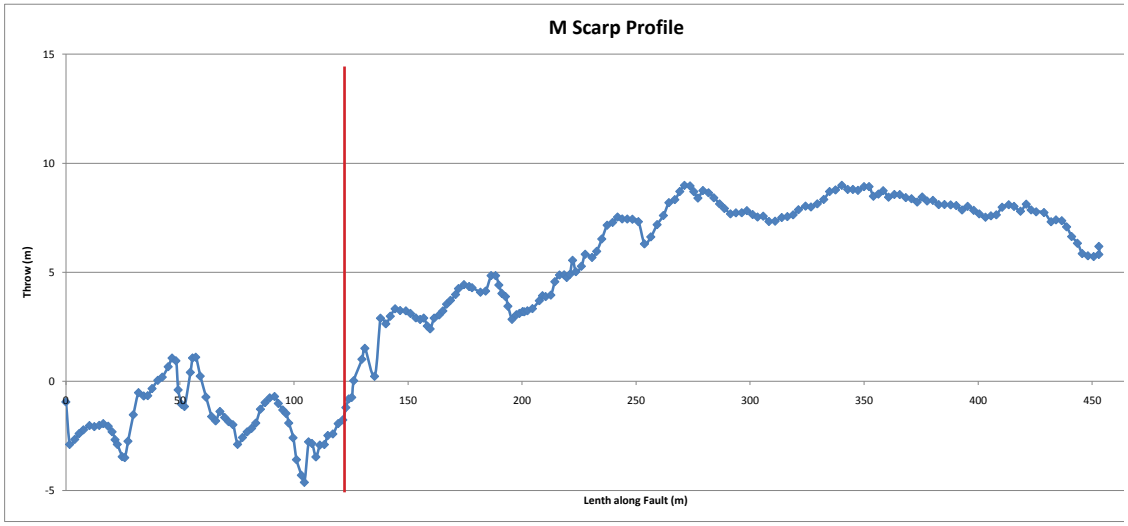


Figure 3.15 Profiles along scarps covered by the historical lava flow. The red lines mark the contact between the fault and the historical lava flow. A) Fault scarp profile for fault J. B) Fault scarp profile for fault M. C) Fault scarp profile for fault N. D) Fault scarp profile for fault P.

C

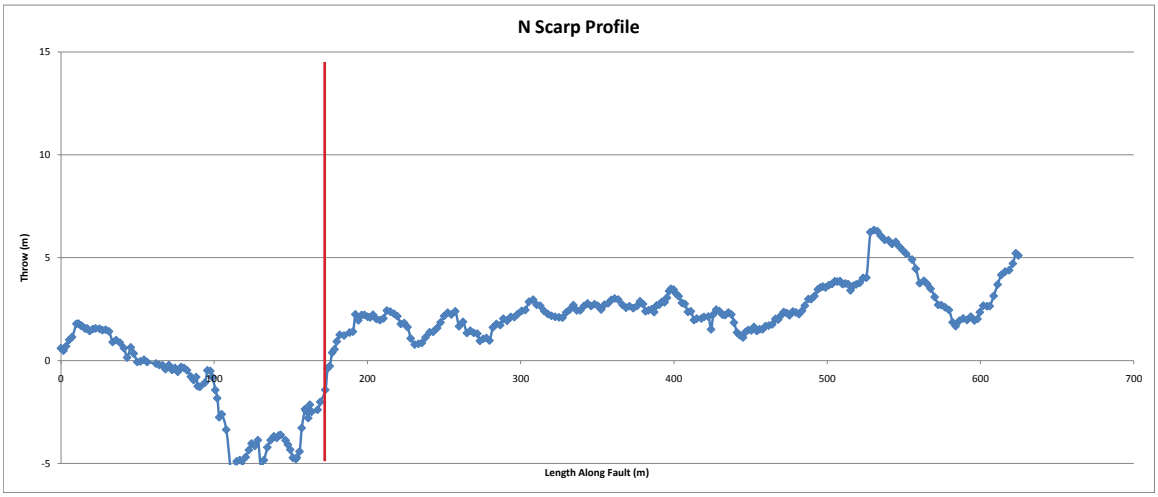
N Scarp Profile
Throw (m)
15
10
5
0
-5
0
100
200
300
400
500
600
700
Length Along Fault (m)

D

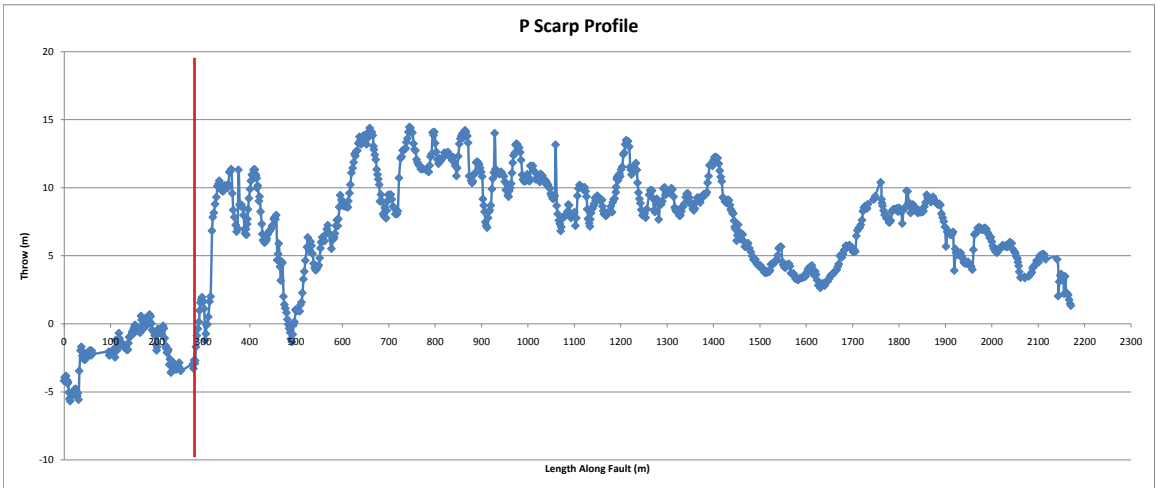
P Scarp Profile
Throw (m)
20
15
10
5
0
-5
-10
0
100
200
300
400
500
600
700
800
900
1000
1100
1200
1300
1400
1500
1600
1700
1800
1900
2000
2100
2200
2300
Length Along Fault (m)

### *3.2.2 Fissures*

Twenty five fissures were identified through field work and aerial photographs. Fissures are characterized by openings that display <1 m of offset (Fig. 3.16). They range from a few meters in length to 1 km, with longer ones (>100 m) displaying sinuosity (Fig. 3.1b). They were found between faults, and at the ends of faults as described previously. One eruptive fissure was found in the southwest area of the field study (Fig. 3.17). The fissure was approximately 75 m in length and was surrounded by pieces of scoria. The scoria was found only out to about five meters from the vent, hence the volume of lava erupted from the fissure was very small.

### *3.2.3 Cross Section*

A transect was conducted across the field area intersecting both faults in the shield lava and the historical lava flow (Fig. 3.18). The data was analyzed in ArcMap and Excel to create a 1:15 scale profile (Fig. 3.19). The 1:15 profile shows a very shallow graben over the 7 km wide area. The change in elevation between the bottom and top of the walls was approximately 70 meters. The moderately dipping scarps on the northern wall with throws >10 m are apparent in the profile. It also shows very rough topography in the lavas over the field area. All of the lavas are offset by the faults except for the historical lava, which has covered the faults in the shield basalt (Fig. 3.19). The cross section also shows the direction of flow of the lavas. The flow direction of the shield basalt was north, and the first fissure lava also flowed south to north. The other fissure lavas all flowed into the field area from west to east. The flow direction of the supraglacial lava could not be determined.

Figure 3.16 Non-eruptive fissure seen in the bottom of the graben. Field notebook for scale.

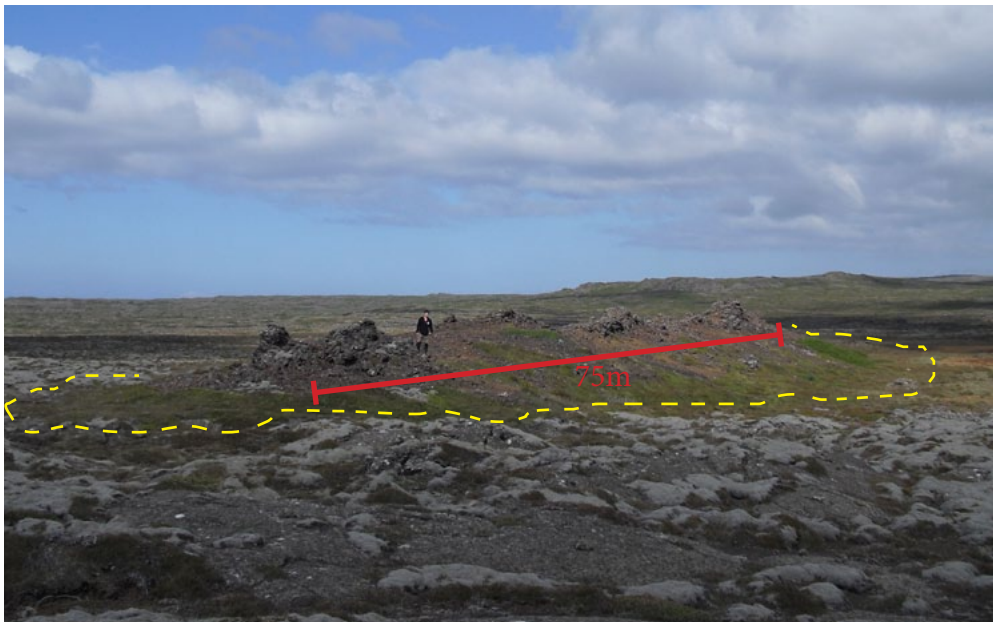


Figure 3.17 Eruptive fissure seen in the southern portion of the field area, yellow line indicates extent of scoria. Kenjo Augustsson (1.7m) for scale.

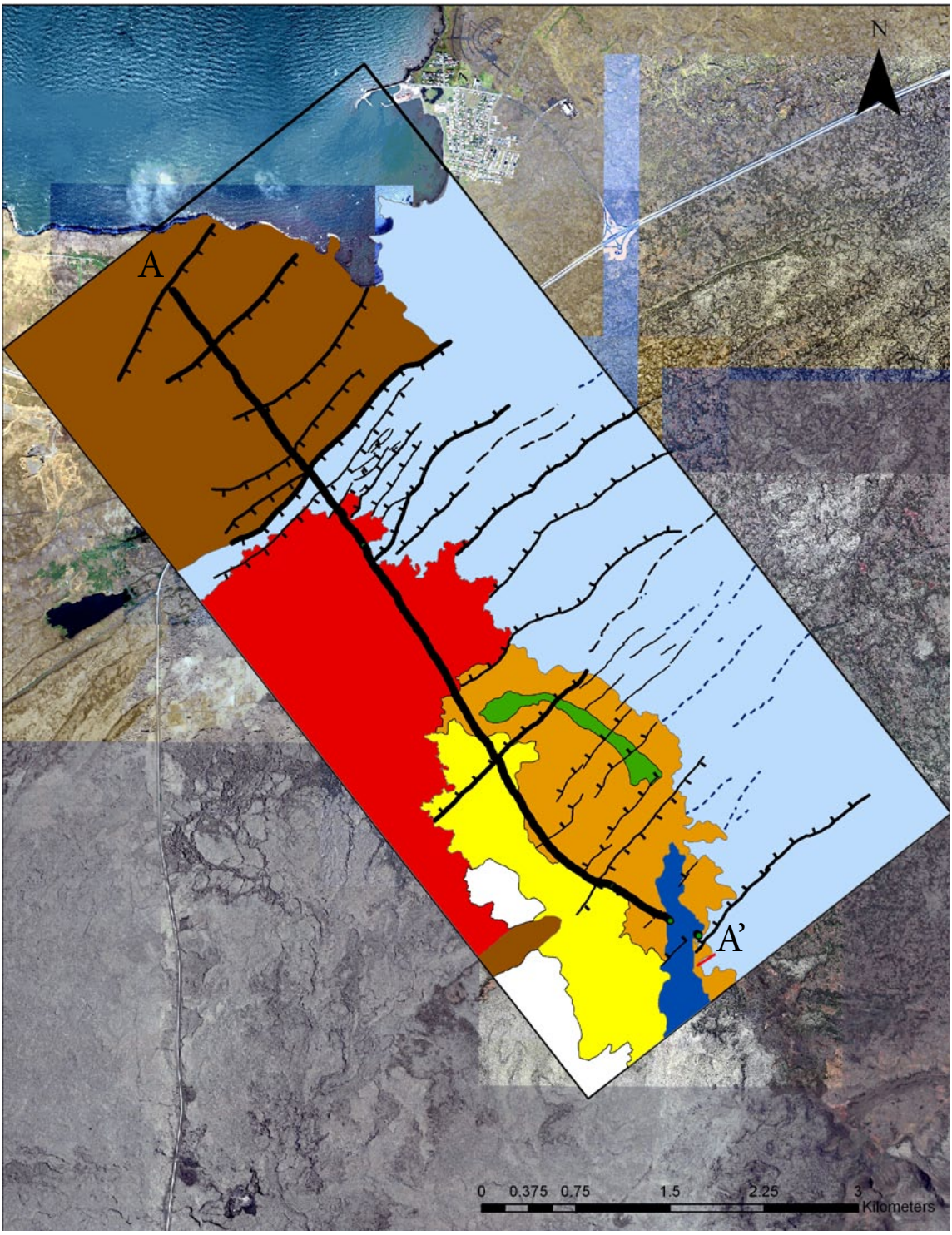


Figure 3.18 Map showing the transect that was conducted to create the cross section in Figure 3.19. The transect cuts six different lava flows.

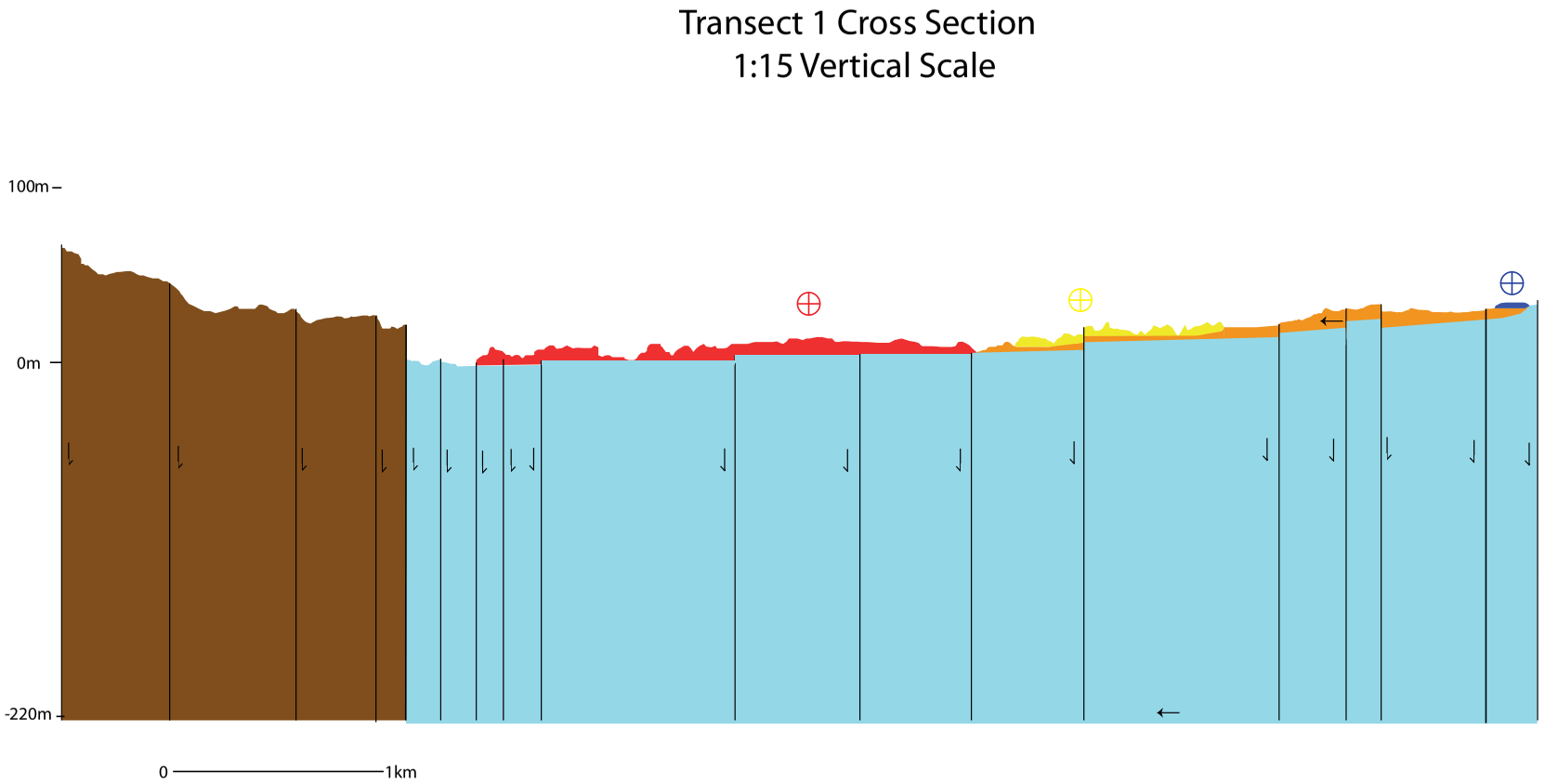


Figure 3.19 Schematic cross section of the fissure swarm down to 220 m depth. The faults are all vertical to this depth. Cross hairs and full arrows show flow direction of the lavas. Faults display offset in all the lava flows except the historical lava flow.

## 3.3 Petrology

### *3.3.1 Optical Properties*

Samples were taken from the supraglacial, shield, lava channel, second fissure, new and unknown lava flows (Fig. 3.1b). The dominant minerals in all the samples are twinned, blade shaped plagioclase grains of a variety of textures which will be described below. Olivine phenocrysts are the next most abundant mineral of varying grain size, followed by pyroxene and clinopyroxene, which was confined mostly to the groundmass.

The supraglacial lava is relatively coarse-grained, with plagioclase grains ranging from .5 to 1.5 mm long and euhedral to subhedral olivine crystals between .25 and .75 mm wide (Fig. 3.20). The texture of the grains is interstitial, where there is little groundmass and most of the phenocrysts are touching. The vesicles are unfilled, and make up 30% of the slide. Excluding the vesicles, plagioclase makes up 50% of the slide, olivine 30%, pyroxene 15%, and clinopyroxene and plagioclase rich groundmass constitutes the remaining 5%.

The shield lava is finer grained than the supraglacial, with bladed plagioclase crystals between .25 and 1 mm long (Fig. 3.21). The olivine crystals are between .1 and .6 mm wide, and are mostly euhedral with some subhedral grains existent. Subhedral pyroxene grains are also present and are .1-.3 mm wide. The texture of the sample is glomeroporphyritic, with clusters of olivine crystals and plagioclase in a fine grained matrix of clinopyroxene and plagioclase. The vesicles are 50% completely filled by fragmented rock material, and 50% not filled at all, and make up 20% of the slide. Excluding vesicles, the sample consists of 30% plagioclase, 10% olivine, 5% pyroxene, and the remainder is matrix material.

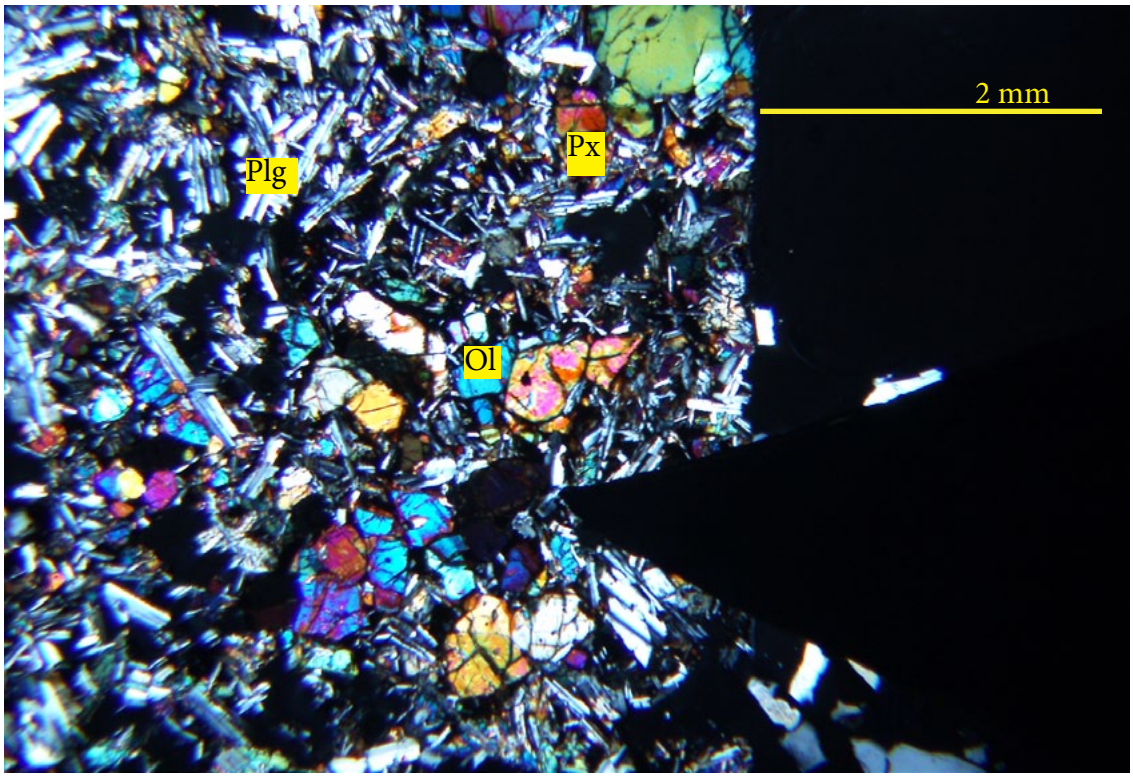


Figure 3.20 Cross polarized view of the supraglacial lava at 40x magnification. Phenocrysts are large and made up of plagioclase, olivine, and pyroxene.

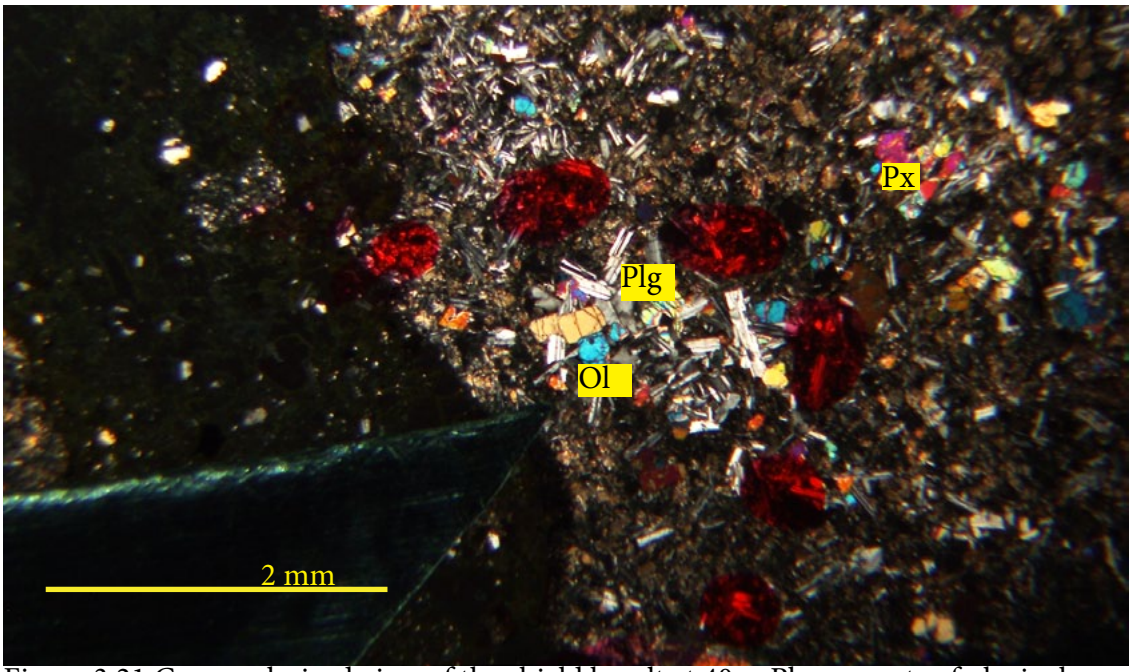


Figure 3.21 Cross polarized view of the shield basalt at 40x. Phenocrysts of plagioclase, olivine, and pyroxene. Large black areas are vessicles Groundmass consitutes majority of sample.

The lava channel flow has crystals of plagioclase that range from .2 to .5 mm in length (Fig. 3.22). The grains of olivine are between .1 and .5 mm wide, and are subhedral. The texture is glomeroporphyritic, with clusters of plagioclase and olivine. The vesicles constitute 30% of the slide and are either completely filled or not filled at all. Excluding the vesicles, about 90% of the sample is a fine grained groundmass. The remainder is course-grained and composed of 5% plagioclase and 5% olivine.

The second fissure lava is comprised of .15 to .6 mm long grains of plagioclase and .2-.4 mm sized olivine in a matrix of smaller plagioclase and pyroxene grains (Fig. 3.23). The sample has a seriate texture, but some clusters of phenocrysts exist. The olivine crystals are euhedral to subhedral in shape. The vesicles in the sample have some orange staining around their edges, and comprise 30% of the sample. The remaining sample is comprised of 60% glass and clinopyroxene rich groundmass, 20% plagioclase, 10% olivine and 10% pyroxene.

The texture of the historical lava is glomeroporphyritic, with clusters of intertwined plagioclase and olivine crystals (Fig. 3.24). The sample has vesicles that are unstained and account for 30% of the area. The plagioclase crystals range from .1 to .5 mm. The olivine crystals are .1-.3 mm wide and mostly euhedral in shape. The groundmass can be described as both intergranular and interstitial, and mostly made up of glass. The sample is 30% plagioclase, 5% olivine, 5% pyroxene and 60% groundmass of mostly clinopyroxene and plagioclase.

In the sample of the unknown lava, the groundmass of clinopyroxene constitutes about 80% of the non vesicular parts of the sample (Fig. 3.25). The vesicles make up about 40% of the overall sample. Crystals of plagioclase are .25 to 1 mm long. Some large (>1 mm) olivine crystals are clustered with the plagioclase crystals, but most are about .15 mm wide and subhedral in shape. The overall texture of the sample can be described as both seriate and glomeroporphyritic. Of the sample that is not groundmass, 10% is plagioclase, 5% olivine, and 5% pyroxene.

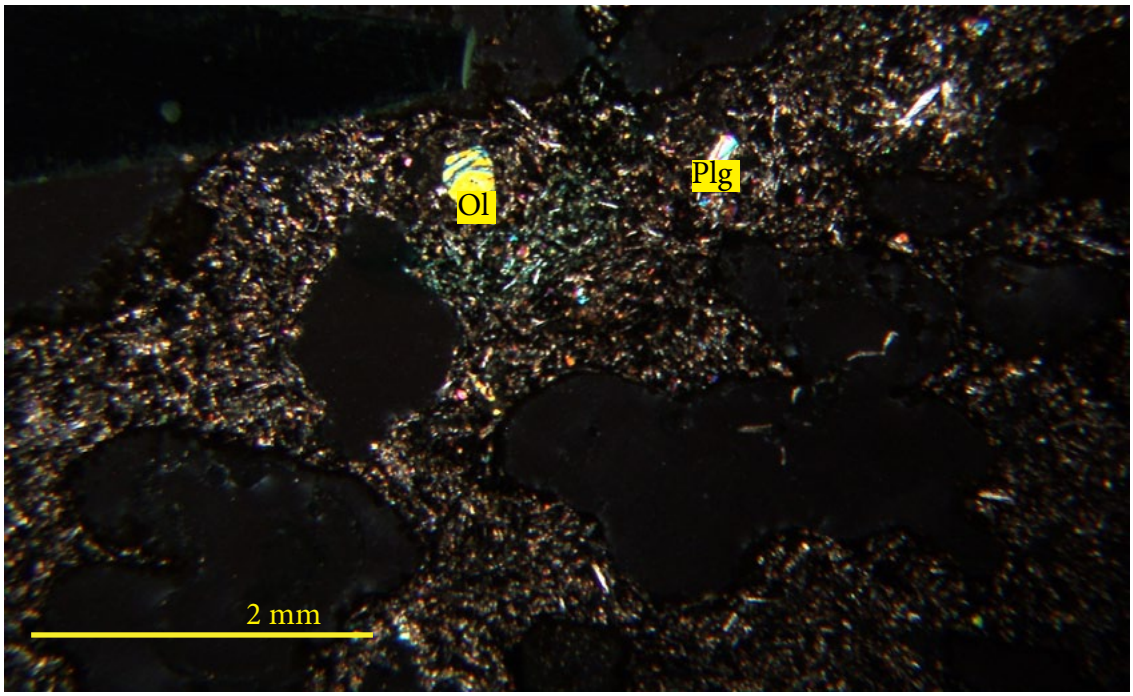


Figure 3.22 Cross polarized view of the lava channel flow at 40x. The large black areas are vesicles, and phenocrysts of olivine and plagioclase are present. The groundmass is fine grained.

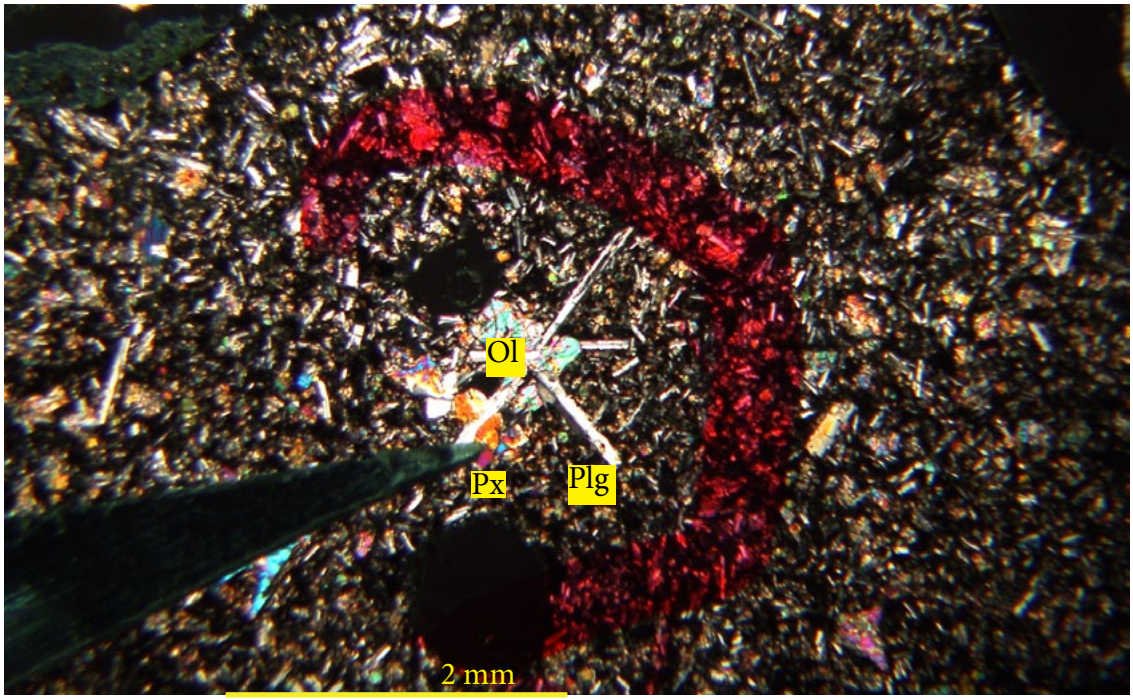


Figure 3.23 Cross polarized view of the second fissure lava at 40x. A cluster of phenocrysts including olivine, plagioclase, and pyroxene is seen at the center.

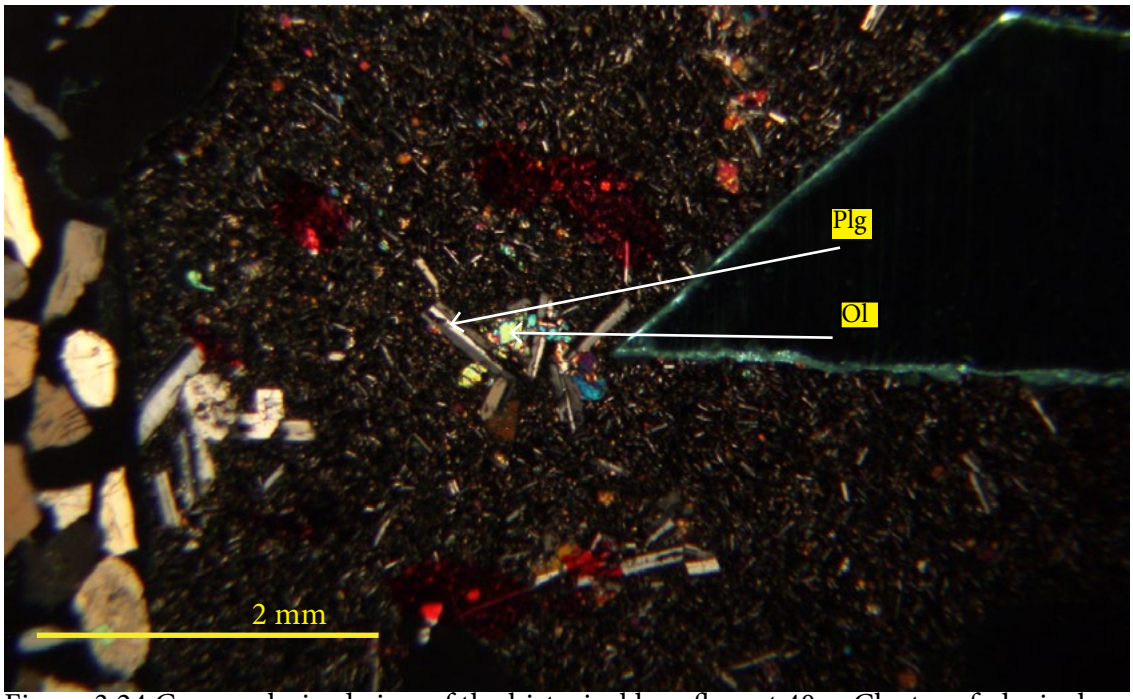

Figure 3.24 Cross polarized view of the historical lava flow at 40x. Cluster of plagioclase and olivine seen at the center. Dark black spots are vessicles.

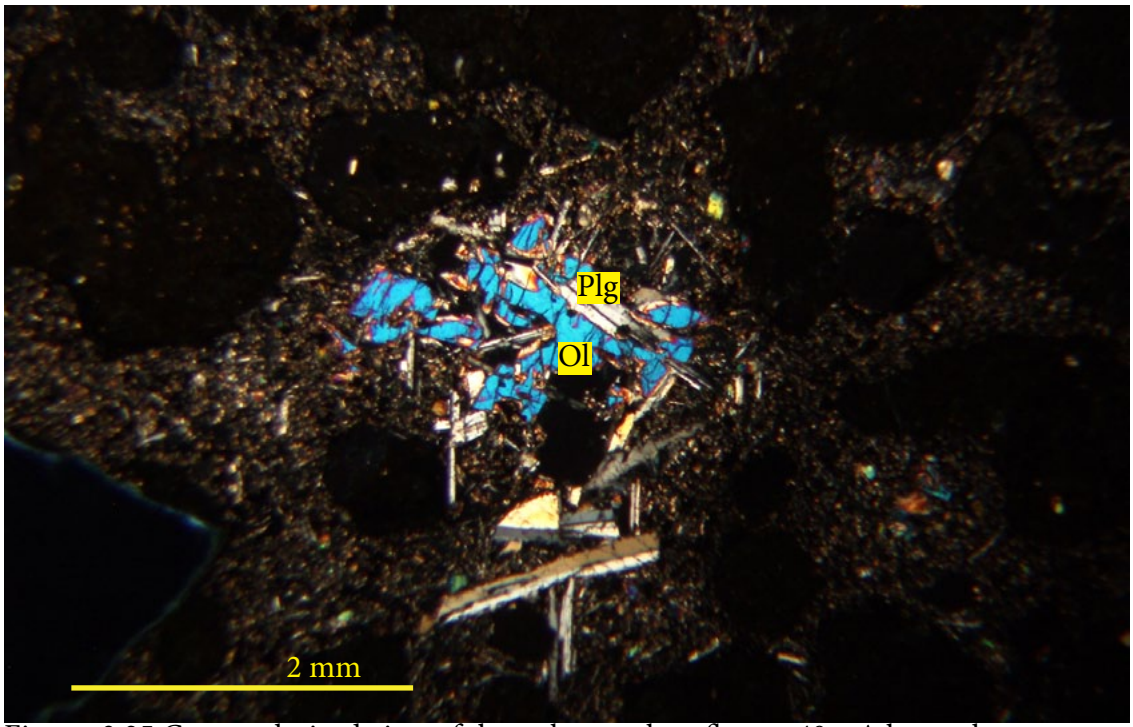

Figure 3.25 Cross polarized view of the unknown lava flow at 40x. A large phenocryst of olivine is seen at the center, with pieces plagioclase embedded in it. Dark round areas are vesicles.

*3.3.2 Mineral Chemistry*

Each of the samples were analyzed using the SEM-EDS to determine weight percentage oxides and the number of cations in order to calculate the specific chemical formulas of olivine and plagioclase in each sample.

*Olivine:*

The elemental analysis and resulting formulas in each flow for olivine are shown in Figure 3.26. For the purpose of analysis the fissure lavas will be looked at separately than the shield and supraglacial lavas, as it has been demonstrated that they are naturally separated in their mineral chemistry trends (Jakobsson et al., 1977). The analysis of the shield lava shows a more enriched content of MgO and less enriched FeO content than the supraglacial (Fig. 3.27). In the fissure lavas the MgO content does not show any statistically significant trend since the error bars are overlapping. The FeO content on the other hand increases as one moves from older lavas to newer ones, and can be considered significant as the error bars do not overlap. The value of FeO in the unknown lava falls in the trend before the channel lava. Overall the number of cations totaled up 3 ±.02 for all the samples confirming these minerals were olivine.

| | | Cation # | | | | | |
|---|---|---|---|---|---|---|---|
| Element | Formula | Supraglacial | Shield | Lava flow | Fissure 2 | Historic | Unknown |
| **O** | | 0.00 | 0.00 | 0.00 | 0.00 | 0.00 | 0.00 |
| **Mg** | MgO | 1.58 | 1.64 | 1.67 | 1.48 | 1.41 | 1.68 |
| **Si** | SiO2 | 1.00 | 0.99 | 0.99 | 1.01 | 1.00 | 1.02 |
| **Mn** | MnO | 0.02 | 0.01 | 0.01 | 0.02 | 0.02 | 0.01 |
| **Fe** | FeO | 0.40 | 0.36 | 0.35 | 0.49 | 0.58 | 0.27 |
| **Ni** | NiO | 0.01 | 0.01 | 0.00 | 0.01 | 0.01 | 0.00 |
| **Total** | | 3.00 | 3.01 | 3.02 | 2.99 | 3.00 | 2.99 |

Figure 3.26 Number of each cation in olivine in the six different samples.

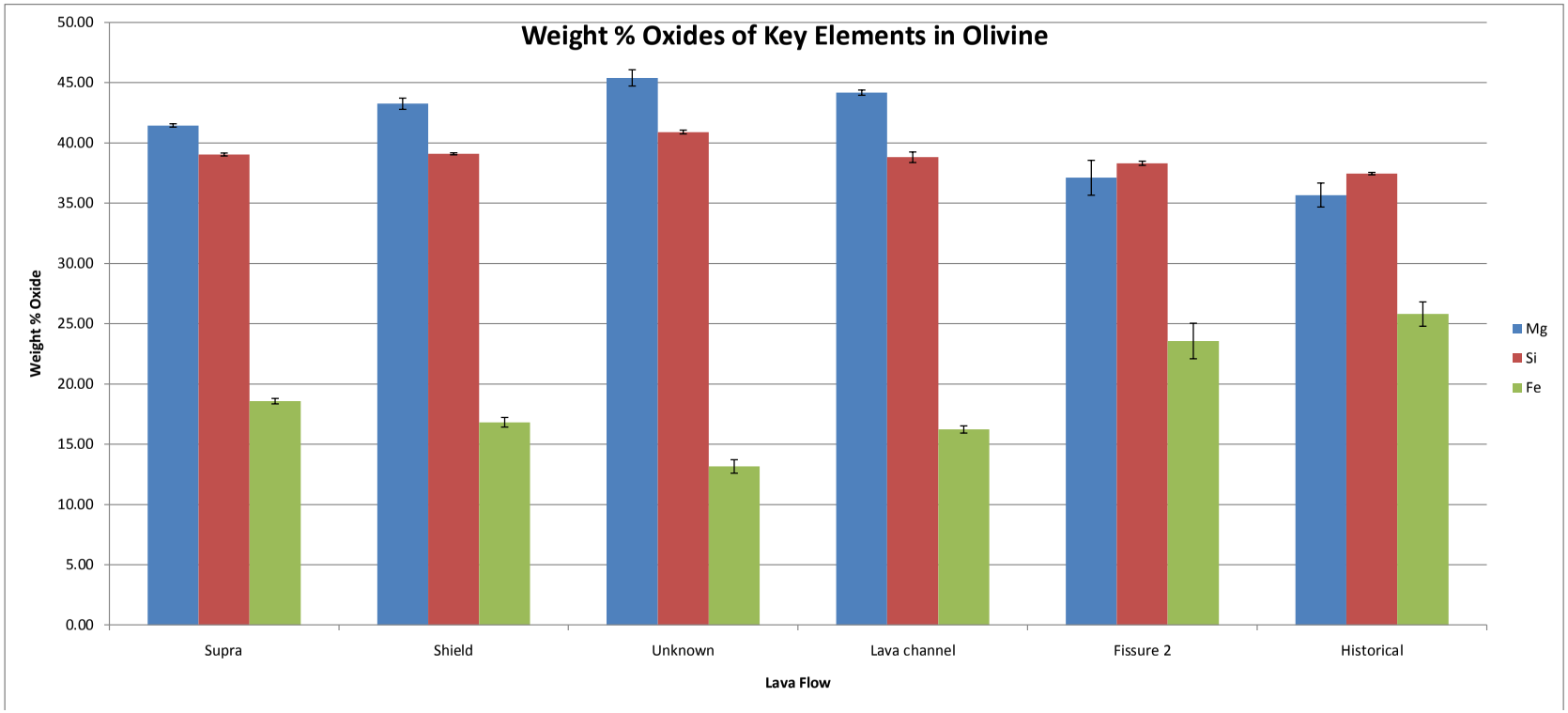


Figure 3.27 Bar graph displaying the average weight % oxides of Mg, Si, and Fe with error bars. Flows are aranged by relative age from oldest to youngest along the x axis. The unknown sample has been fitted in according to contact relationships and the Fe trend. Mg shows a lower percentage in the two more recent flows than in the older flows. The Si percentage is almost constant throughout all the flows. The Fe content shows a statistically significant enrichment as one moves from oldest to youngest in the fissure flows.

*Plagioclase:*

The elemental analysis and resulting formulas for plagioclase in each sample are shown in Figure 3.28. In all the samples the analysis showed the plagioclase was Ca rich An65 (Fig. 3.29). The compositions of the different samples were relatively homogenous. Ca values were more depleted in the fissure lavas than in the earlier shield and supraglacial lavas, and Na values were more enriched. Overall the number of cations in each sample added up to 5.07 ±.04 confirming these minerals were plagioclase, but no real trends were found in the analysis.

| | | Cation # | | | | | |
|---|---|---|---|---|---|---|---|
| Elt | Formula | Supra | Shield | Lava flow | Fissure2 | Historical | Unknown |
| **O** | | 0.00 | 0.00 | 0.00 | 0.00 | 0.00 | 0.00 |
| **Na** | Na2O | 0.32 | 0.26 | 0.36 | 0.41 | 0.48 | 0.32 |
| **Mg** | MgO | 0.01 | 0.01 | 0.01 | 0.01 | 0.01 | 0.01 |
| **Al** | Al2O3 | 1.71 | 1.73 | 1.67 | 1.65 | 1.59 | 1.76 |
| **Si** | SiO2 | 2.25 | 2.23 | 2.29 | 2.30 | 2.33 | 2.24 |
| **K** | K2O | 0.01 | 0.01 | 0.01 | 0.01 | 0.01 | 0.01 |
| **Ca** | CaO | 0.75 | 0.77 | 0.69 | 0.67 | 0.64 | 0.67 |
| **Ti** | TiO2 | 0.00 | 0.00 | 0.00 | 0.01 | 0.01 | 0.00 |
| **Fe** | FeO | 0.03 | 0.03 | 0.03 | 0.04 | 0.05 | 0.02 |
| **Sr** | SrO | 0.00 | 0.00 | 0.00 | 0.00 | 0.00 | 0.00 |
| **Total** | | 5.06 | 5.04 | 5.06 | 5.09 | 5.11 | 5.04 |

Figure 3.28 Number of each cation in Plagioclase in the six different samples.

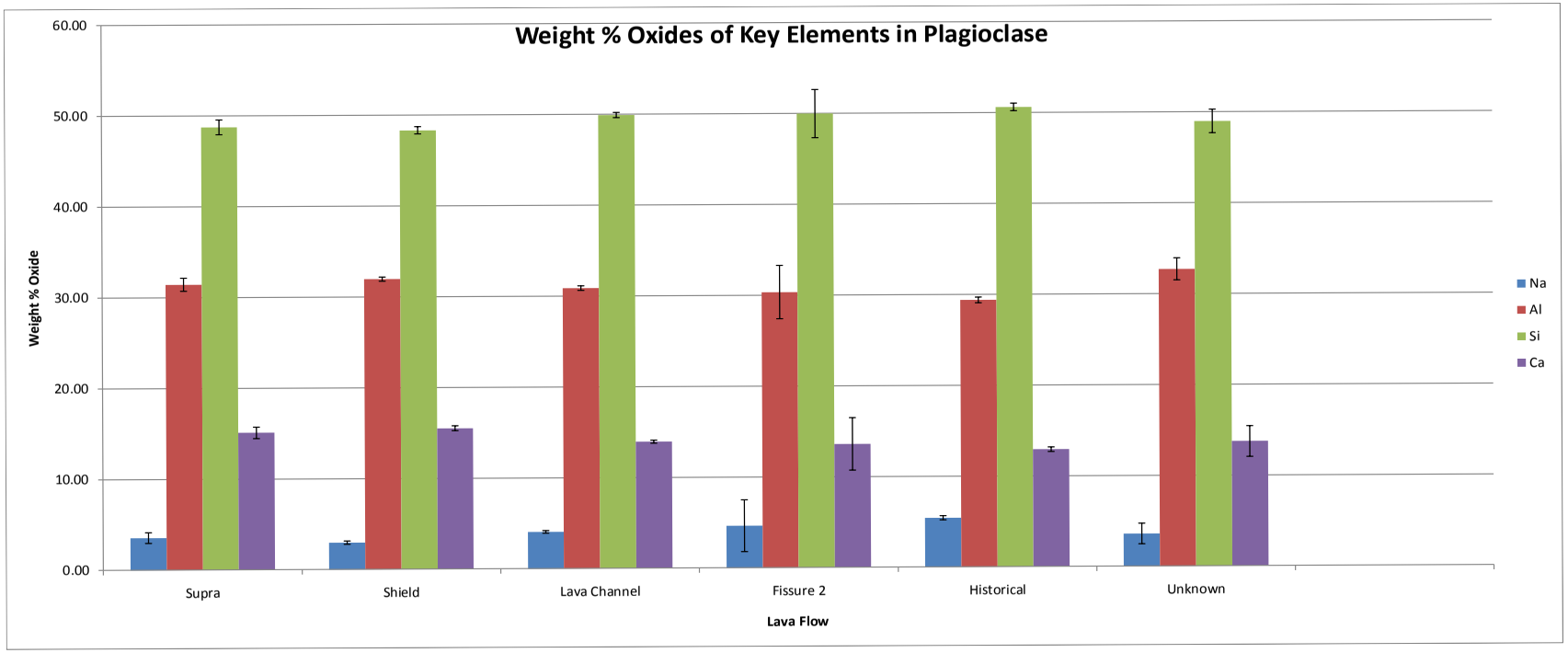


Figure 3.29 Bar graph displaying the average weight percent oxide of Na, Al, Si and Ca. There are no real trends in the values. Silicon hovers around 50% in all the samples. Aluminum is around 30% followed by Ca around 15% and Na at about 5%.

# CHAPTER 4: DISCUSSION

### 4.1 Timing of Lava Flows

The analysis of the thin section samples confirmed that they were all tholeiitic basalts with compositions of plagioclase, pyroxene, and >5% olivine. Chemical and optical data was used to try and constrain the relative age of the unknown lava flow. The flow was known to be younger than the shield basalt and older than the second fissure flow due to contact relationships in the field. Chemical data of the elemental and oxide composition of plagioclase and olivine crystals in the known samples were compared to see if they were similar to that of the unknown flow. They showed no clear similarity in composition, but there was a trend that emerged from the samples of known relative age. The FeO contents in the fissure flows showed a statistically significant increase as the flows became younger (Fig. 3.27). Using this information the unknown lava was cautiously interpreted as having been the first fissure flow within the field area. A sample of the mapped first fissure flow (Fig. 3.1b) was unable to be taken, but it is known to be the oldest fissure flow through contact relationships. The unknown lava is most likely part of this lava unit.

### 4.2 Fault Activity

The mechanism of faulting in the Vogar Graben is a topic of debate. There have been leveling studies carried out by Tryggvason (1970) that show there was movement on some of the faults between 1966 and 1969. This was mostly contributed to an earthquake swarm that occurred 25 km to the southwest of the leveling profile. The most widely accepted theory of faulting however is that these normal faults are activated during magmatic events, when the principal stresses are changed. It is this aseismic magmatic mode that is attributed to the majority of the deformation seen within the Vogar graben. However, some scarps appear to offset even the youngest historical flow and thus question this model, since there have been no magmatic events since the historic lava was

erupted.

For example, aerial photographs of the historical lava flow indicate that there are apparent structures that continue from some of the shield lava faults into the historical lava (Fig. 4.1). Field observations and GPS profiles of the fault scarps that intersect the historical lava flow all show an apparent change in the hanging wall at the contact implying at first glance a reversal of slip (Fig. 3.15). These profiles fit well with the observations made in the field that there appeared to be zones of higher topography in the historical lava along strike of the faults in the shield lava. This can be explained by looking at the flow properties of the historical lava (Fig. 4.2). As the lava flowed from southwest to northeast along the graben, it cooled as it got further from the source. The cooling of the lava increased the viscosity. Eventually the front of the lava reached its present day location in the Vogar Graben. The fault blocks, which are dipping back towards the fault scarps themselves, caused the lava to concentrate against the scarp walls. The lava would eventually overflow the entire scarp, but the scarp would still have enough of an influence that it would allow the viscous lava to pile up against it higher on the hanging wall than on the foot wall.

This is affirmed by field observations of historical lava that is present on the foot wall of the northern most fault in G, but not on the hanging wall (4.3). The lava is piled up higher along the hanging wall than the height of the footwall. This piling up of the lava is only observed closer to the contact of the fault and the historical lava. The reason it may not be observed further into the historical lava is either the fault ends, the viscosity of the lava is not high enough to build up against the fault scarp, or there was enough lava that it eventually overwhelmed the scarp.

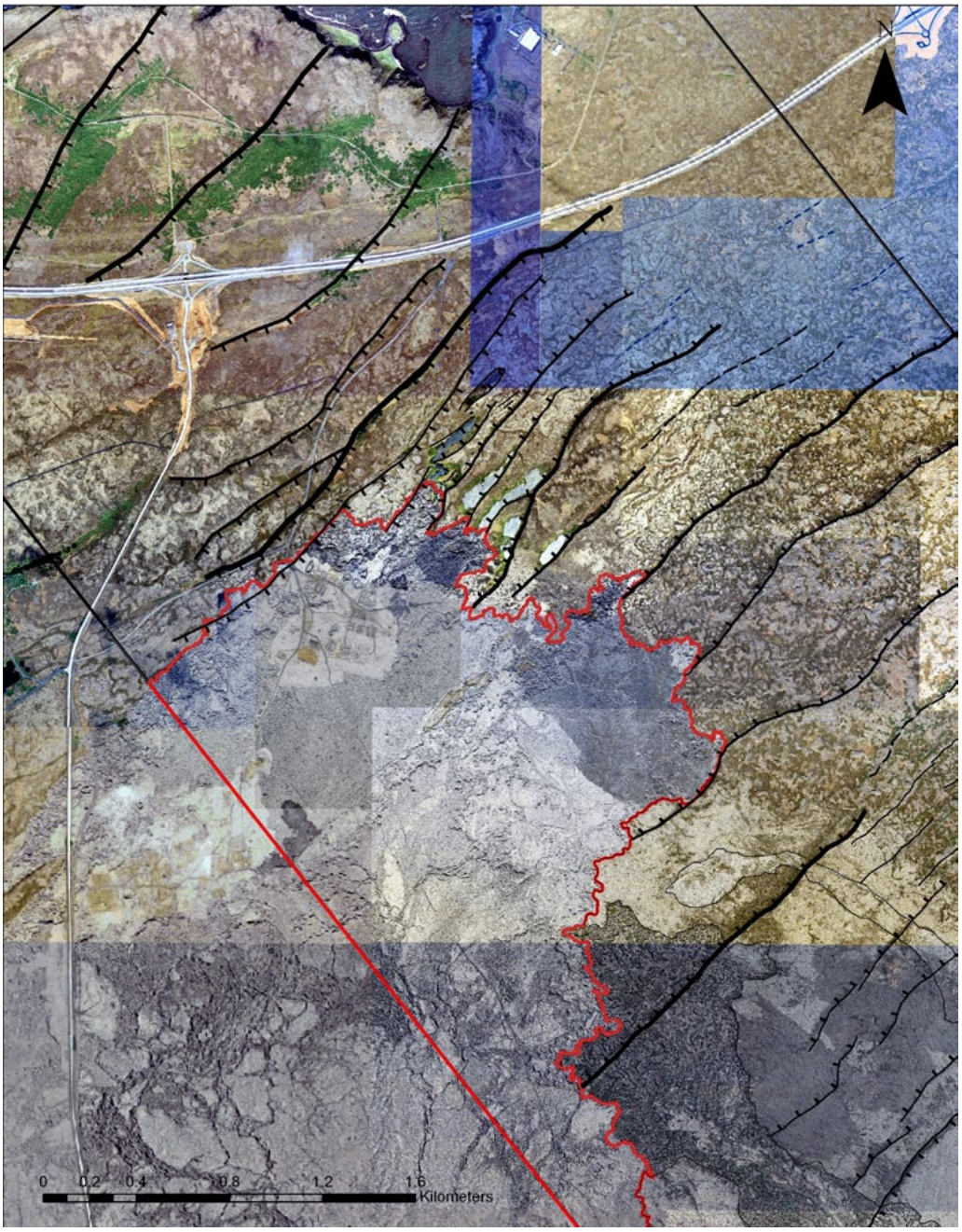


Figure 4.1 Aerial photograph showing the faults and the outline of the historical lava flow. Some of the faults can be seen to apparently cut the historical lava flow.

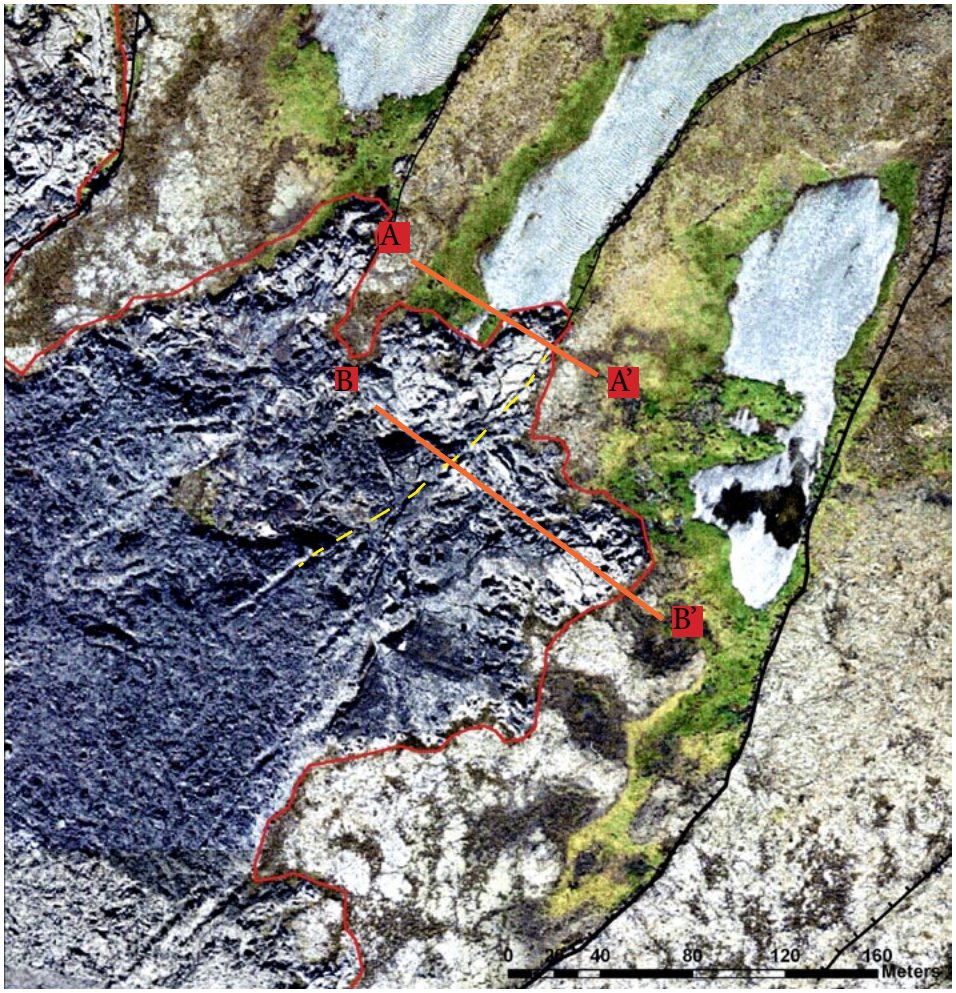


A A’

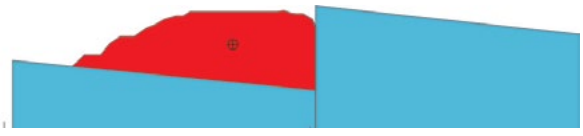

B B’

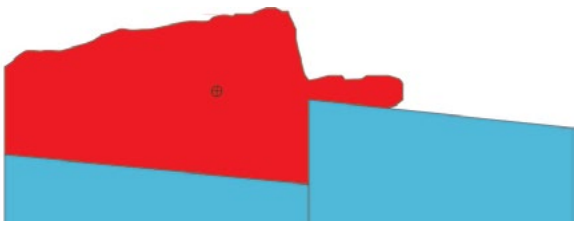

Figure 4.2 Aerial photograph and two cross sections showing the advancement of the historical lava. In the photograph the yellow line marks the apparent continuation of the fault. The subsequent cross sections show the interpretation of this structure.


Figure 4.3 Photograph of the northern most scarp of G (dashed yellow line) that has the historical lava piled up against it. I am standing on the footwall which is comprised of the shield lava, while the historical lava is on the hanging wall and piled up higher than the footwall.

Fissures can be observed along strike of these apparent faults in the historical lava. These are thought to be lava flow structures that can be mostly described through cooling processes of the lava. Differential cooling can account for the apparent change in offset and the fissures seen in the lobes of historical lava that overflow fault scarp F (Fig. 3.1b). When lava cools it contracts, with the thickness of the unit largely determining the cooling and contraction rate (Long and Wood, 1987). Thicker lava units contract more, but take longer to cool. The lobes that overflow scarp F are not as thick as the lava that is on the hanging wall (Fig. 4.4). Therefore these lobes of lava cooled and contracted much faster than the thicker body of lava on the other side of the scarp. This quicker cooling could have led to a fracture at the contact between the lobe of lava and the larger lava body. This contact is defined by the scarp. This process could explain the presence of some fissures and fault-like features along smaller lobes of the historic lava that has covered the scarp.

Many of the faults observed in the shield lava had open gaps or fissures at their bases, some of which were over 15m deep. If one of these openings was present along the fault as the historical lava flowed against it, the historical lava would flow into the crack. This was observed during the Krafla rifting episodes where magma flowed back into the upper crust through open fissures (Einarsson, 1991; Buck et al., 2006). This would again create a unit of the historical lava that was of a different thickness than the unit above it (Fig. 4.5a). Depending on the size of the opening and the volume of lava that flowed into it, secondary rifting structures could form over the older fault scarp. The lava in the opening is insulated from the cooler atmosphere, and therefore cools at a much slower rate. Depending mostly on the temperature, thickness, thermal conductivity, and any water that is present on or in the cooling unit, 60%-80% of the vertical cooling in the unit occurs from the surface down (Grossenbacher and McDuffie, 1995). If the unit of lava above the fissure completely cools and solidifies first, the subsequent cooling and contraction of the lava that has flowed into the open fissure creates open space at depth in

the fissure (Fig. 4.5b). If this space fills in with pieces of the flow above it, it will create secondary rifting structures (Fig. 4.5c). These secondary structures may be fractures or even small normal faults that appear on the surface.

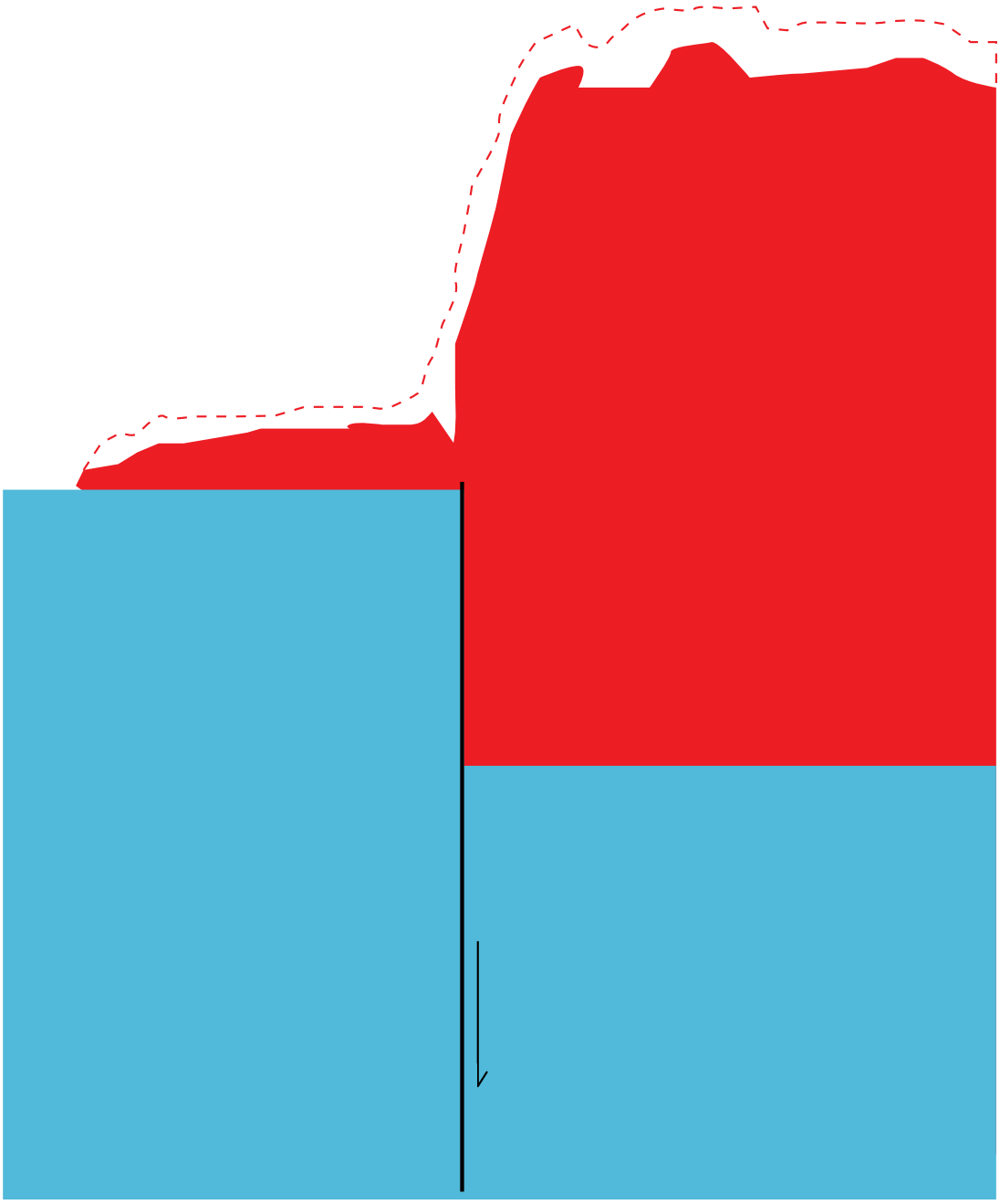

Figure 4.4 Model of the proposed theory of differential cooling leading to a crack along the contact of the overflowed lobe and the larger body of lava. Dashed line indicates the lava surface before it cooled.

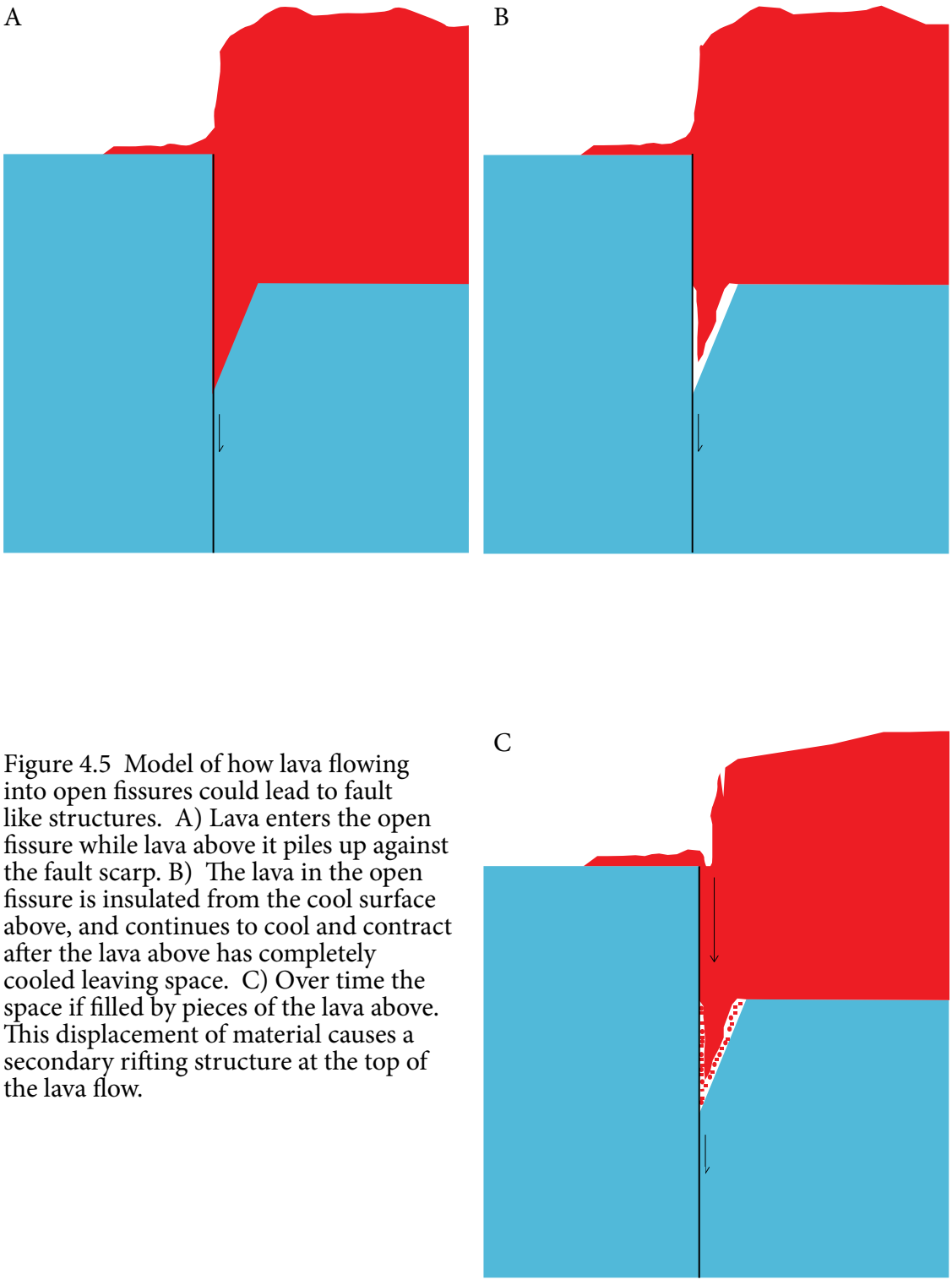


Figure 4.5 Model of how lava flowing into open fissures could lead to fault like structures. A) Lava enters the open fissure while lava above it piles up against the fault scarp. B) The lava in the open fissure is insulated from the cool surface above, and continues to cool and contract after the lava above has completely cooled leaving space. C) Over time the space if filled by pieces of the lava above. This displacement of material causes a secondary rifting structure at the top of the lava flow.

The above mechanisms are theories to explain the apparent offset, in the historical lava, and the fractures that are seen along strike of the faults in the historical lava. Both of these can be explained by differential cooling without an episode of seismicity, and contribute to the idea that faulting in the Vogar graben is primarily aseismic and happens during magmatic episodes on the peninsula. This is concluded because the historical lava from the last eruptions does not show any consistent offset along the faults that it covers. This, coupled with the non-eruptive activity on the peninsula, is evidence that the faults primarily move when the peninsula is experiencing an eruptive or intrusive period. This is in agreement with observations of the Krafla rifting episode where up to 2 m of slip preceded fissure eruptions (Einarsson and Brandsdottir, 1980). This study can only constrain movement in the Vogar graben to the youngest fissure flow that is cut by a fault. Aerial photographs show the 2000 year old Sundhnukur lava flow in the southwest corner of the study area (Fig. 3.2b) being cut by at least one fault. The oldest flow that was confirmed to be faulted in the field was the second fissure flow, which is underneath the Sundhnukur lava and can therefore be constrained to an approximate age between 2000 and 12,000 years old. Therefore it is possible that the graben has not been active in the period of time since the eruption of the second fissure lava.

### 4.3 Fault Geometry

The faults at the surface displayed irregular curvilinear strikes at the surface, as well as left stepping en echelon segments within the fissure swarm. They varied in length and throw, and had generally northeast striking orientations. The observations of the faults fit well with current models of their formation. Faults were originally thought to propagate from the surface down using joints in the cooled basalt (Gudmundsson, 2002; Gudmundsson, 1992). In a model of normal faults along the Ethiopian Rift, Acocella et al. (2003) propose an initial dilational fracture that propagates to some critical depth at which point the fracture continues propagation as an inclined normal fault. In another model for fissure swarms in northern Iceland, it is proposed that faults form at depth

above dikes, and propagate upwards, typically linking with downward propagating extensional fractures above their tips (Tentler, 2005). This coincides with the findings of this study in that there has been no slip in the historical lava flows. Changes in stresses of the dikes below the fissure swarm are associated with eruptive events on the peninsula. Injections of magma into the shallow crust increases the magmatic pressure and allow the dikes to propagate along planes perpendicular to $\sigma_3$ or the minimum principal stress as produced by the plate boundary movements.

Tentler (2005) proposes a model where planar magma filled fractures are initiated at the interface of the magma and the crust when stress conditions are high enough (Fig. 4.6). These fractures propagate upwards until the horizontal compressive force of the overlying crust becomes greater than the pressurized ascending magma. Here, Tentler (2005) proposes that due to the extensional regime created by the plate boundary, the shear velocity of the fracture is great enough to continue as an inclined normal fault. The dip of such normal faults was determined by Slunga et al. (2005) who used data from 96 earthquakes measured in southern Iceland to derive an average dip of 63°. High concentrations of stress above the tip of the fault plane may allow for pure extension fractures to form at the surface above the fault plane, and propagate downwards along weak planes in the lava flow units.

Grant and Kattenhorn (2004) propose a model that accounts for the en echelon segments, seen in Figure 3.8, that proposes oblique slip along the fault plane at depth. Their model is based on the observed left stepping en echelon segments of the faults, and accounts for this through right lateral oblique motion along the faults at depth. In analogue models of an oblique rift zone modeled after the Reykjanes Peninsula, Clifton and Schlische (2003) show there are long N-S dextral oblique slip faults that are created through the rift center. Subsequent mapping of the rift zones showed evidence of these dextral strike slip faults in the field, but they were only found in the zone of active rifting and not along the rift margins (Clifton and Kattenhorn, 2006). There were no dextral

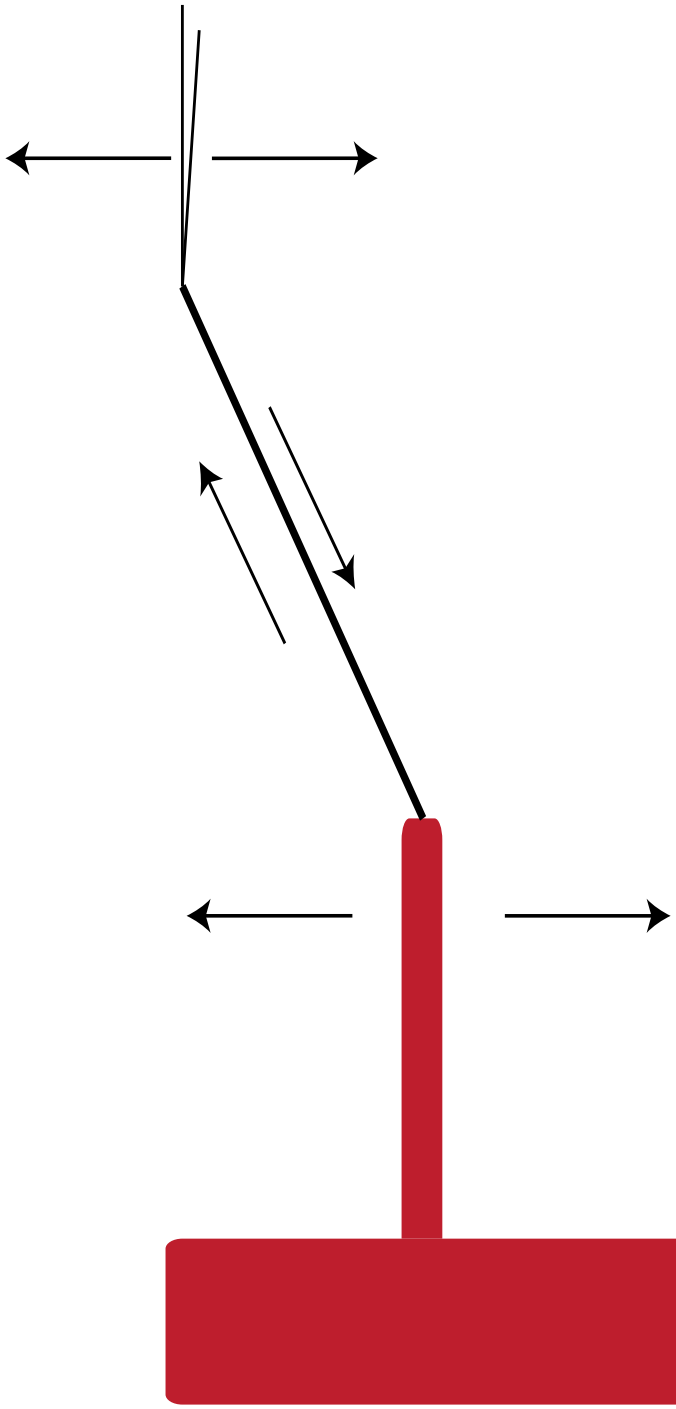

Figure 4.6 A model of the formation of normal faults in fissure swarms from Tentler (2005). A dike intrudes from a larger reservoir until the pressure of the acsending magma is equal to the overlying pressure of the crust. At this point the dike stops but an inclined normal fault continues due to the unique stress conditions of the left lateral transform zone. At the surface a dilational fracture initiates above the tip of the propagating fracture, and propagates downwards along cooling joints in the basalt lava flows until the fracture and fault meet.

strike slip faults found in the Vogar area, but it is possible that this right lateral motion on the rift margin is manifested along already established zones of weaknesses that are the normal faults and associated fissures. This would account for the right lateral motion indicated by the en echelon segments that make up the scarps.

The control on the orientations of the faults are complicated, and dictated by the obliquity of the ridge, the proximity of the faults to the ridge axis, their location in reference to magma reservoirs, proximity to preexisting structures, and the variable strain of the peninsula as a whole (Clifton and Schlische, 2003). With all these factors influencing the geometry of the faults, it is difficult to constrain their development within the context of only one variable. Clifton and Kattenhorn (2006) separated the faults by strike, and related their strikes to different strain environments (Fig. 1.4). They attributed most of the fracture development to upwardly propagating dikes, but found that fractures on the outskirts of the fissure swarms furthest from the volcanic centers had strikes rotated clockwise up to 40° with respect to those in the fissure swarm. The strikes of these faults are almost parallel to a region of subsidence found by Gudmundsson et al. (2002) along the trace of the plate boundary. This subsidence is most likely due to loading of the crust in the region as it is the epicenter of most of the volcanic activity. Clifton and Kattenhorn (2006) attribute the faults to a crustal flexure that is related to this zone of subsidence.

The faults within the field area did display various strikes, but most were striking at approximately 40°. The northern most faults in the study area had a strike slighty counterclockwise to this orientation, which can be attributed to the counter clockwise rotation of the structures as they are rifted away from the plate boundary in a left lateral transform zone (Clifton and Kattenhorn, 2006). These faults are the oldest and furthest from the plate boundary and therefore have had enough time for this rotation to effect them. The longer faults that stretch past the study area display a gradual clockwise rotation, as described by Clifton and Kattenhorn (2006). However an alternate theory to

crustal flexure may explain this occurrence. Strain rates and subsequent accumulation are very localized within the Reykjanes Peninsula as evidenced by GPS velocities measured by Keiding et al. (2008). The two velocity vectors around the Vogar region display different orientations and velocities (Fig. 4.7), with the more eastern vector rotated slightly more clockwise than its counterpart. If these vectors are roughly the σ3 orientations, then the faults would be propagating perpendicular to them. The slight clockwise rotation of σ3 orientations of extension could account for the slight clockwise orientation in the faults as they move from west to east across the graben. Of course these strain rates reflect modern rates that were almost certainly not constant in the past, and the strain of that region has most likely changed many times since the fault nucleation. However, local variations in velocity fields is an alternate explanation that accounts for the change in orientation of the faults.

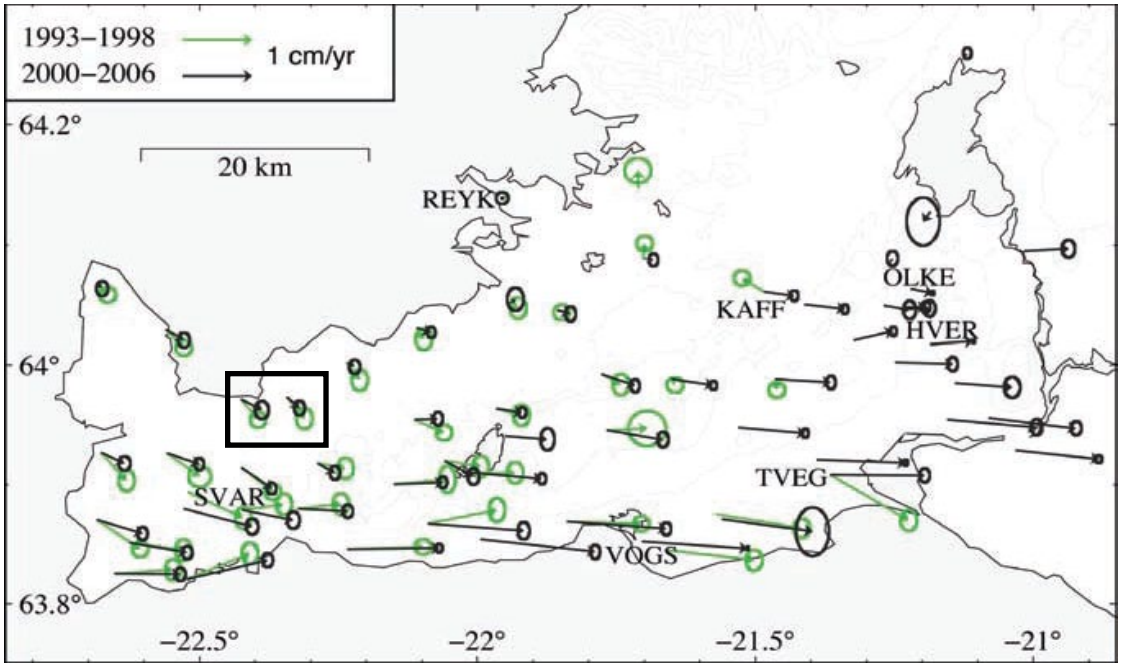


Figure 4.7 Figure modified from Keiding et al (2008) displaying horizontal GPS velocities over the Reykjanes Peninsula in reference to the REYK station. Black display displacement measured between 2000 and 2006 while green display displacement between 1993 and 1998. The blue box in the center indicates the two stations that fall in close proximity to the Vogar Graben. The easternmost station on the edge of the fissure swarm shows a displacement vector rotated slightly clockwise to the western station.

Something that was noted throughout the study area was the significant scarp erosion and degradation observed on many of the faults. This occurrence makes it hard to take field measurements and in some cases make accurate field observations. However, it also provides a method of determining relative ages, with more eroded scarps indicating more exposure and thus an older age. The northern faults A-D displayed the most erosion, with no clearly defined vertical scarp seen (Fig. 3.1b), lending evidence they were the oldest. Scarp N in Figure 3.13 displays how certain parts of a fault can be weathered faster than others. This can make it hard to determine the presence or absence of some structures in the field. For example, some faults have fissures at their bases, and the eroded rock can fill up the fissure over time depending on the amount of erosion and the rate of slip or widening of the fissure. This can make it difficult to determine the presence of fissures at the base of the fault, and to measure existing fissures as they may have been altered by eroded material. It also appears from Figure 3.13 that this eroded material can make an apparent monocline at the base of the scarp. Monocline development has been described through field observations by Grant and Kattenhorn (2004), but they make no mention of this mode of formation. It is something to be considered when evaluating these older scarps in the field.

### 4.4 Cross Section of graben

A true scale cross section of the peninsula was created along a GPS transect using observations of the surface expressions of the faults, and through use of different models in the literature (Fig. 4.8). This model is hypothetical and without more seismic data it is hard to constrain many of the aspects of the cross section. The thickness of the crust at the spreading center is approximately 5 km, and gets steadily thicker moving away from the plate boundary. Dikes that are injected laterally from the plate boundary propagate along the least compressive stress, and it is generally assumed that the fissure swarms mark the dike propagation direction (Einarsson, 2008). Therefore in this cross section the

main dike initiated at the interface of the crust and the mantle, and propagated upwards during multiple injections.

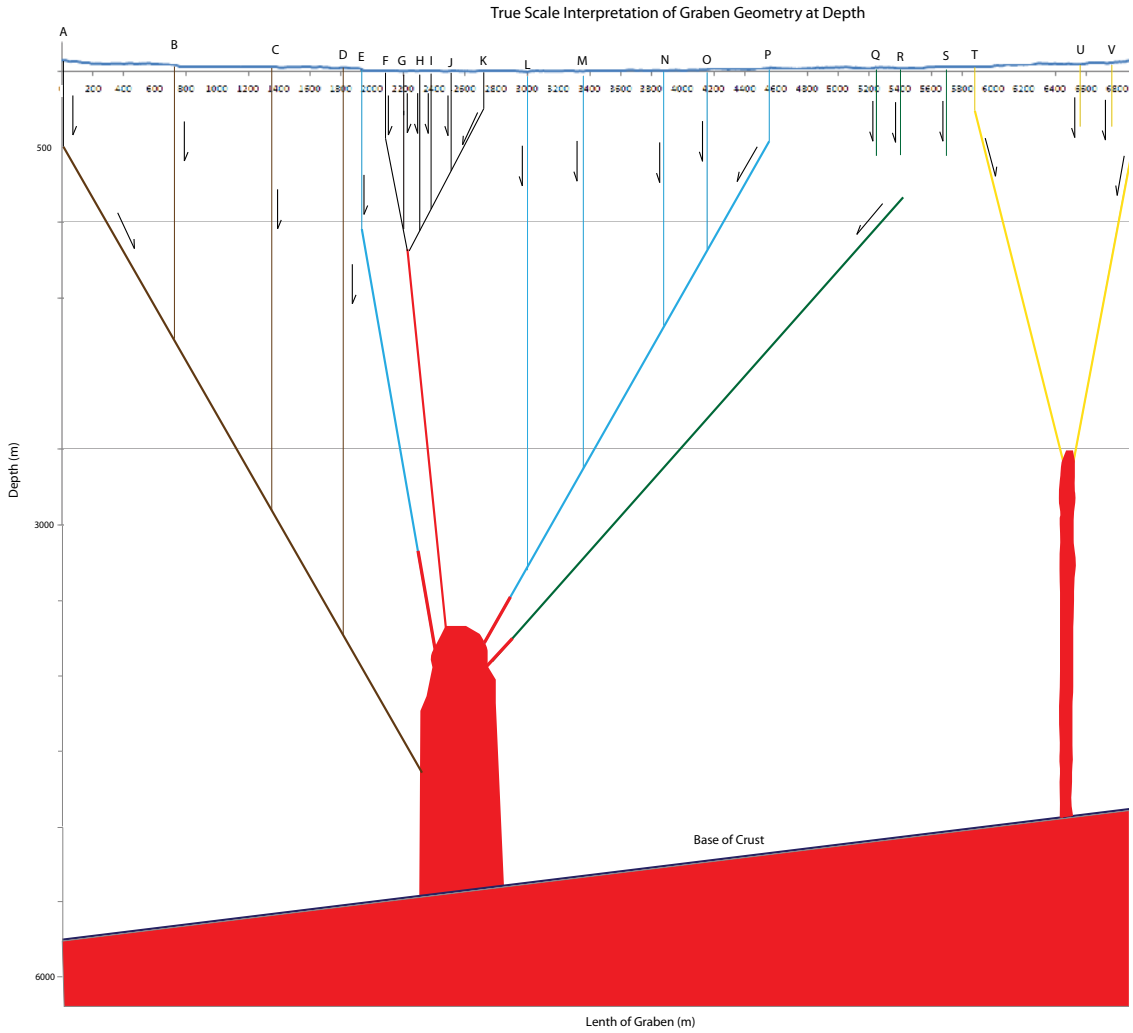


Figure 4.8 True scale interpretation of the faults at depth across the Vogar fissure swarm. Colors indicate faults that formed at the same time. Faults that demonstrated larger throw were considered to have deeper faults. Faults that had longer lengths were considered to be more developed and therefore older. Faults are labeled according to figure 3.1b.

The major faults (A-D) in the supraglacial lava in the north western section of the graben are thought to be the oldest, and represent faults that occurred during glaciation. They have been extinct for a long period of time as they display a significant amount of erosion and don't seem to continue into the Thrainskjoldur lavas to the northeast. The main part of the graben is bounded by faults E and P. These faults display the largest amount of throw and are two of the longest fault scarps in the area. Tentler (2005) describes fault formation as first lateral propagation, followed by vertical displacement. Therefore scarps of similar length are considered to be formed around the same time, and related to the same system of faults. Scarps with larger throws are thought to be connected to normal faults that extend the deepest. Since faults E and P display the largest throws they are considered to be the deepest extending faults and define the graben edges. Faults L-O are all considered to be part of the same fault system as P because they display similar lengths but less throw, indicating they formed at the same time but with less of a normal fault component. The throw of the faults decreases as one moves from M-O, indicating their depths may be decreasing as well. Faults F-K are thought to have formed at the same time because of their similarities in length and throw. They display shorter lengths and smaller throws, and are thought to be the youngest faults representing the shallowest dike. F and K are the two faults with the largest displacement, and therefore are modeled as the largest faults at depth, with the other faults coupled to them. Faults Q-S are relatively short and display the least throw of the faults with 2 m of slip. They are thought to have formed at the same time as each other because of their similar lengths and throws. They are considered to be a surface manifestation of a propagating normal fault at depth that never intersected the downward propagating dilational fractures. They also may be the least developed faults in the graben because they are furthest from the center.

It is hypothesized that instead of one structure, the Vogar graben is actually

comprised of two grabens. The evidence for this is found in the structures seen as well as published data on geothermal systems of the peninsula. Fault scarp T has its hanging wall on the southern side, consistent with being the western boundary fault of a graben east of it. It is thought to be a bounding scarp of a second, smaller dike close to the plate boundary in the southern section of the study. It has a similar orientation to the Eldvorp crater row, and thus their structures may be controlled by the same source (Jenness and Clifton, 2009). This source could be a small shallow dike that has intruded the thin and warm relatively new crust. A resistivity survey conducted by Arnasson et al. (2008) showed that there appears to be a small geothermal system near the Eldvorp crater row. The observed structures and published data lead to the hypothesis that the graben is actually comprised of one large graben related to the larger Reykjanes dike system, and a smaller graben indicative of a small dike, with both protruding laterally from the plate boundary and containing an associated geothermal system.

The overall asymmetry of the graben may be controlled by the crustal thickness and temperature. Stresses may travel easier through the warmer, thinner crust closer the plate boundary as opposed to the thicker colder crust at the edges. This could account for the fact that large scarps with >10 m throw characterize the northern wall of the first graben, while a larger number of scarps with smaller throws characterize the southern wall of the graben. The bottom of the graben may be indicative of the zone of greatest crustal transition, from warm thin crust at the plate boundary to cold thick crust at the edges of the rift zone, creating an area of weakness.

### 4.5 Implications for the Whole Reykjanes Peninsula

Analysis of the Vogar graben provides information on the kinematics of a fissure swarm as it moves from the center of the axial rift zone to its edge. Moving away from the plate boundary in an oblique spreading zone changes the stresses that act on these zones of fissuring and faulting. The fissure swarms are overall controlled by dikes that are injected laterally from the plate boundary at depth. The structures in the Vogar graben

trend at 40°, oblique to the overall plate spreading direction (105°) and the azimuth of the plate boundary (70°). Using the model proposed by Clifton and Kattenhorn (2006), the average strike of the structures falls right in between the values they assign to structures seen at the plate boundary and structures on the edges of the fissure swarms. This is logical since the northeastern edge of the graben is closer to the end of the fissure swarm and the southwestern edge is close to the plate boundary. This change in strike from the plate boundary to the edges of the fissure swarms is controlled by the stress imparted by the left lateral oblique transform zone of the peninsula. The Reykjanes Peninsula is neither a pure extensional nor pure shear environment, but shearing does exceed extension (Clifton and Schlische, 2003). The shear component of 16.8 mm/yr on the peninsula predicted by the NUVEL-1A plate motion model proposed by Demets et al. (1994) is in agreement with GPS measurements from Hreinsdottir et al. (2001). However the extensional component of 8.5mm/yr predicted by the NUVEL-1A is not seen with the GPS-data of 1993-1998. It is concluded by Hreinsdottir et al. (2001) that there are different modes and time periods of deformation. During dry or amagmatic cycles on the peninsula, faulting is primarily along dextral strike slip faults related to the left lateral transform zone. During magmatic or aseismic periods the extensional component is accommodated through fissuring and normal faulting. The analysis of the Vogar graben provides evidence for this theory that the fissure swarms are activated only during wet or eruptive episodes. Contrary to suggestions by Clifton and Kattenhorn (2006), there was no evidence found along the faults in the Vogar graben that there has been any movement along them since the last eruptive episode that ended 800 years ago. Therefore, aseismic faulting and fissuring associated with dike injections during eruptive episodes is the inferred mode of deformation. The presence of the two subswarms was also determined from field observations (Fig. 4.9). This fits well with the locations of the eruptive fissures in the Reykjanes fissure swarm, which lie almost parallel to the proposed strike of the dikes.

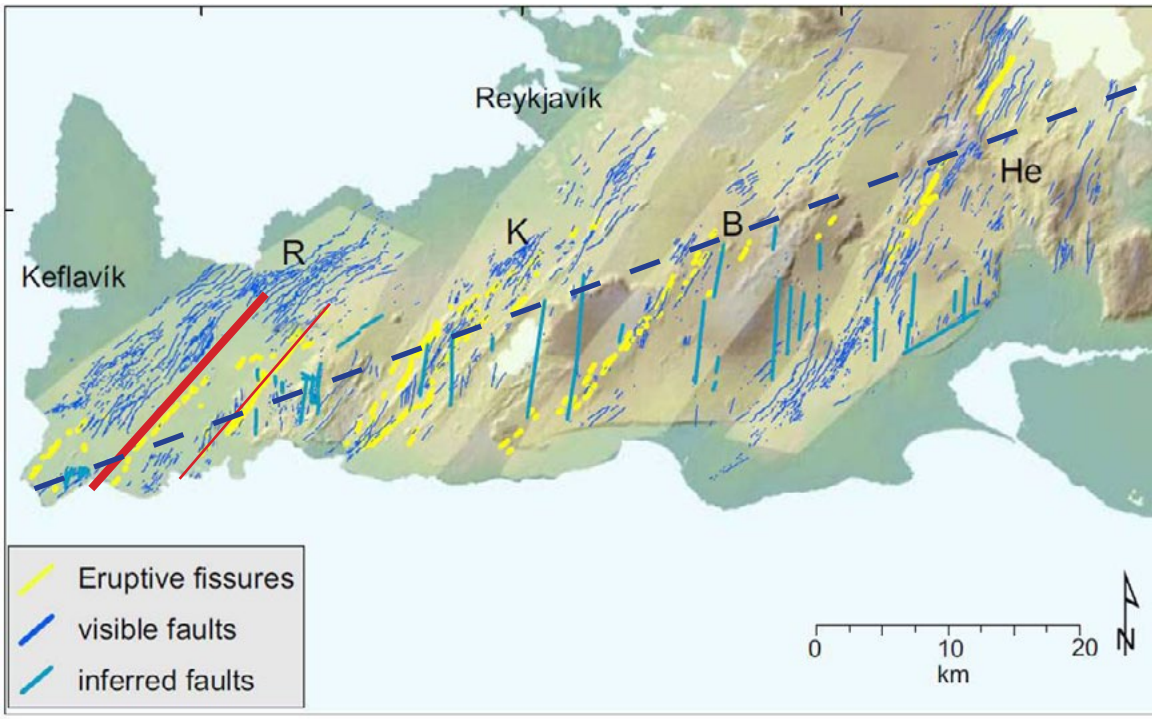


Figure 4.9 Map of the faults and eruptive fissures on the Reykjanes Peninsula with the two proposed dike injection zones superimposed. The trend of the plate boundary is highlighted by the dashed line. The presence of the two subswarms within the Reykjanes Fissure Swarm fits well with the location of eruptive fissures. (Modified from Jenness and Clifton, 2009).

The peninsula is still very much active, and experiences persistent seismicity along the length of it. There is currently an earthquake swarm occurring along the Krisuvik fissure swarm, which lies adjacent to the Reykjanes fissure swarm. The swarm peaked in late February 2011, with a series of over 500 recorded earthquakes between the 27th and 28th (Iceland Meteorological office, 2011). The earthquaked originated in the uppermost few kilometers of the crust, with an average magnitued of 1.5. There was also observed inflation within the swarm and some alteration of the Krisuvik geothermal system (Einarsson, 2011). Large quantities of small earthquakes with small magnitudes coupled with inflation, usually indicate movement of magma under the crust. This was evidenced recently by the eruption of the subglacial volcano Eyjafjallajokull in southern Iceland, which was preceded by large swarms of earthquakes and inflation. The activity in Krisuvik could be an indicator of the start of the next magmatic episode on the peninsula, which has been dormant for 800 years.

# CHAPTER 5: CONCLUSIONS

## 5.1 Conclusions and Future Work

Detailed mapping of the Vogar fissure swarm was carried out in an effort to better constrain the kinematics of the fissure swarms that make up the Reykjanes Peninsula oblique rift. It has been speculated that movement along the normal faults that characterize the fissure swarms occurs primarily during eruptive or magmatic episodes on the peninsula. However, movement during amagmatic periods has also been observed. Primarily, attention was paid to whether the faults that were observed in the Thrainsskjoldur shield lava continued into the historical lava flow that covered many of these fault scarps. Evidence of movement in the historical lava would indicate that since the last eruptive episode ended, 800 years ago, there has been normal slip along the faults, and thus the faults are related seismically to the rifting of the North American and Eurasian plates. If no slip is seen in the historical lava then movement along the faults can be constrained to magmatic events.

Although fault related structures were observed along strike of some faults in the historical lava, they were determined to be related to flow and cooling properties of the lava and not to faulting. The main structures were an apparent change in the hanging wall and the footwall, and fissures observed along strike of faults in the historical lava. GPS data confirmed the apparent change in hanging wall and footwall to occur right at the contact of the shield lava and historical lava. This apparent change in the walls of the fault was attributed to lava piling up against the scarps as it flowed, influenced by the dipping blocks associated with the hanging walls of the faults. The viscosity of the lava allowed it to pile up against the scarp, higher than the footwall. In some cases where the lava overflowed onto the footwall of the bounding scarp, fissures at the contact of the overflowed lobe and the larger body of lava formed due to differential cooling. Another method of formation of these fissures may have been due to open fissures at the bases of the faults. Lava that flowed into them would have cooled, creating space that was eventually filled in by lava above and manifested itself at the surface as a fissure or

secondary rifting structure.

Confirming that there was no observed normal slip along these faults since the last eruptive episode on the peninsula, a cross section of the graben was hypothesized with dikes at depth controlling the geometry of the faults. It was determined that the graben represented four main sets of the deformation, controlled by two dikes or injection zones at depth. The oldest, largest, most eroded faults characterized the oldest set, followed by the main set defined by the next largest and longest faults. The southern end of the section was hypothesized to be controlled by a second smaller dike which would explain the opposite dipping scarp that was observed. The fourth set represents the youngest and shallowest dikes, defined by the bottom of the graben.

Evidence is provided that the fissure swarm has been only marginally active since the latest magmatic episode which ended in 1240 AD. This lends support to the suggestion that the fissure swarms are mainly active during magmatic episodes and not during the intervening periods when the plate boundary deformation is characterized by brittle failure and earthquakes on strike-slip faults (e.g. Hreinsdottir et al., 2001). The true scale cross section of the graben gives one interpretation of the processes happening at depth in the graben, but is still highly speculative. Detailed seismic data from the region would provide much more information as to the kinematics of the faults under the surface. Future work may also involve further investigation of exposed dikes in the northeastern section of Iceland in order to get a clearer picture of dikes mechanics and propagation tendencies within the rift margin.

# REFERENCES

Acocella, V., Korme, T., Salvini, F., 2003, Formation of normal faults along the axial zone of the Ethiopian rift: Journal of Structural Geology, v. 25, p. 503-513

Arnason, K., Karlsdottir, R., Eysteinsson, H., Flovenz, O., Thor, S., 2008, The resistivity structure of high-temperature geothermal systems in Iceland: Proceedings of the World Geothermal Congress, Kyushu-Tohoku, Japan, 923-928

Buck, W.R., Einarsson, P., Brandsdottir, B., 2006, Tectonic stress and magma chamber size as controls on dike propagation: Constraints from the 1975-1984 Krafla rifting episode: Journal of Geophysical Research, v. 111, B12404

Clifton, A.E., Kattenhorn, S.A., 2006, Structural architecture of a highly oblique divergent plate boundary segment: Tectonophysics, v. 419, p. 27-40

Clifton, A.E., Schlische, R.W., 2003, Fracture populations on the Reykjanes Peninsula, Iceland: comparison with experimental clay models of oblique rifting: Journal of Geophysical Research, v. 108, p. 2074–2091

Darbyshire, F.A., White, R.S., Priestly, K.F., 2000, Structure of the crust and uppermost mantle of Iceland from a combined seismic and gravity study: Earth and Planetary Science Letters, v. 181, p. 409-428

DeMets, C., Gordon, R., Argus, D., Stein, S., 1994, Effect of recent revisions to the geomagnetic reversal time scale on estimates of current plate motions: Geophysical Research Letters, v. 21, p. 2191-2194

Dyment, J., Lin, J., Baker, E.T., 2007, Ridge-hotspot interaction: What mid-ocean ridges tell us about deep earth processes: Oceanography, v. 20, p. 102-115

Einarsson, P., 2011, Personal Communication.

Einarsson, P., 2008, Plate boundaries, rifts and transforms in Iceland: Jökull, v. 58, p. 35-58

Einarsson, P., 1991 Earthquakes and present-day tectonism in Iceland: Tectonophysics, v. 189, p. 261-279

Einarsson, P., Brandsdottir, B., 1980, Seismological evidence for lateral magma intrusion during the July 1978 deflation of the Krafla volcano in NE-Iceland: Journal of Geophysical Research, v. 47, p. 160– 165

Foulger, G.R., Anderson, D.L., 2005, A cool model for the Iceland hotspot: Journal of Volcanology and Geothermal Research, v. 141, p. 1-22

Grant, J.V., Kattenhorn, S.A., 2004, Evolution of vertical faults at an extensional plate boundary, southwest Iceland: Journal of Structural Geology, v. 26, p. 537-557

Grossenbacher, K.A., McDuffie, S.M., 1995, Conductive cooling of lava: columnar joint diameter and stria width as functions of cooilng rate and thermal gradient: Journal of Volcanology and Geothermal Research, v. 69, p. 95-103

Gudmundsson, A., 2000, Dynamics of volcanic systems in Iceland: example of tectonism and volcanism at juxtaposed hot spot and mid-ocean ridge systems: Annual Review of Earth and Planetary Sciences, v. 28, p. 107–140

Gudmundsson, A., 1992, Formation and growth of normal faults at the divergent plate boundary in Iceland: Terra Nova, v. 4, p. 464-471

Gudmundsson, A., 1987, Geometry, formation and development of tectonic fractures on the Reykjanes Peninsula, Southwest Iceland: Tectonophysics, v. 139, p. 295-308

Gudmundsson, S., Sigmundsson, F., Carstensen, J.M., 2002, Three dimensional surface motion maps estimated from combined InSAR and GPS data: Journal of Geophysical Research, v. 107, B102250

Hreinsdottir, S., Einarsson, P., Sigmundsson, F., 2001 Crustal deformation at the oblique spreading Reykjanes Peninsula, SW Iceland: GPS measurements from 1992 to 1998: Journal of Geophysical Research, v. 106, p. 13,803-13,816

Icelandic Meteorological Office, Web. 29 Feb., 2011. <http://en.vedur.is/earthquakes-and-volcanism/earthquakes/reykjanespeninsula/>.

Jakobsson, S.P., Jonsson, J., Shido, F., 1978, Petrology of the Western Reykjanes Peninsula, Iceland: Journal of Petrology, v. 19, p. 669-705

Jenness, M.H., Clifton, A.E., 2009, Controls on the geometry of a Holocene crater row: a field study from southwest Iceland: Bulletin of Volcanology, v. 71, p. 715-728

Keiding, M., Arnadottir, T., Sturkell, E., Geirsson, H., Lund, B., 2008, Strain accumulation along an oblique plate boundary: the Reykjanes Peninsula, southwest Iceland: Geophysical Journal International, v. 172, p. 861-872

Long, P., Wood, B.J., 1986, Sructures, textures, and cooling histories of Columbia River basalt flows: Geological Society of America Bulletin, v. 97, p. 1144-1155

Mittelstaedt, E., Ito, G., Behn, M.D., 2008, Mid-Ocean ridge jumps associated with hotspot magmatism: Earth and Planetary Science Letters, v. 266, p. 256-270

Paquet, F., Dauteuil, O., Hallot, E., Moreau, F., 2007, Tectonics and magma dynamics coupling in a dyke swarm of Iceland: Journal of Structural Geology, v. 29, p. 1477-1493

Saemundsson, K., Einarsson, S., 1980, Geological map of Iceland, sheet 3, SW-Iceland, second ed. Museum of Natural History and the Iceland Geodetic survey, Reykjavik.

Slunga, R., Rognvaldsson, S.T., Bodvarsson, R., 1995, Absolute and relative locations of similar events with application to microearthquakes in southern Iceland: Geopysical Journal International, v. 123, p. 409-419

Sonnette, L., Angelier, J., Villemin, T., Bergerat, F., 2010, Faulting and fissuring in active oceanic rift: Surface expression, distribution and tectonic-volcanic interaction in the Thingvellir Fissure Swarm, Iceland: Journal of Structural Geology, v. 32, p. 407-422

Tentler, T., 2005, Propagation of brittle failure triggered by magma in Iceland: Tectonophysics, v. 406, p.17-38

Thordarson, T., Larsen, G., 2007, Volcanism in Iceland in historical time: Volcano types, eruption styles and eruptive history: Journal of Geodynamics, v. 43, p. 118-152

Tryggvason, E., 1970, Surface deformation and fault displacement associated with an earthquake swarm in Iceland: Journal of Geophysical Research, v. 75, p. 4407-4422

White, R.S., McKenzie, D., O'nions, K., 1992, Oceanic crustal thickness from seismic measurements and rare earth element inversions: Journal of Geophysical Research, v. 97, p. 19,683-19,715